NUREG/CR-4157
ARAP No. 472

A Scientific Critique of Available Models for Real-Time Simulations of Dispersion

Prepared by W. S. Lewellen, R. I. Sykes

Aeronautical Research Associates of Princeton, Inc.

Prepared for
U.S. Nuclear Regulatory
Commission

GPO Printed copy price: $5.50

NUREG/CR-4157
ARAP No. 472
RB

A Scientific Critique of Available Models for Real-Time Simulations of Dispersion

Manuscript Completed: January 1985
Date Published: March 1985

Prepared by
W. S. Lewellen, R. I. Sykes

With Contributions by
S. F. Parker, A. K. Varma, R. W. McCullough,
H. Philander, G. Sandri, D. A. Oliver

Aeronautical Research Associates of Princeton, Inc.
50 Washington Road
P. O. Box 2229
Princeton, NJ 08540

Prepared for
Division of Radiation Programs and Earth Sciences
Office of Nuclear Regulatory Research
U.S. Nuclear Regulatory Commission
Washington, D.C. 20555
NRC FIN B0446

ABSTRACT

This report provides a scientific evaluation of several available dispersion models to determine their suitability for providing the capability for estimating the effects of accidental discharges of radioactive material at nuclear power plants. A critique of the assumptions involved and a review of existing verification studies are made for models ranging from the Gaussian plume with straight line winds to models which attempt a complete solution of the primitive equations of motion. It is demonstrated that although even the simple models are capable of providing reasonably accurate predictions under ideal conditions, there are reasons to expect relatively severe limits on plume predictability when certain emission conditions are combined with certain meteorological conditions. The usefulness of a real-time dispersion model is thus likely to be dependent on a complementary estimate of the variability expected about the mean dispersion for the conditions existing at that time.

This report is one of a set of three dealing with real-time dispersion models. The other two deal with the uncertainties involved in the deposition module of dispersion models and the results of testing some of the dispersion models reviewed in this report by comparing them with the data collected at the Idaho National Engineering Laboratory in July, 1981 during an NRC sponsored field test.

TABLE OF CONTENTS

LIST OF FIGURES

LIST OF TABLES

ACKNOWLEDGEMENTS

We wish to thank Frank Kornegay of Oak Ridge National Laboratory for his technical assistance, and Robert Abbey and Robert Kornasiewicz of the NRC for the technical monitoring of this work.

CHAPTER 1
INTRODUCTION

The Nuclear Regulatory Commission has established the requirement that the operators of nuclear generating plants maintain the capability for estimating the effects of an accidental discharge of radioactive material (NUREG 0654). The requirements call for two classes of predictive capabilities reflecting the requirements of the two emergency planning zones for "plume exposure" and "ingestion". A Class A model designed to predict plume exposure within 10 miles of the site must produce initial estimates of atmospheric transport and diffusion within 15 minutes of the accident. The model is to include the plume dimension and position as well as the relative concentrations at various downward locations. The NRC has required that "seasonal, diurnal, and terrain induced flows" be included in the model as well as the "source characteristics" such as "building complex influence". The Class B model is to be used for the prediction of deposition and relative concentration within the ingestion zone which extends out 50 miles from the site. This model should provide, within approximately 45 minutes, a detailed spatial and temporal map of the expected radioactivity for the duration of the release. Both of the models will be required to use site-specific algorithms as well as local meteorological data.

It is the purpose of this report to conduct a preliminary evaluation of several candidate models to determine their ability to satisfy the requirements for Class A or Class B models.

The next section discusses the evaluation criteria. This is followed by an overview of existing models which might be considered as candidates for a real time dispersion model. From this large list we have selected 10 models for detailed critiquing. These are chosen to cover the spectrum of different

types currently available. These models can be divided into four generic categories: gaussian plume with straight line winds; gaussian puff with spatially and temporally varying winds determined by interpolated data; more sophisticated diffusion models with mass-adjusted winds; and models which attempt a complete solution of the primitive equations. This report provides a general scientific critique of the assumptions involved in each type model and a review of existing verification studies for each model chosen for detailed consideration.

It is demonstrated that most candidate models provide a reasonably accurate prediction under the ideal conditions often chosen to test dispersion models. In spite of this favorable result, there are a number of reasons to expect large errors under more realistic conditions. Further testing in comparison with high-quality, tracer concentration data obtained with coincident meteorological data for a number of realistic full scale programs is required to establish definitive error bounds. Results from such a test are given in a comparison report.

CHAPTER 2
EVALUATION CRITERIA

2.1 Overall Criteria

Although the most important criterion in evaluating a model is its accuracy, it is also appropriate to consider its responsiveness, costs, and growth potential. Unless a model can provide a timely response at an affordable cost, its superior accuracy may be of little use. Growth potential is desirable, but not essential.

The responsiveness required by NRC for a Class A model is that an initial estimate of transport and diffusion out to 10 miles be available within 15 minutes following the classification of an incident. This Class A requirement effectively dictates an automated system which ties the on-site meteorological data system directly to a computer dispersal model. Any meteorological data needed to run a Class A model needs to be routinely available.

The response requirements for Class B models are somewhat less stringent. No precise time limit has been imposed by NRC, but if the response time stretches much beyond an hour it would appear to seriously degrade the utility of any model. These time requirements will be discussed for those models for which it appears that response time will be an important factor.

The total cost of implementing a model is composed of the cost of establishing both the on-site data system to collect the meteorological data needed to drive the model and the computer equipment to run the model; the cost of maintaining both the meteorological data system and the model on a standby basis; and the costs of individual runs. We have performed no economic analyses for this report, but have noted where increased data requirements may be expected to drive up costs with little demonstrated improvement in model output accuracy.

Growth potential is provided by a model with a sound scientific foundation, since it should be improvable by incorporating more of the physical features which are not currently being adequately modeled. This possibility is enhanced if modular construction is used in the computer model, such that an improved wind or diffusion model should be readily incorporable into the system.

2.2. Accuracy

Our top priority is to determine how accurate the different models may be expected to be under realistic conditions. The foremost accuracy requirement is that of reasonably representing the spatial and temporal distribution of the plume concentration. A number of attempts have been made to outline procedures for evaluating the performance of atmospheric dispersion models (e.g., Hilyer et al., 1979; Fox, 1981; Pepper, 1981; Hilst, 1978; and Ruff et al., 1979) but there are no generally accepted standards. This literature does stress the importance of judging model performance based on the particular needs of the desired application. Any statistical measures used should directly relate to the desired model output.

Models developed for EPA have generally emphasized the accurate prediction of maximum ground level concentrations that may occur for some specified short period of time, such as an hour, over some specified period of operation, such as a year. For a typical accidental release, this maximum ground level concentration is most likely to occur within a few hundred meters of the plant and within a few minutes of the time of maximum release. Although of some use in decisions regarding controlled releases, this single performance measure is of little use for emergency decisions. A sensible evacuation decision requires estimates of the specific area over which the concentration will exceed some critical level defined by health effects. Unfortunately, the ratio of this critical concentration contour level to the maximum ground level concentration is not likely to be known in advance. For a minor accident with low emissions, the maximum ground level concentration, $C_{o_{max}}$, may remain below the critical level defined by health effects, $C_{o_{he}}$,

while for a major accident with high emissions the ratio of $C_{o_{max}}/C_{o_{he}}$ may be a large number. In this latter case the critical concentration level could be several orders of magnitude smaller than $C_{o_{max}}$. Since the emission rate is unknown until the time of the accident, and perhaps even after the accident, a model can best be judged on how well it predicts the spatial and temporal concentration patterns of a normalized unit release. Although the elevated concentration is of some importance due to the radiation received at a distance ("shine dose") we will concentrate more on ground-level concentration patterns. We feel there are ample reasons for this bias. First, inhalation dose is likely to be more serious than shine dose for the low-level releases anticipated in most accident scenarios. Second, reliable ground-level concentration data is more readily available to use for model evaluation. Third, the ground-level concentration will be the major factor determining dry deposition. At any rate, a close agreement between ground-level observations and calculations should provide reasonable assurance that the vertical distributions of the associated plumes are also in reasonable agreement.

The spatial distribution appears to be more critical than the temporal distribution, since health effects tend to depend on time integrated dosage and thus temporal variations may be integrated over time periods of a few hours. What is desired is a quantitative measurement of how well the predicted spatial distribution of ground-level, time-integrated concentration agrees with real field observations. A pattern comparability test designed to measure this is described in Section 2.3. We expect to utilize this tool in evaluating how well different models perform under real field test conditions. However, due to the scarcity of appropriate data which define the spatial distribution of plumes out to distances of 10-100 km, other somewhat more subjective tests will also be used.

Since opportunities for real field tests under conditions similar to those which may exist at the time of actual incidents are so limited, it is also important that candidate models be judged on the basis of their scientific validity. This provides the best chance that a model's accuracy under a few diverse test conditions will extrapolate to equal accuracy under

untested conditions. For this reason our present evaluation emphasizes a scientific critique of the individual codes. An essential adjunct is a numerical analysis of the sensitivity of the models to uncertainty in the inputs using both ideal analytic tests and real field tests. An important part of our evaluation is a critical review of published verification tests.

2.3. Proposed Measure of Surface Pattern Comparability

The most commonly used measures of model performance are direct comparisons of calculated values versus observed values for the available data observations. These comparisons are generally either paired in time and space or paired in time only. Neither comparison provides adequate information on how much spatial variability there is between observed and calculated contours of some concentration level. Precise pairing in time and space imposes too strong a penalty for small misalignments, while paired in time only provides no information on spatial variability.

We propose herein a more quantitative measure of the spatial comparison between observed and calculated patterns by allowing the comparison to be made at increments of decreasing spatial resolution. This involves a measure of how much the calculated pattern must be shifted in space to cover all of the observed values. For this purpose, let us define the area A sketched in Fig. 1 centered at an arbitrary observation point x_o. This $A(x_o,\delta\theta)$ is completely defined by its position in polar coordinates (r_o,θ_o) centered on the emission point and an angular displacement $\delta\theta$. The area is bounded by $\theta-\theta_o < \delta\theta$ and $r-r_o < r_o\delta\theta$. The calculated concentration field within the area A is bounded by lower and upper values which we define as $C_c^1(A)$ and $C_c^2(A)$, respectively. With the observed concentrations $C_o(x_i)$ given at a number of points $i = 1,\ldots,M$, let us define the calculated concentrations at these points to be the following function of $\delta\theta$:

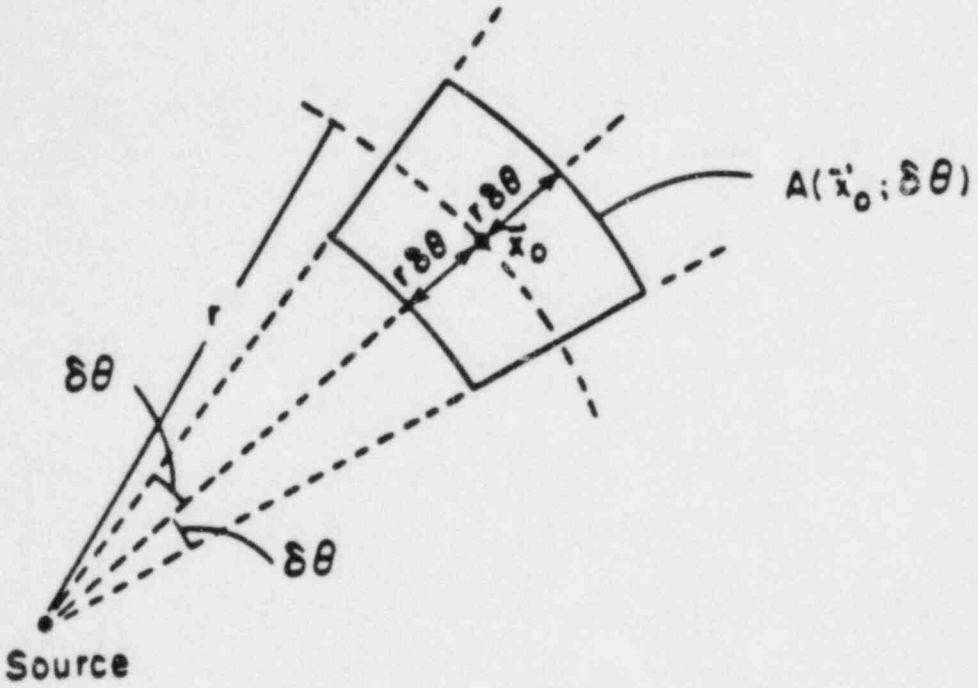

FIGURE 2.1 - Schematic of Area Segment A (x_o,$\delta\theta$).

$$C_c(x_i,\delta\theta) = \begin{cases} C_c^1(A) & \text{if } C_o(x_i) < C_c^1(A) \\ C_o(x_i) & \text{if } C_c^1(A) < C_o(x_i) < C_c^2(A) \\ C_c^2(A) & \text{if } C_o(x_i) > C_c^2(A) \end{cases} \qquad (2.1)$$

Any statistical measure of the comparison between C_c and the observed C_o can now be made as a function of spatial resolution, $\Delta\theta$. Our principal measure will be the number of calculated points which fall within specified bands about the observed data. For this purpose $f_N(\delta\theta,N)$, is defined as the fraction of the test points which yield calculated concentrations within a ratio N of the observed value within the area defined by the sector $\delta\theta$, and calculated from

$$f_N(\delta\theta,N) = \frac{1}{M}\sum_{i=1}^{M} H\left(N - \exp\left|\ln\frac{C_c\ x_i,\delta\theta}{C_o\ x_i}\right|\right) \qquad (2.2)$$

with H(t) the Heaviside step function equal to 1 or zero, depending upon whether $t \geq 0$ or $t < 0$.

A plot of $f_N(\delta\theta,N)$ gives a direct measure of how the calculated spatial distribution compares with the observations. As an example, Figure 22 from Lewellen, et al. (1982) is repeated here as Figure 2. The level of accuracy desired can be set by specifying the ratio N. For N = 2, Figure 2 shows that 90% of the observations are covered by a shift of 15° in the pattern, and that this rises to 100% for a 25° shift. An emergency planner should be happy to expand a potentially affected area by 15° in order to cover model uncertainty. Unfortunately, Figure 2 represents unusual test conditions so that the general results are not expected to be this good.

We do not wish to imply that the use of f_N will eliminate all ambiguity regarding comparisons between the model calculated dispersal pattern and the actual test pattern. Ideally the sum in Equation (2.2) defining f_N should include all points where either the calculated or the observed concentration

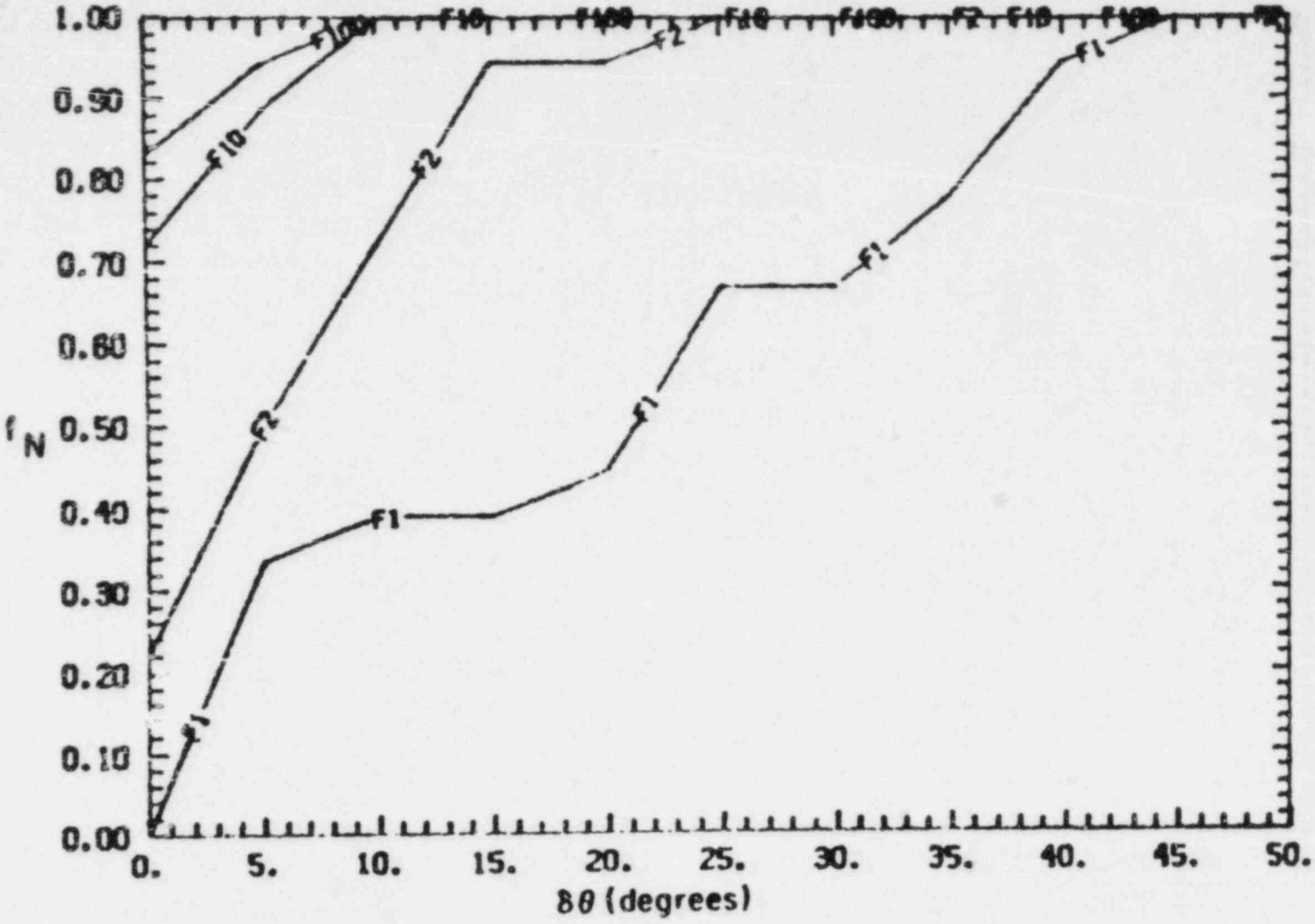

FIGURE 2.2 - Pattern Test Result using the MATHEW/ADPIC Calculations. f_N equals the fraction of data points covered within a factor of N by the calculated pattern expanded through an angle $\delta\theta$. (From Lewellen et.al., 1982)

is greater than background values. However, it can only be applied at points where observed values are available. Clearly, if the observed data points are so sparse as to leave the actual test pattern undefined, it would be possible to design calculative procedures to yield high values of f_N without necessarily showing good agreement with the actual test pattern. For instance, if the plume is modeled as a hopscotch pattern with alternating high and zero values of concentration, only a small angular shift in pattern would be required to match observed data. Although this model is very unlikely to be a true model, the test is unable to discriminate against it. We believe that the best safeguard against this is a combination of requiring that the model be scientifically sound, and that the model be tested against a variety of observed data.

A variation of the pattern test which we will use for some purposes is to compare only the maximum value of the concentration with the maximum observed within the defined area. In the limit of large areas this would go to the standard paired in time only comparison. It will also defeat the simple strategy of predicting the previously mentioned hopscotch pattern. The principal drawback of this version of the comparison would be an undue penalty to the model when the observations are not adequate to capture the maximum concentration at that time.

CHAPTER 3

INHERENT UNCERTAINTIES DUE TO THE STATISTICAL NATURE OF TURBULENCE

Before critiquing some specific models, we wish to discuss the inherent uncertainties involved in any simulations of atmospheric dispersion. Atmospheric motions cover a range of scales from small dissipative eddies on the order of 10^{-3} meters, to the large synoptic weather features of the order of 10^{6} meters. It is essential to average over, at least, the lower end of this spectrum of scales, particularly since the smallest scale motions tend to be random in character, and thus most susceptible to statistical analyses. However, it is somewhat arbitrary where the break between resolved wind features and unresolved turbulent motion is placed. It is well to keep in mind that these unresolved turbulent motions will induce some essentially random variation on the plume. That is, even if it were possible to introduce two separate plumes into the same resolved wind field, there would be some variance in the dynamics of the two plumes due to the unresolved turbulence.

All available models implicitly assume that transport by the mean wind can be clearly separated from diffusion by turbulence. This is only true if a distinct spectral gap exists between the wind fluctuations inducing diffusion and those responsible for transporting the plume. There is evidence of some reduction in wind energy in the frequency range between 10min and one hour as exhibited by van der Hoven (1957), but seldom is there a complete absence of energy in this mesoscale range. In fact in the presence of mesoscale forcing this range may be expected to be particularly active. Under such conditions it is important to keep in mind that dispersion models are designed to simulate the distribution of the ensemble mean concentration and that the ensemble mean may be significantly different from a time average. This is particularly important in attempting to evaluate the accuracy of real-time dispersion models. The model user would like to obtain an estimate of the concentration distribution in time and space being realized over one particular domain of time and space. Even though some averaging is permitted it is the results of a single realization which is desired rather than a prediction of the ensemble mean. When there is a large variance between the

ensemble mean and the particular time and space average considered, then even a perfect model prediction of the ensemble mean may provide little indication of what is happening in the single realization. This natural limit on predictability plays an essential role in model evaluation and a large part of our effort has been devoted to our attempt to elucidate this role.

A clear specification of the limits to predictability as a function of available meteorological conditions would not only provide an upper bound on model accuracy but it would also provide a precise measure to use when comparing model predictions and field observations. We have not achieved this level of specification, but have gained a healthy appreciation of the obstacles which must be overcome and have formulated a framework for achieving a model which provides for an estimate of the variability expected to complement its prediction of a mean distribution. This work is detailed in Appendices A thru D for the interested reader. We will only summarize the most important results here.

Our principal conclusion from our predictability work is that it is as important for a real-time dispersion model to provide an estimate of variability as it is to provide an estimate of the mean dispersion. Further, this variability is not simply a function of the model chosen but rather is a complicated function of the meteorological data and the nature of the source of emissions. We recommend that any model adopted for real-time emergency use be supplemented by, at least, a simple model of the concentration variance expected under the conditions at that time. A relatively simple model of the mean concentration together with a compatible model of its variance should be more useful than a sophisticated model which even provides a better estimate of the mean if the latter includes no estimate of the variability expected.

The technical obstacles to be overcome are discussed in Appendix A. There we discuss how the measured meteorological data define the ensemble of possible realizations. The scale of the wind motions which must be included in the ensemble turbulence, as distinct from the larger scale motions which may be resolved as transporting winds, is determined by the time and space resolution of the available data. A schematic delineation of six different

boundaries of possible interactions between a plume are provided on a real wind spectra obtained from the EPRI plume model validation study. These six different boundaries ranging from the low frequency end of the spectra are:

1) The upper boundary on frequencies included in the mean transport of the plume;

2) The lower bound on frequencies included as part of the turbulence;

3) The upper bound on motions transporting the time-averaged plume as a coherent entity;

4) The lower bound on motions which contribute to diffusion of the time-averaged plume;

5) The upper bound on motions which contribute to the variance in the instantaneous plume; and

6) The lower bound on motions which contribute to the diffusion of the instantaneous plume.

The first and second boundaries are controlled by the spatial domain which the data is to represent. The third and fourth are controlled by the concentration sampling time, and the fifth and six by the spread of the instantaneous plume. If there is a well defined mesoscale gap in wind energy so that boundaries one and two are widely separated and boundaries three and four fall between one and two then variability is not a problem. In this case the time average result will agree with the ensemble average. The actual wind spectra shown provides for some reduction in energy in the mesoscale gap but leaves plenty of energy to drive variability in time-averaged plumes.

A framework for analytically estimating the natural uncertainty is presented in Appendix B. Further work is required before the framework presented there can be used with any quantitative precision, but it does show that large uncertainties should be expected when the sampling time of the measurement is not much greater than the time scale of the turbulence. The ratio of the source size to the length scale of the turbulence also is an important parameter in determining the uncertainty, with the uncertainty increasing as the ratio of the source size to the turbulent length scale decreases.

As an example of the importance of the natural uncertainty, consider afternoon conditions with light winds and relatively strong convection. The analysis of Appendix B involves 3 steps: 1) the prediction of the ratio of the ensemble variance to the ensemble mean, 2) relating the ensemble variance to the variance expected in time-averaged samples for a particular sampling time, and 3) the interpretation of the time-averaged variance as a measure of the expected uncertainty. When the ratio of the source size to the turbulent length scale, Λ, is of the order of 10^{-2}, as it would be for a 10 m plume released into a boundary layer with $\Lambda \sim 1$ km, then both the simple model and laboratory experiments indicate that a significant part of the plume will have $\sigma_c/\overline{c} \geq 3$. Then according to either Fig. B.1 or B.2, an instantaneous sample of the concentration in this region of the plume would have less than a 50% chance of being within an order of magnitude of its mean value. Thus even a perfect prediction of the mean will lead to an order of magnitude scatter in the comparison between the predicted and the instantaneously observed values in these regions of the plume. The predictability for a given sample time is increased as the time-averaged variance is significantly reduced below its ensemble value. According to Eq. (B.1), $\sigma_c/\overline{c}$ is reduced by less than 30% from its ensemble value when the sample time is equal to the turbulent time scale. The sampling time must be greater than 20 times the turbulent time scale before the time-averaged value of $\sigma_c/\overline{c}$ is reduced to less than 10% of its instantaneous value. For a turbulent length scale of 1 km and a wind speed of order 1 m/sec, the turbulent time scale will be order 10^3 sec. The regions of the plume which had instantaneous values of $\sigma_c/\overline{c}$ in excess of 3 will still have hour averaged values in excess of 1. Again referring to either Fig. B.1 or B.2, this still provides a 50% probability of missing the mean value by more than a factor of 2 with a perfect model.

Appendix C demonstrates that it is possible to provide a model which will correctly predict the ensemble variance under a number of conditions existing in the laboratory. This provides a firm foundation for the expectation that it should be possible to carry out the procedure outlined in Appendix B. We have also included Appendix D which provides an analytical model of the influence of source size on time-averaged concentration variance. This is

useful in estimating the variance during the INEL tests which are used to compare different model results against field data.

CHAPTER 4

SELECTION OF MODELS FOR DETAILED TESTING

There are a large number of dispersion models which have been used for various purposes. Recent reviews of available models have been given by Turner (1979), Drake (1979), Bass (1980), Bass and Smith (1981) Hanna (1981), and Liu et al. (1982). Our purpose in the present section is to select a modest number of representative models for detailed consideration. We have divided the available models into four generic categories: steady-state gaussian plume models, unsteady puff models, transport and diffusion models, and primitive equation models.

The Gaussian plume models use a steady-state, parameterized solution for diffusion in the presence of straight line winds. A representative list of some of the available models of this type is given in Table 1. These models are sufficiently simple that many users modify the parameterization slightly to suit their own perceived needs. These modified models then may or may not be elevated to the level of named models. Chapter 5 will discuss this category of models and critique three particular ones: two established models, ISC and TEM, and a third model, GP, which we designed for this purpose. These are not chosen as the best available, but rather because they should be quite representative of this category of models. Models in this category are prime candidates for selection as a Class A model. They are considerably less likely to be appropriate as a Class B model due to temporal variations in the meteorological conditions.

For longer times and greater distances, models need to account for some temporal variations in the wind. The simplest approach to this is to represent the plume as a series of puffs or plume segments. Table 2 lists a number of available models in this category. Most of these models are flexible enough to serve either as a Class A or Class B model. Chapter 6 will discuss this category and five particular models: Mesodif, MESOI, the ARL trajectory model, and two new models, MESOJ and MESOT we have introduced as diagnostic models to determine the potential of this type of model.

Table 1

Gaussian Plume Models

Model Name	Organization	Reference
AIRDOS	Oak Ridge National Laboratory	Moore (1977)
AIRMOD	U.S. ARMY	Webster, et al. (1978)
APRAC2	EPA	Ludwig and Obinata (1974) Illinois EPA (1976)
AQSTM	Illinois EPA	
ARAC Gaussian	LLNL	Dickerson and Orphan (1975,1976)
ATDL	NOAA/ATDL	Gifford (1973)
ATM	NOAA/ATDL	Culkowski and Patterson (1976)
COMRADEX-4	Rockwell International	Otter and Chung (1977)
DEPA	NOAA/ATDL	Rao (1981)
DIFOUT	Sandia National Lab.	Luna and Church (1969)
DWNWND	Oak Ridge National Laboratory	Fields and Miller (1980)
EDMS	RAS/NUC	Wilkie and Garry (1981)
GEM	Science Applications Inc.	Fabrick, Sklarew and Wilson (1977)
GLUMP II	MESOMET	Lyons, et al. (1981)
MESOPLUME	ER&T	Berkley and Bass (1979)
MIDAS	Pickard, Lowe, and Garrick, Inc.	Woodard (1975)
PAVAN	Pacific Northwest Lab.	Bander (1982)
RADOS	DuPont/SRL	Cooper
SWAGA	ER&T Inc.	-
SRDFM	NOAA/ARL	-
STRAM	Battelle PNL	Hales, et al. (1977)
SUBDOSA	Battelle PNL	Strenge, et al. (1976)
UNAMAP Series (CDM,CRSTER,ISC, MPTER,PAL,PTDIS, PTMAX,PTMTP,VALLEY)	EPA	Turner (1979)
TEM	Texas Air Control Board	Christiansen (1976)
XOQDOQ	NRC	Sagendorf and Goll (1977)
3141	Enviroplan, Inc.	Ellis and Liu

Table 2

Gaussian Puff and Plume Segment Models

Model Name	Organization	Reference
ADPLUM	DuPont/SRL	Huang (1980)
ASTRAP	ANL	Shannon (1981)
ATAD	NOAA/ARL	Heffter (1980)
AVACTA	AeroVironment	Chan and Tombach (1978)
AVPPM	AeroVironment	Zannetti (1980)
DRAX2	NOAA/ARL	Draxler (1979)
JEREMIAH	DuPont/SRL	Kern (1977)
MESODIF	NOAA/ARL	Start and Wendell (1974)
MESODIF-II	Battelle PNL	Powell, et al. (1979)
MESOPUFF	ER&T, Inc.	Benkley and Bass (1979)
MESOI	Battelle PNL	Ramsdell and Athey (1981)
PFPL	DuPont/SRL	Garret and Murphy (1981)
PSM	TVA	Lott
RETADD	NOAA/ATDL	Begovich, et al. (1978)
TRAGGY	Meteorological Evaluation Service, Inc.	- Smith
REED	H.E. Cramer Co.	Bjorklund and Dumbauld, (1978)

The division between our last two categories is somewhat arbitrary. The category labelled transport and diffusion models in Table 3 are more complex than those in Table 2, either because they attempt a more continuous solution of the diffusion equation, or because they attempt adjustments to the wind field rather than rely on a straightforward interpolation of the data. Table 4 is reserved for those models which attempt to solve dynamical equations for the wind field. Models in the first three categories, Tables 1-3, are primarily dispersion models, although some type of wind model must be used to drive them, while models in category 4 view the prime task as predicting a wind field with the addition of a dispersion model as almost subsidiary. We have chosen four models in category 3; Patric, Impact, Mathew/Adpic, and a hybrid NOABL/Adpic, for detailed review. The models listed in category 4 are all research models which do not have the status of currently available candidates for selection as real-time dispersion. The potential of some of these models is discussed in Chapter 8.

Bass and Smith (1981) have compiled the results of questionnaires to the developers of a number of the models listed in Tables 1 to 3. The goal of their questionnaire was to provide a short-list of attractive candidate models as potential Class A and Class B models. They conclude that a few of those listed in Table 2 here are the most attractive, partially because they can be used as either a Class A or B model. Two of their preferred models Mesodiff II and the ARL trajectory model are on our list for detailed review. Their third preferred model Mesopuff has been replaced by MESOI a model not included in their questionnaire.

Eleven of the models critically reviewed here, ranging in complexity from the simplistic Gaussian plume models to relatively complex transport and diffusion models, were used to simulate final test results of an experiment carried out at INEL in the summer of 1981. Results are given in a companion report.

Table 3

Transport and Diffusion Models Based on Mass Continuity

Model Name	Organization	Reference
ATMOS	Los Alamos National Laboratory	(None)
BLM/TM	NOAA/NWS	Long, Schaffer and Kemler (1978)
CHAPEAU	Savannah River Laboratory	Pepper and Baker (1979)
IMPACT	Form and Substance Inc.	Fabrick, et al. (1977)
MATHEW/ADPIC	Lawrence Livermore National Laboratory	Sherman (1978) Lange (1978)
MESOGRID	E.R.&T, Inc.	Morris, Berkley and Bass (1979)
PATRIC	Lawrence Livermore National Laboratory	Lange (1978)
PHOENIX	Oak Ridge National Laboratory	Murphy (1979)
PIC	Systems, Science & Software	Sklarew, et al. (1971)
RADM	Dames and Moore	Runchel et al. (1979)
PDM	Systems Applications, Inc.	Liu, et al. (1976)

Table 4

Primitive Equation Models

Model Name	Organization	Reference
UVMM	University of Virginia	McCumber (1978)
Argonne Model	Argonne and Los Alamos	Yamada (1978)
Penn State Model	Penn State and NCAR	Anthes and Warner (1978)
ARAP MODEL	A.R.A.P. Inc.	Lewellen (1981)
UK Meteorological Office Mesoscale Model	UK Meteorological Office	Tapp and White (1976)

CHAPTER 5
GAUSSIAN PLUME MODELS

5.1 General Features of the Models

Gaussian plume models are based on a steady state solution for diffusion in a flowing medium. If a point source releases a substance at a rate, Q, in a medium of constant diffusivity D, flowing at velocity, U, then the concentration χ is given by

$$\chi = \frac{Q}{4\pi Dr} \exp\left[-\frac{u}{2D}(r - x)\right] \tag{5.1}$$

If we limit our considerations to downstream distances where $x >> y,z$, then the approximation $r \approx x$ and

$$r - x \approx x\left(\frac{y^2 + z^2}{2x^2}\right) \tag{5.2}$$

can be used to give

$$\chi = \frac{Q}{2\pi u\sigma^2} \exp\left(-\frac{y^2 + z^2}{2\sigma^2}\right) \tag{5.3}$$

where

$$\sigma = \sqrt{\frac{2Dx}{u}}$$

The distribution is the form of a gaussian distribution with a spread σ, which increases with distance downstream.

In atmospheric transport, the dominant dispersion mechanism is the turbulent fluctuation of the bulk fluid flow; molecular diffusion plays a relatively minor role. The fluid equations can be cast in the form of a diffusion equation with the diffusion "coefficient" given in terms of a correlation between transverse velocity and concentration fluctuations. However, it is not necessary to deal with the diffusion equation in order to use a gaussian model for concentration distributions in atmospheric transport. All that is required to utilize Equation 5.3 as a model for dispersion, is some specification of $\sigma(x)$. This is generally parameterized as a function of the thermal stability of the atmosphere. The most popular parameterization uses the Pasquill-Gifford classifications of stability (Pasquill, 1974). As long as conditions under which the model is to be applied are sufficiently similar to those used to determine the empirical curves of $\sigma(x)$, reasonable results should be assured.

5.2 Variable Sensitivity

The general expression for a Gaussian plume is given by

$$\chi = \frac{Q}{2\pi u \sigma_y \sigma_z} \exp\left(- \frac{(y-y_o)^2}{2\sigma_y^2} - \frac{(z-z_o)^2}{2\sigma_z^2} \right) \tag{5.4}$$

The input parameters to the model then are: u, the mean wind velocity; Q(t), the source strength function; the horizontal, σ_y, and vertical, σ_z, spread and y_o and z_o, the plume centerline coordinates. If we perform an uncertainty analysis on χ, we get

$$\frac{\delta\chi}{\chi} = \frac{\delta Q}{Q} - \frac{\delta u}{u} + \left(\frac{(y-y_o)y_o}{\sigma_y^2} \right) \frac{\delta y_o}{y_o} + \left(\frac{(z-z_o)z_o}{\sigma_z^2} \right) \frac{\delta z_o}{z_o}$$

$$+\left(\frac{(y-y_o)^2}{\sigma_y^2}-1\right)\frac{\delta\sigma_y}{\sigma_y}+\left(\frac{(z-z_o)^2}{\sigma_z^2}-1\right)\frac{\delta\sigma_z}{\sigma_z} \qquad (5.5)$$

Thus we see that a 1% error in u or Q will propagate through to produce a 1% error in χ, but that uncertainties in y_o, z_o σ_y, or σ_z can be amplified or reduced. For thin vertical plumes the dominant uncertainty in surface concentration will be associated with uncertainties in z_o or σ_z, while for narrow plumes the dominant uncertainty is likely to be that associated with uncertainty in wind direction, ϕ. Since $y_o = x \tan \phi = xy$ the multiplier in uncertainty due to an uncertainty in y is proportional to $(x/\sigma_y)^2$ which can easily be of order 10-100.

5.3 Fundamental Limitations

Limits of applicability exist for all models. For the gaussian plume these limitations tend to fall in four categories: those associated with temporal changes in the wind, those associated with extrapolating the σ parameterization beyond its empirical basis, those associated with spatial variations in the wind, and those associated with the statistical nature of a turbulent plume discussed in Chapter 3.

The simplest limit to consider is the maximum range of applicability of the model determined by the persistence of the wind. If the wind is persistent for a length of time, τ, then the distance that a particle travels is given simply by $\ell = u\tau$. The gaussian plume model then can be valid, at most, for

$$\frac{x}{u} < \tau \qquad (5.6)$$

Thus, the distance of applicability scales directly with the wind speed. For example, if there is a 5 m/sec wind with a persistence of 1 hour, then by the end of the hour we would expect the plume to extend to x = 18 km. Of course,

simultaneously, the plume source must persist at a constant strength. The error expected in the average concentration over the period of persistence may be approximated as a function of x, u, and τ as

$$E = \frac{\overline{C}observed - \overline{C}calculated}{\overline{C}observed} \simeq \left(\frac{\tau u}{x} - 1\right)^{-1} \qquad (5.7)$$

provided $x/u\tau < 1$. For greater distances the error is unbounded. This error bound is schematically demonstrated in Figure 4.1. It is readily seen that strong, persistent winds are required to keep this source of error from being large at distances beyond 10 km.

The other three categories of limitations are not as straightforward to quantify. Although many models still use the five stability class parameterization for both the vertical and horizontal spread (σ_z and σ_y) of the plume, it is quite widely recognized (Hanna et.al., 1977) that this is not very appropriate for σ_y, since horizontal wind variance is not as much a function of stability as it is a function of other factors, such as vertical wind shear, mixed layer depth, and mesoscale atmospheric turbulence. Pasquill (1976) has recommended that direct measurements of horizontal wind direction variance be used in estimating σ_y (x). A surprisingly small number of models appear to be designed to take advantage of such direct measurements. The standard stability class parameterization provides a somewhat better measure of vertical spread, but the scheme is designed more as a measure of surface-layer stability and is not reliable for elevated plumes. The standard deviation of the vertical wind angle is a better indicator of vertical mixing but it is sometimes difficult to measure accurately.

Spatial variations in the wind can essentially invalidate the common σ_y predictions. Vertical wind shear can often be the dominant factor in spreading the plume horizontally, since a turning of the wind with respect to altitude of 30° or more often occurs within the boundary layer, particularly under stable conditions. Irwin (1979) has attempted to incorporate vertical wind shear into a general algorithm for σ_y. Considerable uncertainty remains

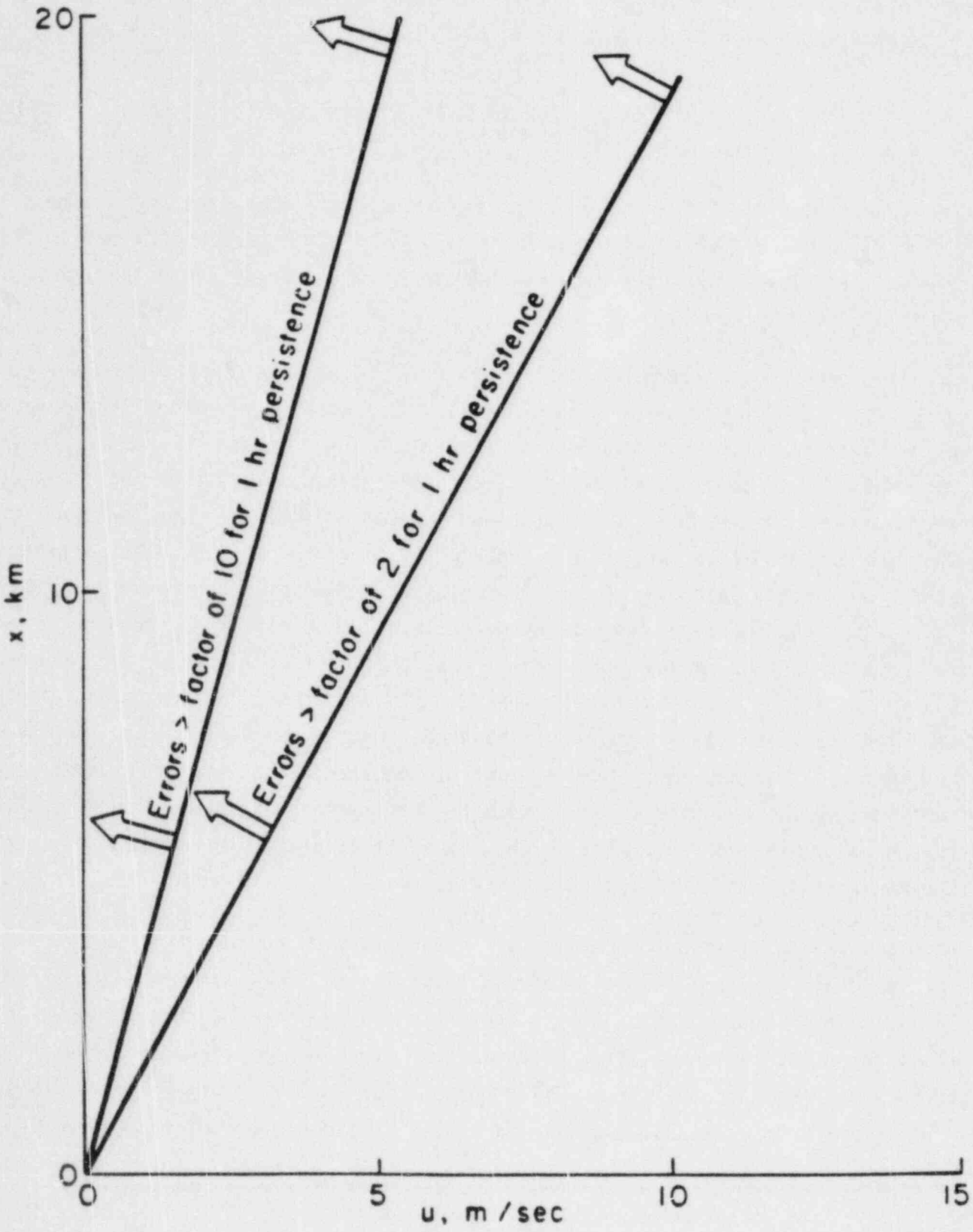

Figure 5.1 - Error Bounds on the Steady State Plume for 1 Hour Persistent Winds as a Function of Distance and Wind Speed.

as to the correct evolution of σ_y at downwind distances greater than 10 km (Gifford, 1983). As discussed in Appendix A the largest uncertainty in dispersion models is likely to be caused by eddies in the size range of 1 to 10 km. These may be responsible for either an uncertainty in position of the transported plume or concentration level of the plume depending upon the sampling time period. In general the empirical foundation on which the σ_y and σ_z algorithms are constructed do not extend to this eddy size.

5.4 Specific Models

We considered two models: TEM and ISC. TEM was designed by the Texas Air Control Board to evaluate ground level, short-term concentrations of atmospheric pollutants. It is a relatively straightforward steady state Gaussian plume model with no adjustments for building effects, terrain adjustments or deposition. ISC was designed for the EPA to evaluate the effect of an industrial source of pollutants on nearby communities. It can handle both short term and long term computations, and it appears that the short term model has received a fair amount of attention. Allowances have been made for deposition, ground reflection, and inversions as a capping layer. The theory for plume rise and building effects is relatively elaborate, probably more complex than is warranted. Both codes have the ability to treat area sources as well as point sources. The latter features may be useful in predicting accidents in which debris is spread over an area.

Both models account for the anisotropic structure of atmospheric turbulence by allowing differing dispersion coefficients in the lateral and vertical directions. The distribution is then given by Eq. 5.4.

Both models allow σ_y and σ_z to vary with distance, x. The functional variation depends upon the local atmospheric stability criterion as given by the Pasquill-Gifford-Turner stability classification. Somewhat different parameterization of these empirical functions are used in the two codes. The standard deviation functions for ISC are given in Tables 5 and 6, while those for TEM are given in Tables 7 and 8.

Table 5

Parameters Used to Calculate σ_y in ISC

Pasquill Stability Category

$\sigma_y = 465.11628\ x(km)\ \tan(TH)$

$TH = 0.017453293\ (c - d \ln[x(km)])$

	c	d
A	24.1670	2.5334
B	18.3300	1.8096
C	12.5000	1.0857
D	8.3330	0.72382
E	6.2500	0.54287
F	4.1667	0.36191

Table 6

Parameters Used To Calculate σ_z in ISC

Pasquill Stability Category	x, (km)	$\sigma_z = ax(km)^b$ a	b
	0.10 - 0.15	158.080	1.05420
	0.16 - 0.20	170.220	1.09320
	0.21 - 0.25	179.520	1.12620
A*	0.26 - 0.30	217.410	1.26440
	0.31 - 0.40	258.890	1.40940
	0.41 - 0.50	346.750	1.72830
	0.51 - 3.11	453.850	2.11660
	> 3.11	**	**
	0.10 - 0.20	90.673	0.93198
B*	0.21 - 0.40	98.483	0.98332
	> 0.40	109.300	1.09710
C*	> 0.10	61.141	0.91465
	0.10 - 0.30	34.459	0.86974
	0.31 - 1.00	32.093	0.81066
D*	1.01 - 3.00	32.093	0.64404
	3.01 - 10.00	33.504	0.60486
	10.01 - 30.00	44.053	0.51179

*If the calculated value of σ_z exceeds 5000 m, σ_z is set to 5000 m.

**σ_z is equal to 5000 m.

Table 6

Parameters Used To Calculate σ_z in ISC

Continued

Pasquill Stability Category	x, (km)	$\sigma_z = ax(km)^b$ a	b
	0.10 - 0.30	23.331	0.81956
	0.31 - 1.00	21.628	0.75660
	1.01 - 2.00	21.628	0.63077
E	2.01 - 4.00	22.534	0.57154
	4.01 - 10.00	24.703	0.50527
	10.01 - 20.00	26.970	0.46713
	20.01 - 40.00	35.420	0.37615
	> 40.00	47.618	0.29592
	0.10 - 0.20	15.209	0.81558
	0.21 - 0.70	14.457	0.78407
	0.71 - 1.00	13.953	0.68465
	1.01 - 2.00	13.953	0.63227
F	2.01 - 3.00	14.823	0.54503
	3.01 - 7.00	16.187	0.46490
	7.01 - 15.00	17.836	0.41507
	15.01 - 30.00	22.651	0.32681
	30.01 - 60.00	27.074	0.27436
	> 60.00	34.219	0.21716

Table 7

Parameters used to compute σ_z in TEM

$$\sigma_z = ax^b$$

Atmospheric Stability Class	Downwind Distance, meters $100 < x \leq 500$		Downwind Distance, meters $500 < x \leq 5000$		Downwind Distance, meters $5000 < x$	
	a	b	a	b	a	b
A1	0.383	1.281	.0002539	2.089	.0002539	2.089
B2	.1393	.9467	.04936	1.114	.04936	1.114
C3	.1120	.9100	.1014	.926	.1154	.9109
DD4	.0856	.8650	.2591	.6869	.7368	.5642
DN5	.0818	.8155	.2527	.6341	1.297	.4421
E6	.1094	.7657	.2452	.6358	.9204	.4805
F7	.05645	.8050	.1930	.6072	1.505	.3662

Table 8

Parameters used to Compute σ_y in TEM

$$\sigma_y = cx^d$$

Atmospheric Stability Class	Downwind Distance, meters $x < 10{,}000$		Downwind Distance, meters $x \geq 10{,}000$	
	c	d	c	d
A1	.495	.873	.606	.851
B2	.310	.897	.523	.840
C3	.197	.908	.285	.867
DD4	.122	.916	.193	.865
DN5	.122	.916	.193	.865
E6	.0934	.912	.141	.868
F7	.0625	.911	.0800	.884

TEM includes an adjustment to σ_y for differing averaging times. The values given in Table 8 are assumed to be valid for 10 minute averaging times as indicated by Turner (1970). For longer time averaging periods, σ_y values are increased in an attempt to represent the plume meander due to fluctuations in wind direction. The adjustment is computed as

$$\sigma_{y_{total}} = \sigma_{y_o} \left(\frac{t}{10 \text{ min}} \right)^R$$

where R is given in Table 9.

Table 9

Stability Category	R
A	0.675
B	0.55
C	0.425
D	0.3
E	0.175
F	0.175

Both models account for reflections at the ground and the mixing layer height, H_m. If $\sigma_z/H_m \geq 1.6$, ISC assumes the material to be uniformly distributed within the mixing layer, while TEM pegs the distance at which the vertical distribution becomes uniform at twice the distance where $\sigma_z/H_m = 0.47$. If the effective stack height exceeds the mixing layer height, at least part of the plume remains elevated, and the ground level concentration is appropriately reduced. When the mixing height elevates above the stack height, it is unclear from the documentation whether all of the material is deposited in the mixing layer, or just that fraction of the plume below the mixing layer.

ISC includes some parameterization for dry and wet deposition. Dry deposition rates are based upon surface concentrations, while wet deposition rates depend on local centerline values. As material is depleted from the plume, the concentration of the overall plume is reduced in either case. In other words, the loss of material at the boundary is instantaneously felt throughout the plume. This is not appropriate for dry deposition where the material is deposited from the layer closest to the ground. This reduces the driving potential for deposition, and so the program will tend to over predict deposition rates. In practical situations this inaccuracy is probably masked by the uncertainties in the deposition parameterization. Deposition is analyzed in a separate companion report.

The effects of building interference on the plume are accounted for in the ISC model by increasing the initial plume dispersion. The building wake is assumed to contain a uniform dispersion of plume material, and so the building dimension is used. The model accounts for the increased initial dispersion by using a virtual distance to the source for computing a lateral and vertical dispersion. The model first computes the plume height and compares it to the building heights. If the plume height is greater than 2.5 building height, the building effects are neglected. The model uses the lesser of the two building dimensions, h, (height or width) and corrects the variance as follows:

$$\sigma_z' = \begin{cases} .7\ h(m) + .067[x(m) - 3h(m)] & 3h < x < 10h \\ \\ \sigma_z\ (x + x_z) & x \geq 10h \end{cases} \qquad (5.8)$$

$$\sigma_z' = \begin{cases} .35\ h(m) + .067[x(m) - 3h(m)] & 3h < x < 10h \\ \\ \sigma_y\ (x + x_y) & x \geq 10h \end{cases} \qquad (5.9)$$

where the vertical distances are given by

$$x_z = \left(\frac{1.2h}{a}\right)^{1/b} - .01h \qquad (5.10)$$

$$x_y = \left(\frac{.85h}{p}\right)^{1/q} - .01h \qquad (5.11)$$

and the coefficients a, b, p, and q are given as a function of atmospheric stability (Bowers, Bjorkland, and Chaney, 1979).

For very tall or very squat buildings, these equations are modified to attempt to account for building shape factor. As the data base from which the expressions are derived is sparse, it is questionable whether the complexity of the expressions is justified. The authors state for a building that is 5 times as long as it is wide, the error can be -40% for winds parallel to the long side, versus +60% for wind parallel to that side for the plume height within a distance of 1.2 building dimensions.

Since in both cases the concentration at the receptor location is inversely proportional to the wind velocity, both models attempt to account for the wind gradient through the atmospheric boundary layer and the initial plume rise. In both models, a power law is assumed of the form

$$\frac{u}{u_o} = \left(\frac{z}{z_o}\right)^{\beta} \qquad (5.12)$$

where u_o is the velocity measured at z_o, and β is assigned a value for each stability condition according to Table 10.

Table 10

Wind Profile Exponents in ISC

Stability Category	β
A	0.1
B	0.15
C	0.20
D	0.25
E	0.30
F	0.30

Both models use plume height computations that trace back to Briggs' (1975) model to compute plume rise, and both models treat the plume as a stabilized layer once it reaches its final height. Terrain effects are ignored in TEM, while a crude attempt is made to include some influence in ISC by taking the height of the plume above ground as

$$h = h_s + \Delta h - h_t \tag{5.13}$$

where

h = effective plume height

h_s = stack height

Δh = plume rise

h_t = local terrain elevation above elevation at base of stack

This can lead to some very unphysical results. For example, in ISC, if the receptor is higher than the effective height, the program produces an error and halts. Conversely, if the terrain is lower than the base of the stack, the program sets it to the elevation of the stack base. This severely limits the program's utility in hilly terrain.

The methods for computing plume rise are similar in both models. The momentum flux from the stack is compared to buoyant terms to determine which mechanism dominates. Both models for plume rise involve power law formulations which account for local atmospheric stability. Plume rise varies with distance downstream until a certain maximum allowed rise has been reached. The physical basis of these models derives from arguments by Briggs based on integral properties of the plume at any cross-section. The properties at a given cross-section depend upon an "entrainment" rate. This rate and other constants are adjusted to achieve a good fit between the prediction of Briggs' plume rise model and experimental observations. The authors of the ISC model note the paucity of data for verification of the

nonbuoyant case.

Both models allow a correction for stack tip downwash when the stack velocity is less than 1.5 times wind velocity. A factor of Δh_{ST} is subtracted from the effective plume height where

$$\Delta h_{ST} = a\left(1.5 - \frac{U_s}{U}\right) \tag{5.14}$$

where for ISC a = 2D and for TEM, a = 3D.

Both models have provisions for an exponential decay of the pollutant material.

The most important difference between the two models appears to be the adjustment in σ_y made for increased meander for averaging times greater than 10 minutes. In our comparisons between models and the INEL dispersion data, we have also included a Gaussian plume model with σ_y determined from direct measurements of σ_θ as recommended by Pasquill (1976). For this GP model σ_y is computed from

$$\sigma_y = \sigma_\theta x/(1+0.003x/\bar{u})^{1/2} \tag{5.15}$$

with x in meters and $\bar{u}$ in m/sec. Irwin (1983) has shown that this type scheme agrees with a number of experiments much better than the standard Pasquill-Gifford scheme.

5.5 Validation Studies for Gaussian Plume Models

Neither of the volumes of documentation for TEM or ISC discussed model validation or the levels of uncertainty associated with the model. However, a number of accuracy estimates have been made for various Gaussian plume models in the literature. It appears the more recent the verification study, the

more modest the accuracy claims.

An AMS position paper (AMS,1978) projected that a factor of 2 accuracy could be expected for these models when compared to measurements in "ideal" situations with steady homogeneous winds. For an elevated stack, the position paper projected an accuracy of 20-40% for the ground level downwind maximum predictions. The study did note, however, a number of situations that would classify the local meteorology as exceptional and hence raise the expected uncertainty in the model predictions. These factors included downwash, buoyant flow, surface conditions different from the surfaces used to collect the baseline data, extremely stable or unstable conditions, and large downwind distances. This qualification probably includes 15% of all cases of practical interest and seriously restricts the utility of the panel's findings.

An independent study (Londergan et al. (1980)) was performed for the American Petroleum Institute to evaluate plume models for Short Term Air Quality. Although ISC was not included, CRSTER was tested. CRSTER is a single source version of ISC with a large number of common subroutines. The study examined predictions for 5 models for 17 tracer release experiments. The experiments were conducted in widely varying terrain, from flat rural to urban or hilly. The study examined the data using statistical tests and concluded that "the standard EPA dispersion models are not reliable within a factor of 2 for predicting concentrations for characteristic dispersion conditions at most locations", and "...systematic departures from observed dispersion behavior were found even for flat, rural conditions." The data were mostly from ground releases, and so conclusions for releases from elevated stacks could not be made. In the study, no attempt was made to say to what factor the models could be used (10 or 100) or to try to explain the "systematic" nature of the error. No pattern shift tests were run to ascertain the contribution to wind shift in the uncertainty. The study did conclude that the agreement between models was much better than the agreement between the models and the data. Furthermore, the API study pointed out that discrepancies between the model predictions and the measured data for these relatively straightforward cases amounted to more than a factor of 5 at the

majority of monitoring stations.

A recent study (Weber and Buckner, 1982) has compared sixteen dispersion models, including several Gaussian plume models, and found that the models agreed with each other substantially better than they agreed with the data. The data base was the Kr 85 released from the Savannah River Plant (SRP) over a year. The study found a relatively high correlation for model predictions averaged over long time periods (yearly or monthly). However, when the models were used weekly or twice daily, the correlation becomes very weak, indicating the model's inability to predict a specific situation. While the high correlation for long time periods may give comfort to planners for air pollution impact studies, it does not provide reassurance to emergency planners who must know the resulting dispersion pattern for a specific event.

Another recent study of CRSTER performed for EPA (Mills, et al. 1981) used SO_2 data collected at several points in the Ohio river valley to evaluate the relative performance of two different algorithms for determining σ_y and σ_z. One was the standard P-G-T relationships, while the other was an algorithm attributed to Irwin designed to correct for some known deficiencies of the P-G-T method. In particular it attempted to incorporate other influences such as wind shear, plume buoyancy, surface roughness, and mixed layer height to modify the dependence of σ_y and σ_z on stability. The study concluded that both versions of the model demonstrated a good correlation between annual highest predicted and observed concentrations for 3 hour and 24 hour averaging times. In fact, these maximum concentrations were predicted within a factor of 2. However, both models also demonstrated poor ability to reliably reproduce observed concentrations for specific events. When the models did predict the correct highest concentration, it did not occur at the observed time and place. Often it was not even associated with the same type of meteorological conditions. From their results, we conclude that this model is much less satisfactory for the current application of emergency planning during a specific event than it is for the EPA application for which it was designed; that is, predicting the frequency with which regulatory standards will be exceeded.

An extensive air pollution data set currently available is the St. Louis RAPS data set. Two studies using this data are of particular interest to the evaluation of Gaussian plume models. Ruff et al. (1980) have used this set to evaluate the EPA RAM model. They conclude that RAM performs fairly well when comparing the frequency distribution of observed concentrations with the frequency distribution of predicted concentrations, but performs poorly on a case-by-case basis when comparing observations and predictions at the same place and same time. The correlation coefficient for hourly concentrations was typically below 0.25.

Hanna (1982) has made an interesting study of how much of the variability in the 1976 RAPS data set are outside the range of predictability by a simple Gaussian model which depends only on wind speed, wind direction, stability, and source emissions. He termed this the natural variability of the observed hourly concentrations. His conclusion was that a perfect model of this type cannot hope to produce results that are better than within a factor of two because of the observed factor of two "natural" variability. We believe this is a very optimistic interpretation of his results. The same analysis could be used to argue that such a "perfect" model based only on these variables cannot make any statistically meaningful prediction of the hourly concentrations.

Hanna's analysis rests on taking the data restricted to a wind direction between 180° and 200° and dividing it into 70 classes depending upon 10 wind speed classes and 7 stability classes. About 30% of these joint classes contain 10 or more hours of hourly data. Since this number is judged to be adequate for a statistical analysis, the mean and standard deviation of $\ln(C/Q)$, the log of the concentration normalized by the source emissions, are calculated for each of these joint classes which contain more than 10 data points. When these standard deviations were averaged over wind speed, stability and monitoring station, the SO_2 samples yielded an average standard deviation of $\sigma[\ln C/Q] = 0.96$. This means that on average, 68% of the data in any individual class are within a factor of 2.61 of the median value within that class. Since the Gaussian model considered here cannot discriminate any

finer than to place any desired hourly prediction within one of the classes, this intra-class variation establishes a limit on the predictability which Hanna terms natural variability. A factor of two as the natural variability does not impose much added restriction on plume predictability since few people would expect Gaussian models to exceed a factor of 2 accuracy in any case.

The data can be used to paint a considerably different picture by recognizing that the sample cumulative distributions of hourly SO_2 concentration observations given for stations 1, 3 and 5 for the total year 1976 imply $\sigma(\ln C)$ is approximately 1. Specifically, the distributions shown indicate a ratio of approximately 20 to 50 between the median SO_2 concentration and the 99.9 percentile concentration. Assuming a log normal distribution, which Hanna argues provides a reasonable fit to the data, this distribution spread yields a $\sigma(\ln C)$ of 0.97 to 1.27, only marginally larger than the intra-class variability. Thus the total spread in the data only appears to be marginally larger than the intra-class variability. It is not apparent that this difference has any statistical significance. At least 4 factors act to reduce further even this small difference. Hanna quotes a value of source emission variability $\sigma_q/Q = 0.17$, which can contribute to the total variance but should not contribute to the normalized intra-class variance. Second, and probably more important, Hanna's value of $\overline{\sigma(\ln C/Q)} = 0.96$ is obtained by averaging the standard deviation rather than more appropriately averaging the variance, σ^2, over all the sub classes. Since $(\overline{\sigma^2}) > (\overline{\sigma})^2$, his average underestimates the true average variability to some degree. Third, we have no way of knowing how representative the total distribution shown for stations 1, 3 and 5 are of the remaining 22 stations. The average total variance may be more or less than that represented by the 3 plots presented. Finally, it is noted that even a sample size as large as 20 permits the computed standard deviation of the sample to underestimate the true standard deviation of the population by as much as 28% at the 90% confidence level according to the chi-squared test. These factors all combine to suggest that there is no firm evidence of a significant difference between the total variance and the intra-class variance. From this, it is possible to

argue that all of the variability observed in the RAPS SO_2 hourly concentration samples is "natural" variation, with the assumed model able to account for very little of the observed variations.

Ruff et. al.'s (1980) conclusion regarding RAM tends to support this latter argument. A correlation coefficient of less than 0.25 means that less than 6% of the variance in the observations is accounted for by the RAM model prediction. Of course, it is possible that the problem lies with the RAM model. However, our interpretation of Hanna's results is that even a "perfect" Gaussian, steady state model would not perform significantly better. Expressed in a slightly different way, the fact that 68% of the intra-class data are within a factor of 2.61 of their median value does not leave the model providing much predictive capability when it is realized that 68% of the total data appear to be within a factor of approximately 3 of the median value. Rather than concluding that a perfect Gaussian model is only limited to predicting the hourly concentration to within approximately a factor of 2, we make essentially the opposite conclusion, that a Gaussian model based only on wind speed, wind direction, stability, and source emissions has little or no predictive capability for hourly concentrations on the regional scale of the RAPS data.

EPRI is currently conducting an intensive plume model validation program (Hilst, 1978). A network of 200 ground-level tracer samples, 30 air quality samplers, 2 aircraft, 3 remote plume sensing devices, and a full complement of upper air and surface meteorological sensors are being used to acquire data on plume behavior downwind of isolated power plants. Results from the most homogeneous site located in the plains of central Illinois lead to the conclusion that the gaussian plume models tested "showed no skill in predicting hour-by-hour concentrations at fixed receptors and exhibited only minimum skill in predicting the position and pattern of the plume foot-print." (Bowne et al. 1981,1983). Some of the models did predict a value within 25 to 50% of the observed maximum of the ensemble of all concentrations; i.e. the highest observed concentration versus the highest predicted concentration not paired in time or space, but as demonstrated in figure 4.2 there is very

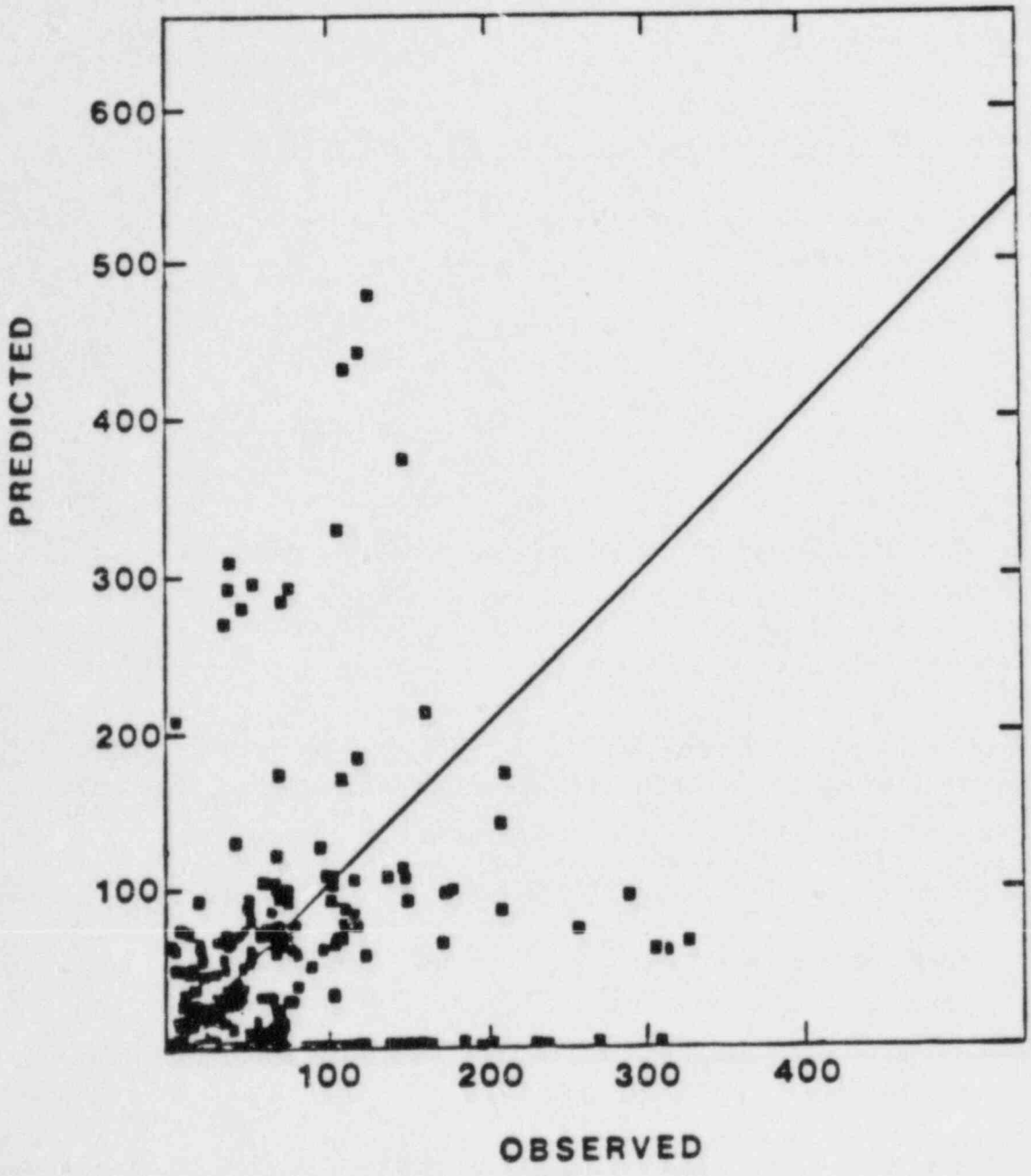

Figure 5.2 - Comparison of highest observed and predicted χ/Q values for 1-hour SF_6 concentration averages, CEQM Ib.

little correlation when the predictions and observations were paired in time.

In summary, recent evaluation tests have not shown the standard gaussian plume models in as favorable a light as did the earlier studies. Their most noteable success has been in predicting maximum 1-hour, ground-level concentration when specific time and location are not considered. It remains to be seen how well they will perform with regard to the pattern test described in Chapter 2.

5.6 Advantages and Disadvantages of Gaussian Plume Models

The advantages and disadvantages of the gaussian plume models are summarized as follows:

ADVANTAGES

1. Can be programmed on small local computers for very fast execution times.

2. Can be used to run a number of possible scenarios to assist in future planning immediately after an event.

3. Minimum amount of meterological data required.

4. Has demonstrated ability to predict maximum hourly concentration over an extended time when time and space variation are ignored.

DISADVANTAGES

1. Existing evaluation tests have demonstrated that these models have very little capability for predicting hourly observations at a specific time and location beyond the immediate vicinity of the release.

2. Unable to track changing meteorological conditions, such as those

leading to fumigation effects.

3. Cannot treat spatial inhomogeneities such as those due to vertical wind shear or terrain specific features.

4. As presently formulated, requires a completely empirical specification of σ's as a function of stability and distance travelled.

5. Does not include any estimate of the expected variance from the predicted value of the expected mean concentration.

CHAPTER 6
GAUSSIAN PUFF MODEL

6.1 General Features

Gaussian puff models are based upon a transient solution to diffusion in a medium with constant diffusivity. If a mass Q of material is released instantaneously at the origin at t = 0, then the solution to the diffusion equation is given by

$$\chi = \frac{Q}{(2\pi)^{3/2}\sigma_x\sigma_y\sigma_z} \exp\left(-\frac{x-ut}{2\sigma_x^2} - \frac{y^2}{2\sigma_y^2} - \frac{z^2}{2\sigma_z^2}\right) \qquad (6.1)$$

where $\sigma_x = \sigma_y = \sigma_z = \sqrt{2Dt}$ when D is equal to a constant.

Since the diffusion equation is linear, the solution to an arbitrary source function can be constructed by superposition. The concentration field at a time t and position x,y,z is given by integrating over the contribution from all earlier emissions that have moved into the domain of interest. The gaussian puff models use this property to predict concentrations from temporally and spatially varying sources. As the predictions are based on numerical modeling, summations of the contributions of a finite number of "puffs" replace the integrals. In principal, it is straightforward to track the movement of any individual puff in a wind field which varies in space and time.

The evaluation of puff models can be divided into considerations of: (a) the number of individual puffs required to resolve a complete plume to a given accuracy; (b) the accuracy with which the center of an individual puff may be tracked; and (c) the accuracy of the algorithms for determining the spread of the individual puffs.

The three specific models considered herein are the mesoscale transport and diffusion model written by Roland Draxler at NOAA's Air Resource Laboratory, MESODIF written by Wendell and Start at INEL and MESOI written by

the Pacific Northwest Laboratory. Even though the models are based upon the same scientific concept, the implementations differ substantially. We also introduce two new models, MESOJ and MESOT as diagnostic models to see how much performance may be improved by correcting certain deficiencies.

6.2 Compatible Wind Field Models

The wind field predictions use data from surface weather stations and rawinsonde readings to compute wind velocity. The resulting velocity fields are two-dimensional and represent the velocity at the level of the center of mass of the puff. This horizontal wind field is used to compute the Lagrangian trajectory of the center of mass of the puff.

The primary advantage of puff models over the plume models considered in the previous chapter is their ability to account for some wind variability in space and time. In order to realize this advantage, it is necessary to provide the puff model with a wind field which provides an approximately valid space and time variation. Counterbalancing this is the fact that the puff cannot account for any wind variations which are on a smaller scale than the size of the puff. Thus, it is most efficient to match a compatible description of the wind field with a given puff model. In general, these models require the following variables specified as a function of x, y, and t: (a) horizontal wind components u,v; (b) mixing layer depth; and (c) Pasquill-Gifford-Turner (PGT) stability class.

The wind model in the ARL transport and diffusion model uses the surface and upper air wind data. The upper air data, are used to compute the average velocity field of the mixing layer, and the surface wind data are used as hourly correction factors. The wind data at each upper air data station are averaged to obtain a average wind speed and direction in the transport layer. The extent and location of the transport layer is determined by the dispersion of the tracer species. It is the intent of the averaging to produce winds that reflect the average value of the portion of the atmosphere that contains the pollutant. This average is not weighted by the mass. The stations within

a radius r of the segment start point are then averaged with a $1/d^2$ weighting factor, where d is the distance from the upper air station to the halfway point on a trajectory segment that started at the start point and has the same direction and velocity as the upper air station. The data is also weighted by the factor $1 - 1/2|\sin\phi_j|$ to give a station aligned with the local wind the heaviest weighting where ϕ_j is the angle between the wind vector and the line connecting the data station and segment origin.

The local surface winds are used to correct the winds interpolated from the upper air stations in the following manner. The spatially averaged transport layer wind data is ratioed to the spatially averaged surface wind data from the upper air stations. These ratios give directional and speed changes between surface and transport layer data as computed from the upper air data. A local surface wind direction and speed is computed by spatially averaging the hourly surface data. This wind speed and direction are then adjusted by the ratios computed to give a corrected transport layer wind speed and direction. The intent of this type of averaging is to provide a better interpolation between upper air data which are taken every 12 hours.

The ARL wind field is computed for each point on the trajectory instead of for a grid. This results in fewer computations, and hence, a more efficient code. The wind model makes no attempt to account for terrain effects such as channeling or thermally induced upslope/downslope winds.

MESOI is a descendent of Mesodif, developed by Start and Wendell, (1974). Both are designed for use with a network of wind towers such as that in existence at INEL. The model is currently programmed to accomodate winds from up to 30 surface locations. The winds, defined on a 16x16 grid that covers the spatial domain of the model, are estimated by interpolation using weighted averages of the winds at the three closest instrument locations. The weight given to each wind included in the average is proportional to the inverse of the square of the distance between the grid point and the instrument location. Wind fields are computed for hourly intervals and two fields are retained in MESOI at all times. The wind at the center of mass of each puff is determined by inverse square spatial interpolation between the grid point and linear

interpolation in time between the two wind fields. The advection wind is the vector average of the wind at the center of mass of a puff at the beginning of an advection step, and the wind at the projected position of the center of mass at the end of the step. Once an advection wind has been determined for a puff, it is assumed to persist until the next puff is released. Thus the puff release rate also controls the variability permitted in the wind advection. The total number of puffs being considered at any one time is limited to 200.

Both MESODIF and MESOI are assumed to be released at ground level, and to remain at this level with no surface deposition. No provision for plume rise is incorporated. Although the puff is assumed to be at ground level for purposes of computing the surface concentration it is advected with the winds obtained from the 10 meter towers. This relationship is held regardless of the spread of σ_z or the evidence of vertical wind shear in the relevant sounding.

6.3 Puff Diffusion Models

All three models emphasize ground level concentrations and consider the rates of horizontal and vertical diffusion separately. If we consider the expression for the puff with separate terms for horizontal and vertical dispersion, Eq. 6.1 can be rewritten as

$$\chi = \frac{Q}{2\pi\sigma_H^2} \exp\left(-\frac{r_A^2}{2\sigma_H^2}\right) g(z) \qquad (6.2)$$

where r_A is the distance between the projection of the center of mass on the ground and the receptor location (i.e., $r_A^2 = x^2 + y^2$) and $g(z)$ is a function that contains the z variation. Written this way, $g(z)$ can be constructed to represent the effects of multiple reflection from the ground and the top of the mixing layer.

The ARL model puts much more emphasis on evaluating vertical diffusion than on horizontal diffusion. It uses a constant growth rate for $\sigma_h, \sigma_h(0.5m/sec)t$, while using a finite difference treatment of the vertical diffusion. At any point on the ground, the concentration is given by

$$\chi = \frac{c_b Q}{2\pi\sigma_h^2} \exp - \frac{r_A^2}{2\sigma_H^2} \tag{6.3}$$

where c_b is a normalized concentration in the lowest vertical slab. This model truncates the puff at $4\sigma_h$. The finite difference vertical model is based on a one-dimensional diffusion assumption which allows a variation in diffusion coefficients with altitude and conditions. The net flux of material into a layer is given by

$$F_i = K_z \rho \frac{\partial \chi}{\partial z}\Big|_i^{TOP} - K_z \rho \frac{d\chi}{\partial z}\Big|_i^{BOTTOM} \tag{6.4}$$

and the time rate of change in the box is given by

$$\frac{\partial \chi}{\partial t} = \frac{F_i}{\rho_i \Delta z_i} \tag{6.5}$$

The diffusion coefficients K_z are computed by using constant values for z > 100 m as indicated in Table 11 from an analysis by Draxler (1979).

Table 11

Vertical Diffusivity

Stability Class	A	B	C	D	E	F	h
Vertical Diffusivity (m^2/sec)	161	101	67	1.5	5	1.5	.13
α	1.44	1.30	1.26	.920	.695	.491	.244

For $z < 100$ m, the values are scaled with a power law in z to the value at 100 m, so that

$$K_z = K_{z=100} \, (z/100)^{a} \tag{6.6}$$

The horizontal and vertical diffusion parameters for MESODIF and MESOI are both determined from the same empirical functions of distance and atmospheric stability. The vertical parameter is also a function of the atmospheric mixing layer. The growth of the vertical diffusion parameter is governed by the following relationships:

$$\sigma_z = \begin{cases} AX^{Y} & \sigma_z/\text{LDEPTH} < 0.465 \\ 0.465 + 0.335 \dfrac{X - X_L}{X_L} \text{LDEPTH} & 0.465 \leq \sigma_z/\text{LDEPTH} < 0.800 \\ 0.8*\text{LDEPTH} & \sigma_z/\text{LDEPTH} \geq 0.80 \end{cases} \tag{6.7}$$

where X is the distance from the source, A and Y are constants that depend upon atmospheric stability, LDEPTH is the thickness of the atmospheric mixing layer, and X_L, a function of stability, is the distance at which σ_z reaches 0.465*LDEPTH, i.e.,

$$X_L = (0.465 \text{ LDEPTH}/A)^{1/Y} \tag{6.8}$$

The relationship between σ_z and X in Equation (6.7) is an approximation to curves originally developed by Markee (Yanskey, Markee and Richter, 1966). Markee's curves are significantly different than the σ_z curves developed by Hilsmeier and Gifford (1962) which are presented in Appendix A of Meteorology and Atomic Energy - 1968 (Slade, 1968) and in NRC Regulatory Guide 1.145. The primary differences occur in extremely unstable or stable atmospheric conditions. In unstable atmospheric conditions at distances greater than 1 km, the growth of σ_z predicted by Markee's curve is

much less rapid than the growth predicted by the Hilsmeier and Gifford curves. Equation (6.19) gives even less rapid growth. In stable conditions, Markee's curves again predict slower growth of σ_z.

Figure 6.1 demonstrates the σ_z curves for MESOI and Mesodif. It also shows the modification of the unrestricted growth caused by imposing limits to vertical mixing by assuming thicknesses of 100 and 1000 m.

The relationships used to define the growth of the horizontal diffusion parameter are:

$$\sigma_H = \begin{cases} BX^{0.85} & X \leq 20{,}000 \text{ m} \\ B'X^{0.50} & X \geq 20{,}000 \text{ m} \end{cases} \qquad (6.9)$$

where B and B' are again stability dependent. Curves showing these relationships are given in Figure 6.2. These curves are based upon diffusion data collected at NRTS and Hanford, and are approximations to curves presented by Yanskey, Markee and Richter (1966).

Table 12 gives the values for the constants required for Equations (6.9) and (6.10). The values of A, B and B' presented in the table are dimensional; if distances are given in units other than meters, appropriate corrections must be applied. The units of A are $m^{(1 - Y)}$, those for B are $m^{0.15}$ and those for B' are $m^{0.5}$.

The MESOI diffusion parameter curves were initially meant to be used with stability classes determined using a scheme based on sky cover, wind speed, time-of-day and insolation. The scheme, developed by Markee for use in the desert climate of INEL, is a modification of the original scheme proposed by Pasquill (1961). Markee's scheme is presented in Table 13.

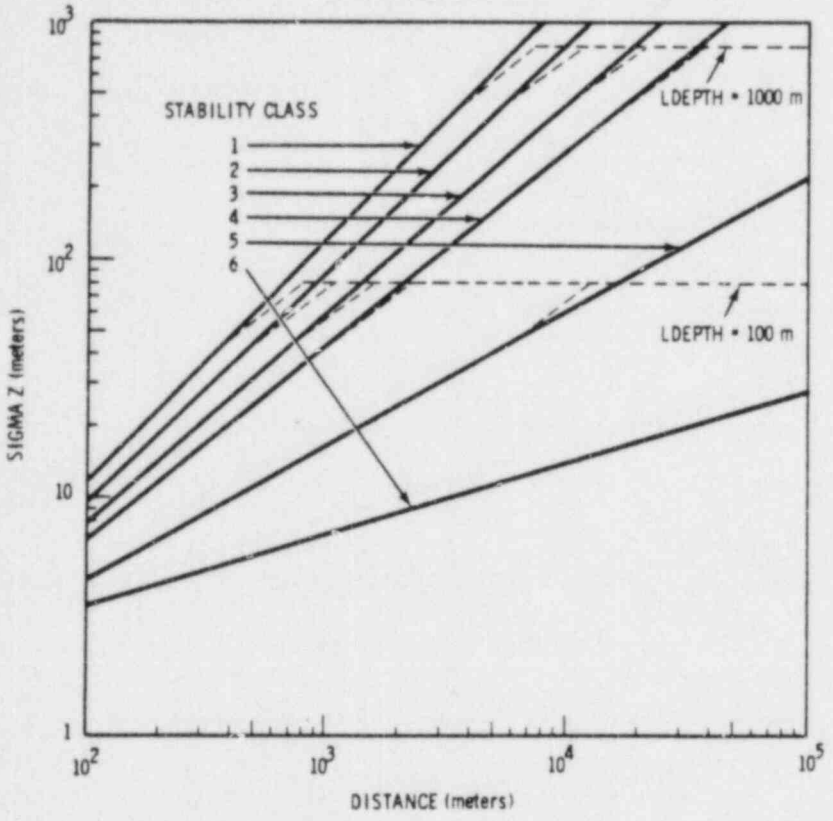

Figure 6.1 Vertical Diffusion Parameter as a Function of Distance and Stability for Mesodif and MESOI.

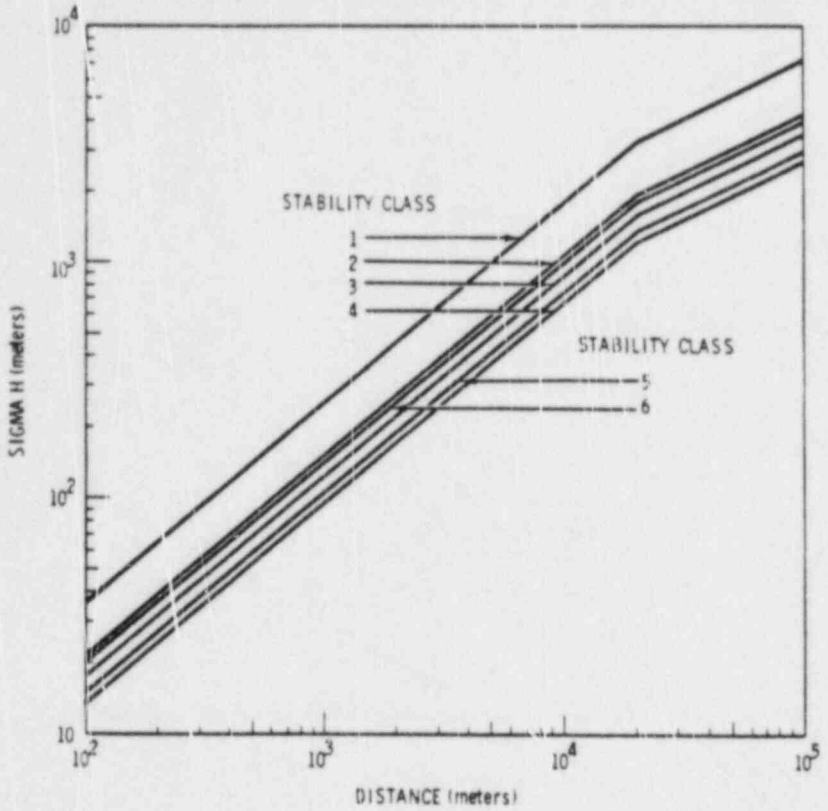

Figure 6.2 Horizontal Diffusion Parameter as a Function of Distance and Stability for Mesodif and MESOI

TABLE 12. Constant Values for Evaluation of Diffusion Parameter Equations

Stability Class	A	γ	B	B'
1	0.100	1.033	0.718	23.0
2	0.105	0.975	0.425	13.6
3	0.128	0.891	0.349	11.2
4	0.146	0.824	0.267	8.55
5	0.331	0.567	0.299	9.57
6	0.812	0.307	0.401	12.8

Time of Day by Season			Windspeed at 8 m (m/sec)	Cloud Cover				
November through January	February through April / August through October	May through July		0 through 5/10	6/10 through 10/10	Heavy Overcast	Insolation	Solar Altitude (degrees)
10 through 12	08 through 11	06 through 09	< 6	B	C	D	Slight	15 through 35
13 through 16	14 through 18	17 through 20	06 through 09	C	C through D	D		
			> 9	D	D	D		
12 through 13	11 through 14	09 through 11	< 6	A	B	C	Moderate	35 through 60
		14 through 17	06 through 09	B	B through C	C		
			09 through 11	C	C	D		
			> 11	D	D	D		
		11 through 14	< 9	A	A through B	B	Strong	> 60
			09 through 11	B	B through C	C		
			> 11	C	C	C		
16 through 10	18 through 08	20 through 06	< 3	G	F	E	None (night)	< 15
			03 through 09	F	E	E		
			09 through 11	E	E	D		
			> 11	D	D	D		

A = Extremely Unstable
B = Moderately Unstable
C = Slightly Unstable
D = Neutral
E = Slightly Stable
F = Moderately Stable
G = Extremely Stable

TABLE 13. Stability Estimates Using Time of Day, Windspeed, and Cloud Cover for INEL (Yansky, Markee, and Richter, 1966).

The use of this scheme at locations other than INEL is open to question. However, it might well be argued that its use at Hanford is reasonable because Hanford diffusion data were used in the development of the scheme. Similarly, the use of other atmospheric stability typing schemes with the curves presented in Figures 6.1 and 6.2 will have an unknown effect on the accuracy of the model. Intercomparisons (e.g. Gifford, 1976; Horst, Doran and Nickola, 1979; Sedefian and Bennett, 1980) do not show a great deal of consistency between schemes. On the average most schemes tend to agree, but in a relatively large number of individual cases there are significant differences among predicted values of diffusion parameters and among concentrations.

Equations (6.8) and (6.10) are appropriate for use in estimating the horizontal and vertical diffusion parameters when the atmospheric stability is constant. When the stability is a function of time, however, the use of these equations results in discontinuities in diffusion parameter magnitudes at the time of the stability changes, and the puffs expand or contract unnaturally. To avoid this problem, the diffusion parameters may be evaluated by numerical integration of derivatives of Equations (6.7) and (6.9). At time increment n following puff release, the diffusion parameters are given by:

$$\sigma(n) = \sum_{i=1}^{n} \left(\frac{d\sigma}{dx}\right)_i \Delta X_i \qquad (6.10)$$

where the index i indicates the time increment, and ΔX_i is the distance moved in the sampling interval corresponding to time increment i. The magnitude of the diffusion parameter in the last sampling interval and the current atmospheric stability are used to define an effective puff travel distance for use in evaluation of the derivative. This approach was used by Start and Wendell in Mesodif for the vertical diffusion parameter; MESOI also extends it to the evaluation of the horizontal spread.

6.4 Validation Studies for Gaussian Puff Models

Puff codes are generally constructed so that the model reduces to the gaussian plume model for steady meteorological conditions. With a high spatial resolution and when the same coefficients for dispersion are used, the accuracy expected should be similar to that discussed for the gaussian plume models in Section 2.6. Under variable wind conditions it should be more accurate, but this advantage has not often been quantified by comparisons with actual data.

The ARL model was developed using experimental data and has undergone several revisions as a result of further comparison with such data. Draxler (1979) compared the model predictions to results of the 1972 INEL experiment near Idaho Falls and the 1972 Savannah river project (SRP)near Aiken, South Carolina. In general, the predictions for the SRP data showed a pattern shift, but very good predictions of absolute levels and pattern. For the INEL experiment, the results at 50 km and 90 km arc were within a factor of two of the measurement data when wind tower data was used in place of rawinsonde data to get the vertical wind profile.

The only validation studies included in the documentation of Mesodif (Start and Wendell, 1974) and MESOI (Ramsdell and Atley, 1981) are comparison with continuous plumes to investigate the sensitivity to puff release rate. The potential advantage of these puff models over plume models has not been demonstrated by statistical tests.

The inherent uncertainties due to the statistical nature of turbulence discussed in Chapter 3 are still relevant for puff models. The greatest difference is that time variations in the wind can now be more readily followed so more of the wind variation may be treated as part of the transport winds, rather than forced to be considered as part of the turbulent diffusion. In practice, the minimum scale of either space or time variations included as part of the transport of the puff is the scale of the puff itself and the resolution of the available meteorological data. Whenever the resolution of the meteorological data is finer than the scale of the puff, errors will be

induced (because the puff algorithms do not include any influence of subgrid variations in the transport winds) but it will not be a statistical error. On the other hand, when the resolution of the meteorological data is coarser than the scale of the puff, there will be a variance in the position of the puff due to the inclusion of all of the wind variations, which must now be considered as part of the turbulence since they cannot be included as part of the resolved wind field. Under such conditions, puff models should be expected to yield uncertainties similar to those deduced from the analysis of Appendix B.

6.5 Introduction of MESOJ, MESOT

In order to aid us in the analysis of how this class of models may be improved, we have introduced two new variations. MESOJ varies only slightly from MESOI in that we have modified MESOI to allow for elevated releases every six minutes. The first modification is important for surface receptors close in during stable release periods of the INEL test series. The second modification is introduced to see if attempting to follow the wind variations closer will improve the results. This should make the results less dependent on the assumptions regarding horizontal diffusivity.

MESOT is introduced to use the tetroon observations directly rather than a wind transport model. The observed tetroon track should provide the best estimates for a model puff track providing the tetroon is at the right height. In this model emissions are divided and lumped at the time of the tetroon releases. Diffusion during the subsequent evolution of the tetroon track is assumed to follow the algorithms given for MESOI.

6.6 Advantages and Disadvantages of Gaussian Puff Models

ADVANTAGES

1. Can be implemented on local minicomputers with reasonable computing requirements.

2. Can track changing wind and stability.

3. Accuracy principally limited only by the resolution of the meterological data and the scale of the tracked puffs.

DISADVANTAGES

1. Requires significant amount of local wind data to represent the wind field sufficiently accurately to realize the potential gain in accuracy over steady plume models.

2. Available models cannot treat the dispersion augmentation due to the wind shear with altitude.

3. As presently formulated, requires a completely empirical specification of σ_s as a function of stability and distance travelled.

4. Does not include any estimate of the expected variance from the predicted value of the expected mean concentration.

CHAPTER 7

TRANSPORT AND DIFFUSION MODELS BASED ON MASS CONTINUITY

7.1 General Features

This class of models combines some objective analysis of available wind data to form a wind field, together with a numerical solution of the diffusion equation to estimate dispersion. The wind field analysis typically provides some means of assuring that the resulting wind field satisfies air mass continuity. The diffusion equation assures continuity of the species of interest. In a previous report (Lewellen, Sykes & Oliver, 1982) we examined two of these models, the MATHEW/ADPIC model and PATRIC, in considerable detail. Results of that study will be used herein without repeating the prior analysis. Also, we consider two additional models of this class.

First we consider the potential advantages or disadvantages of NOABL, a wind field model developed by Science Applications Inc., with respect to MATHEW. The other model considered here is IMPACT, a proprietary model developed by Form and Substance Inc. As noted in Table 3, there are a number of other models which fit in this class. Inclusion of the present four should be adequate to represent the relative potential of this type model for the current application.

7.2 NOABL

7.2.1 Model Description

The coordinate system used in MATHEW is a rectangular Cartesian coordinate system and has difficulties at the boundary for real terrain which must be represented as a collection of rectangular blocks. The principle difference in NOABL is the use of a terrain-following coordinate transformation, which facilitates the specification of the lower boundary condition. In NOABL, as in MATHEW, the wind field is interpolated/extrapolated to produce a three-dimensional gridded field which

is constrained to be divergence free. This condition is met by superimposing a potential flow field on the interpolated field that is irrotational in the horizontal plane. If we let u^o, v^o and w^o be the components of the interpolated field, then a field $\bar{u}$, $\bar{v}$, $\bar{w}$ is added such that

$$\bar{u} = \tau_h \frac{\partial \phi}{\partial x}, \quad \bar{v} = \tau_h \frac{\partial \phi}{\partial y} \tag{7.1}$$

and

$$\bar{w} = \tau_v \frac{\partial \phi}{\partial z} \tag{7.2}$$

where τ_h and τ_v are horizontal and vertical transmission coefficients and are adjusted to represent deviations from neutral stability. Thus if we define

$$\vec{\omega} = \nabla \times \vec{v} \tag{7.3}$$

we see that

$$\omega_x = (\tau_h - \tau_v) \frac{\partial^2 \phi}{\partial y \partial z}$$

$$\omega_y = -(\tau_h - \tau_v) \frac{\partial^2 \phi}{\partial x \partial z}$$

$$\omega_z = 0 \tag{7.4}$$

Thus the added terms introduce no vorticity in the horizontal plane.

With these definitions, the divergence free condition $\bar{\nabla} \cdot \bar{u} 0$ is written in a transformed coordinate system. The transformation is in the z coordinate and z is replaced by σ, where

$$\sigma = \frac{z_t - z}{z_t - z_s} = \frac{z_t - z}{\pi} \tag{7.5}$$

and z_t is the top of the grid and z_s is the surface elevation. The transformed equation is then

$$\frac{\partial}{\partial x}\left(\pi \frac{\partial \phi}{\partial x} + \sigma (z_s)_x \frac{\partial \phi}{\partial \sigma}\right) + \frac{\partial}{\partial y}\left(\pi \frac{\partial \phi}{\partial y} + \sigma (z_s)_y \frac{\partial \phi}{\partial \sigma}\right)$$

$$+ \frac{\partial}{\partial \sigma}\left(\frac{\tau_v}{\tau_h} + \sigma^2\left[(z_s)_x^2 + (z_s)_y^2\right]\right) \frac{1}{\pi}\frac{\partial \phi}{\partial \sigma} + \sigma\left[(z_s)_x \frac{\partial \sigma}{\partial x}\right.$$

$$\left. + (z_s)_y \frac{\partial \phi}{\partial y}\right]\Bigg) = -\frac{1}{\tau_h}\left(\frac{\partial \pi u^o}{\partial x} + \frac{\partial \pi v^o}{\partial y} + \frac{\partial \pi \tilde{w}^o}{\partial z}\right) \tag{7.6}$$

This equation is solved iteratively for ϕ, subject to the following boundary conditions:

$$\frac{\partial \phi}{\partial \sigma} = 0 \tag{7.7}$$

at the top and lateral boundaries and

$$\frac{\partial \phi}{\partial \sigma} = \frac{-\pi\left(\frac{\pi \tilde{w}^o}{\tau_h} + (z_s)_x \frac{\partial \phi}{\partial x} + (z_s)_y \frac{\partial \phi}{\partial y}\right)}{\frac{\tau_v}{\tau_h} + (z_s)_x^2 + (z_s)_y^2} \tag{7.8}$$

on the lower boundary. In the above,

$$\tilde{w}^o = \frac{\sigma}{\pi}\left((z_s)_x u^o + (z_s)_y v^o\right) - \frac{w^o}{\pi} \tag{7.9}$$

7.2.2 Idealized Flow Tests on NOABL

As noted in our earlier report on MATHEW, the solution to the minimization problem for the adjusted velocities is simply potential flow if a uniform velocity is specified as the interpolated field. This feature can be used to investigate the numerical accuracy of the method used to solve the differential problem.

In the MATHEW tests, the flow past a hemisphere was used as the analytic solution, and numerical results were calculated with different grid resolutions. The principle result for MATHEW was that there were always O(1) errors within one or two grid lengths of the surface, due to the step representation of the topography. The same tests were applied to NOABL, and the results for $\delta x = 0.3a$ are shown alongside the MATHEW result in Figure 7.1; δx is the grid-spacing, and a is the hemisphere radius. The graph shows r.m.s. errors normalized by the mean flow speed as a function of radial distance from the center of the hemisphere. Contrary to our expectation, it appears that NOABL also has large errors close to the surface, and in fact runs with higher resolution did not reduce this error. The reason for the O(1) errors in NOABL is that the coordinate transformation involves the derivative of the surface height, which in the case of the hemisphere has a strong singularity around the base. Thus our test is not appropriate for NOABL. The inability to deal with discontinuous slopes or cliffs is not likely to be a real drawback in the practical case, since the flow in the vicinity of such features will be very locally controlled and will not be described accurately by these simple mass-continuity adjustments. There will be no real loss of accuracy in representing real topography with a smooth function, indeed it is desirable, because sharp features will always depend on the numerical resolution.

A second test for NOABL was devised using a smoothly varying lower boundary. This was achieved by using one of the stream surfaces from the hemisphere flow as the lower boundary. Thus the flow is still the same potential flow, but the lower boundary was taken as the stream surface which was 0.2a above the ground plane far upstream. The results for NOABL and

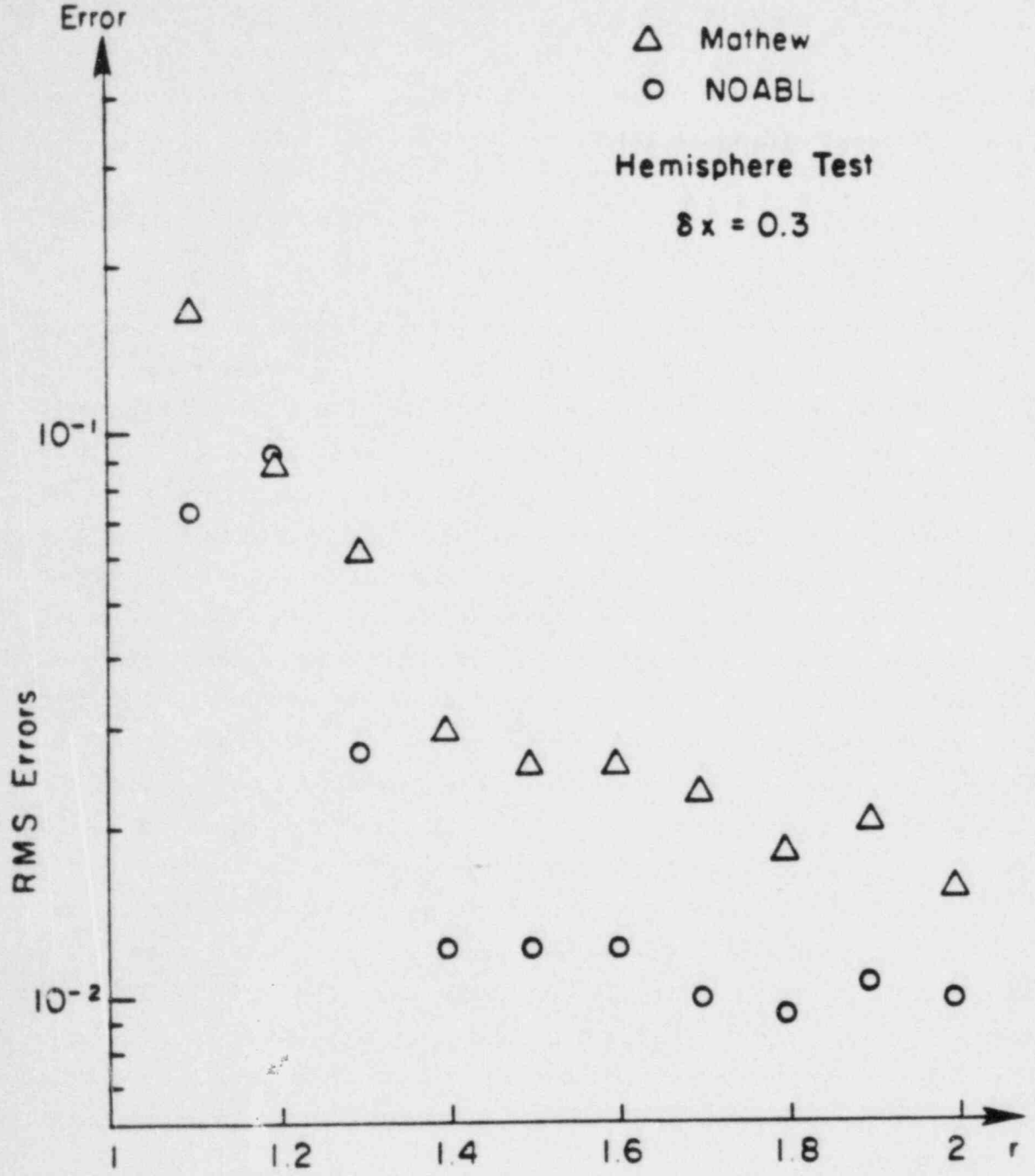

FIGURE 7.1 - Relative Errors Obtained for MATHEW and NOABL for the Ideal Test of Flow about a Hemisphere.

MATHEW with $\delta x = 0.3a$ are shown in Figure 7.2. In this plot, it is clear that NOABL has a distinct advantage over MATHEW, with errors remaining small near the boundary. The NOABL errors can now be made smaller by increasing the resolution since there are no singularities in the problem.

Unfortunately, NOABL does not maintain its clear advantage over MATHEW throughout the whole range of flow situations. Difficulties arise when we consider strongly stratified cases. In both NOABL and MATHEW, the effects of stability are modelled by using different weights on the vertical and horizontal velocity components. As shown in our earlier report (LSO), this procedure is equivalent to solving the unweighted potential problem, but with a stretched vertical coordinate. Thus if the stability parameter is $\alpha \ll 1$, a transform from an object with height H, length L, to an object with height $H\alpha^{-1}$, length L. This effectively forces the flow around the obstacle, and causes no problem for MATHEW. However, the transformation increases the effective slope of the obstacle, and this causes convergence problems for NOABL. There is a "damping factor" in the numerical scheme which the authors of NOABL recommend should be set to a non-zero value for runs with stratification, i.e., α small. This was found to help a little, but even using the damping factor it was not possible to obtain convergence when the effective slope, $H\alpha^{-1}/L$, was greater than about 3.

In summary, NOABL is a terrain-following version of MATHEW which was designed originally for the prediction of wind speed-up effects over topography. It has definite advantages over MATHEW in these cases where the flow goes over the topography; specifically, the errors near the boundary are much reduced, and the coordinate transformation also allows increased resolution near the ground. However, NOABL seems unreliable when computing flows which go around obstacles, because the numerical scheme can diverge if the stability parameter is pushed too far in the direction of no vertical motion.

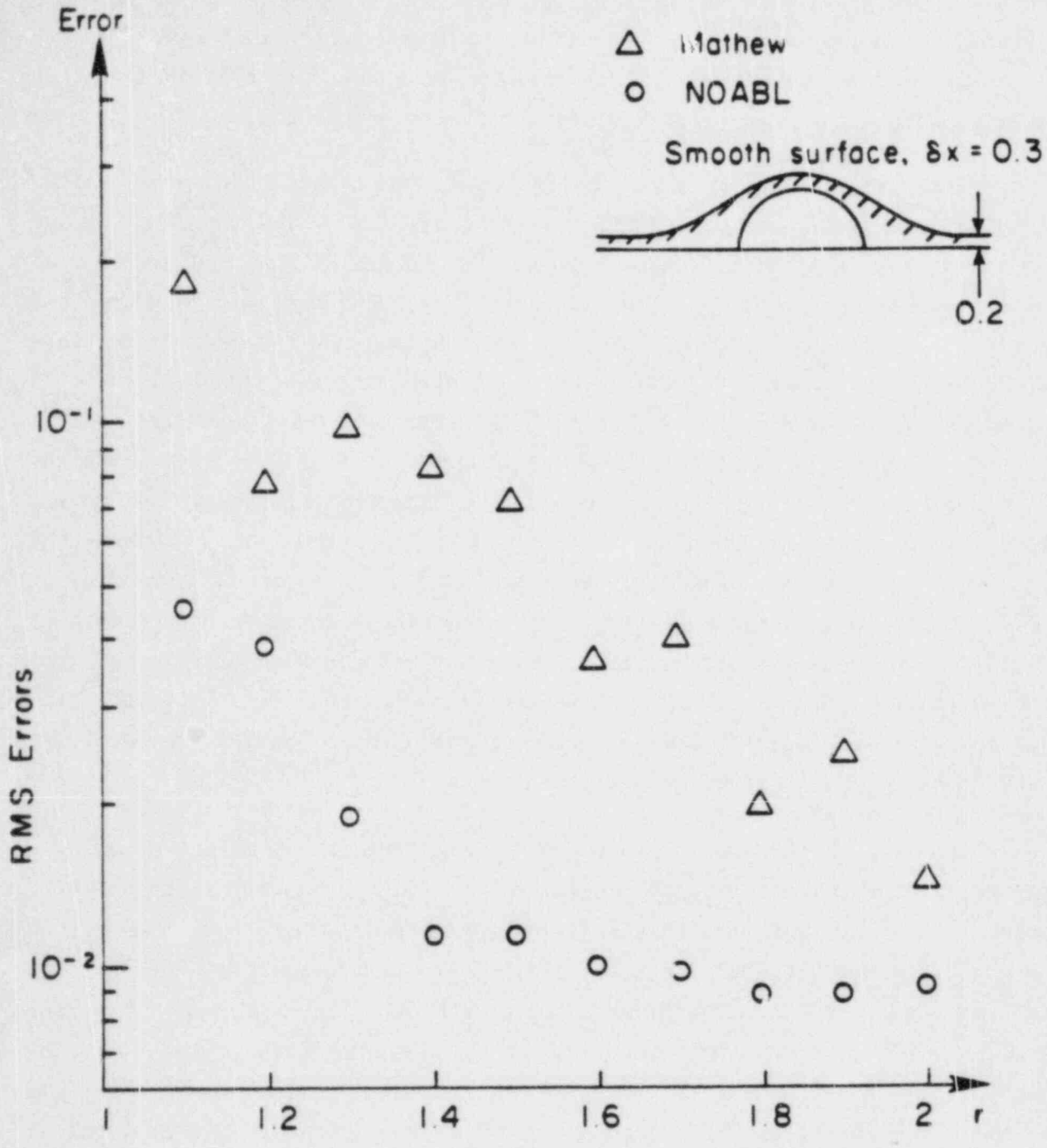

Figure 7.2 - Same as Figure 7.1 Except for the Smooth Surface Sketched.

7.3 IMPACT Description

The IMPACT code has five subprograms to compute: 1) wind field, 2) diffusivity fields, 3) pollution transport, 4) plume rise, and 5) plume chemistry. The wind field prediction has the option of including the effects of thermal drainage winds. Wind fields are calculated using a $1/r^2$ interpolation of existing data to provide the horizontal wind components. Local stability is then used to compute vertical wind components that provide a divergence free field. The stability at each grid point is computed using a $1/r^4$ weighting of stability at the data points. The intent of including stability is to allow the flow over terrain for unstable conditions, and around terrain for stable condition. This feature is implemented through the use of "Transparencies" which vary with stability as shown in Table 14.

Table 14

Stability	A	B	C	D	E	F	G
Horizontal Transparency, T_x, T_y	1.	1.	1.	1.	200.	500.	1000.
Vertical Transparency, T_z	1.6	1.4	1.2	1.0	0.8	0.6	0.4

Terrain cells are assigned zero transparency.

The divergence is minimized by adjusting the velocities by a factor α, so that

$$u_1 \quad u_o + \alpha_u D_o$$

$$v_1 \quad v_o + \alpha_v D_o$$

$$w_1 \quad w_o + \alpha_w D_o$$

where D_o is the divergence computed from first-order backward differencing, and the α's are given by

$$\alpha_u = \frac{\beta T_x}{\frac{\partial T_x}{\partial x} + \frac{\partial T_y}{\partial y}\frac{\Delta x}{\Delta y} + \frac{\partial T_z}{\partial z}\frac{\Delta x}{\Delta z}}$$

$$\alpha_v = \frac{\beta T_y}{\frac{\partial T_x}{\partial x}\frac{\Delta y}{\Delta x} + \frac{\partial T_y}{\partial y} + \frac{\partial T_z}{\partial z}\frac{\Delta y}{\Delta z}}$$

$$\alpha_w = \frac{\beta T_z}{\frac{\partial T_x}{\partial x}\frac{\Delta z}{\Delta x} + \frac{\partial T_y}{\partial y}\frac{\Delta z}{\Delta y} + \frac{\partial T_z}{\partial z}} \qquad (7.10)$$

where β is an overrelaxation parameter set equal to 1.25; Δx, Δy and Δz are the grid spacings, and the derivatives of the transparencies are computed using first-order forward differencing.

The effect of this scheme is to distribute the residue of the divergence among the three wind components. For an equally spaced grid, the A stability case results in a 50% larger correction for the vertical component than the horizontal components, while for the G stability, the horizontal component is weighted 1560 times the vertical. This latter condition effectively eliminates the vertical component and forces the flow around terrain features.

The computation of the wind field for WEST is very similar to the technique used in MATHEW. The principal difference is the use of transparencies which vary with position. The corresponding parameter in MATHEW is fixed (see discussion in Lewellen, Sykes and Oliver, 1982). The codes are slightly different iterative schemes to solve the Poisson equation for the velocity perturbation potential. Comparisons of the two codes have

shown (Fabrick, et.al., 1977) that they produce very similar wind fields when the transparencies are held constant throughout the flow field.

The treatment of thermal drainage winds adds a component to the vertical velocity near the surface. This component is given by

$$w_T = .001 \quad \frac{|T_g - T_a|}{T_g} \tag{7.11}$$

where T_g is the ground temperature and T_a is the ambient temperature. The inclusion of thermally generated winds appears to be attempted without regard to the ground slope. There is no assurance of even getting the sign of the term right.

IMPACT handles diffusion in one of two methods as selected by the user. The simple DEPICT option which is recommended for most cases and a more elaborate Myrup/Ranzies (M/R) model. The DEPICT model computes the vertical diffusivity from the expression

$$D_V = .45\bar{U}\, \sigma_e \ell \tag{7.12}$$

where $\bar{U}$ is the wind speed at the point of interest, σ_e is the standard deviation of the wind fluctuation, and ℓ is the turbulence length side. σ_e and ℓ vary with stability as shown in Table 15.

Table 15

Stability	A	B	C	D	E	F
σ_e	.262	.277	.184	.119	.056	.023
ℓ @ 100 m	105	85	74	64	59	54
ℓ @ 10 m	18	15	12	10	8	7

The computation of diffusivity for the M/R model depends on surface-layer similarity. In this model, the surface wind speed and Monin-Obukhov length scales are computed based on the surface stability and roughness scale. The program assigns different diffusivities for positions below, within and above local inversions.

The diffusivities are computed from expressions of the form

$$D = \frac{k\, u^* z}{\phi} \tag{7.13}$$

where k is Von Karman constant and is set equal to .35. ϕ is the Monin-Obukhov similarity function that varies with stability. For unstable conditions

$$\phi = (1 - 15Z/L)^{-1/4} \tag{7.14}$$

for $-5 < Z/L < 0$. For very unstable conditions, the function $\phi = 1.46(Z/L)^{-1/3}$, which corresponds to the free convection limit. For stable conditions $\phi = 1 + 4.7Z/L$ is used. When an inversion is present, the diffusivity is multiplied by the factor

$$\left(1.1 - \frac{z}{z_{base}}\right) \quad \text{for } .1 < \frac{z}{z_{base}} \leq 1.1 \tag{7.15}$$

This factor reduces the diffusivity near the inversion and reduces transport into the stable layer; this tempers to some extent the error introduced by computing vertical diffusivities strictly applicable only in the surface layer and applying them throughout the mixed layer. Within an elevated inversion Eq. 7.14 is used in a completely arbitrary way by setting L20m and calculating z from the base of the inversion.

The calculation of the horizontal diffusivities is accomplished by scaling the vertical diffusivity calculated by either approach (DEPICT or M/R). The scale factors are shown in Table 16 as a function of stability.

Table 16

Diffusivity Scale Factors

Stability	A	B	C	D	E	F
D_H/D_V	.5	.75	1.05	1.35	1.70	2.0

There is little evidence to support this simplified approach to horizontal diffusivity. The ratio of diffusivities certainly varies by more than the factor of four indicated in this table. Close to the surface D_H/D_V should significantly exceed one for all stability categories and under highly stable conditions may be orders of magnitude higher at any height.

In many simulations the intended horizontal diffusivity is overshadowed by numerical diffusion introduced by an apparent upwind treatment of transport. As long as the coordinate system can be directly aligned with a straight line transporting wind this artificial numerical diffusion will only diffuse the plume along the direction of the wind and cause little problems, allowing this effect to be missed in simple tests. However, when the wind is advecting diagonally across the grid the numerical diffusion, proportional to $V\Delta y$ in the y direction and $u\Delta x$ in the x direction, can easily be an order of magnitude larger than the intended horizontal diffusion. A direct test of the relative influence of numerical diffusion on IMPACT results was made for the

simulation of test case #6 of the July 1981 INEL data. Comparison of two simulations with two orders of magnitude difference in the specified horizontal diffusion resulted in an almost imperceptible change in the spread of the plume, clearly demonstrating that for this case the plume spread was dominated by numerical diffusion.

7.4 Model Verification Studies

7.4.1 Wind Field Comparisons

NOABL has received considerably more attention in the area of model verification than many of the other models considered in this study. The intended application of NOABL was for wind field screening to select favorable sites for wind energy system location. This application requires the ability to accurately predict the wind fields in high wind areas. High wind areas usually occur in rugged terrain. Consequently, the model verification studies for NOABL have tended to concentrate in areas where wind energy may play an important role. The documentation we have on NOABL (wind verification studies) covers Eugene, Springfield Oregon, White Sands Missile Range and additional comparison to wind tunnel data taken at Colorado State University.

A comparison was made to the wind tunnel data recorded at the CSU in the Environmental Wind Tunnel facility. In this study, the two-dimensional flow over four triangular hills with aspect ratios of 1:20, 1:6, 1:4, and 1:2 were recorded as well as a 1:4 sinusoidal hill. The initial flow over the hills was characterized by a boundary layer produced in the tunnel to simulate an inviscid shear layer. This boundary layer was much thicker than the naturally occurring boundary layer on the tunnel walls. The model did a very good job of predicting the flow over the 1:20 1:6, and 1:4 triangular ridges. The simulation included a prediction of a low jet at the summit of the ridge. For the 1:2 ridge, the model predicted a very high speed jet at the summit, whereas the actual experiment underwent separation. The authors indicate that their model would do a better job if they had used downwind data as well as upstream to predict the flow, but no attempt was made to verify this claim in

the study. The model did not perform especially well on the 1:4 sinusoidal ridge, failing to predict the shape of the low level jet at the ridge and missing the boundary layer profile on the upwind side of the ridge considerably.

The authors also compared data from the Eugene/Springfield Oregon area. This area is at the southern end of a mountain valley formed on the east by the Cascade and on the west by the Coast ranges. The model predicted wind speed and direction on a daily and hourly basis. In general, the model predictions were good to within a factor of two on wind speed, and to within 30 to 40 degrees in wind direction. For one particular location, the Creswell airport, the model predicted wind directions which were 150^{o} off at 0600 hours in the morning.

A model verification study was also conducted for data from the White Sands Missile Range (WSMR). The authors selected a particular day to use from a large database because of its near neutral conditions. Attempts by the authors to average data over sequential days were ineffectual because the weather at WSMR was so variable during the period under consideration. The authors used data from eight locations at WMSR. Again the terrain was a north-south running valley which lies to the southwest of the San Andreas mountains, and east of the Sacramento mountains. The study utilized data from eight meteorological stations, each of which included surface and upper air data. Data were compiled during the PASS program. An extensive set of calculations was conducted by SAI to determine the accuracy of NOABL calculations. Again the results predicted the wind speed to within a factor of two for most of the test conditions. The study showed a weak sensitivity to the number of data stations used, with more stations yielding a slightly improved wind prediction. The statistical data were compiled for wind speed only, and no directional considerations were included. One interesting conclusion of the study was that the presence of one data station could bias the predictions substantially. In the case of the study, the particular data station which was labeled "anomalous" was at the base of the southern tip of the San Andreas mountains just on the lee side of a pass. This area

presumably has a very complex wind field, and the difficulties of using data from it are understandable. The wind flow for the experiment considered was from east to west through this particular pass down into the valley, and the experimental station was located roughly at the peak wind speed contour for the experiment.

These model verification studies are consistent with the conclusions from our numerical tests on NOABL and MATHEW. Namely, that when the data is sufficient to define all of the features of interest, models of this type will provide a creditable job of interpolating the wind field over the domain of interest. They should appropriately be thought of as models for interpolating available wind data and not as models for solving the wind field. This also holds for the wind module of IMPACT.

7.4.2 Diffusion Verification Studies

None of the published studies contain a detailed statistical analysis with multiple receptors, but rather they argue the models validity qualitatively on the basis of a few selected measurements. These type studies for the MATHEW/ADPIC model have been discussed in our earlier report (Lewellen, Sykes, Oliver, 1982) where we argued that it was yet to be established that this model performed better under actual tests than the simpler puff models considered in the last chapter.

There have been no published model verification studies of IMPACT to date. IMPACT has been widely used, however, for air pollution studies. These studies differ from model verification studies in that the local meteorological data generally comes from one or two stations. IMPACT studies have been conducted for an Anaconda smelter near the continental divide at Anaconda, Montana. The input meteorological data consisted of a single wind profile, and the IMPACT Program predicted measured concentrations at 1.2 km and 8.7 km downwind of 29 ppm SO_2 and 4.6 ppm SO_2, respectively. These compare to the measured values of 38 ppm SO_2 and 15 ppm SO_2. Similar studies have been published for Garfield, Utah, the Los Angeles basin, and Geyser, CA.

Additional studies have been performed, but not published, for an area in the Rocky Mountains and Vancouver, B.C. In an earlier study by Fabrick et.al., (1977) IMPACT predictions were compared to measurements taken in coastal areas. The authors assert that the studies indicate that the IMPACT model is accurate to a factor of 2 for both coastal and complex terrain situations for short-term averaging of 1-3 hours. However, these conclusions are reached for only a very limited number of computations, and a detailed statistical analysis substantiating these figures was not included.

7.5 Introduction of SPLITPUFF

Our analysis indicates that the most important advantage this transport and diffusion class model has over the simpler puff models considered in Chapter 6 is a better representation of wind shear. In order to test whether this feature could be incorporated into a puff model rather than utilizing a model with the complication of either a complete representation by particles in a cell or finite differencing of the diffusion equation, we have constructed a new model which we call SPLITPUFF. The most important new feature introduced into this puff is the ability to either merge existing puffs into a new combined puff or to split an existing puff which has grown too large into a number of smaller puffs. The goal is to condense the information contained in several thousand particles in ADPIC or IMPACT to a few hundred puffs by continually checking to see that the puffs are efficiently used.

The rules used for splitting or merging are designed to conserve the first and second moment of the concentration distribution about the center of mass of the puff being divided or the puffs being merged. As in the simpler puff models, only the diagonal components of the second moment tensor are calculated, i.e., σ_x^2, σ_y^2 and σ_z^2. Rate equations are used to advance σ_x^2, etc. in time using the Gaussian model diffusivities. At each step, the size of the puff is checked, and if σ_x exceeds $2\Delta x$, where Δx is the grid-spacing in the x-direction, then the puff is split. Similar rules apply in the y- and

z-directions, but the puff is only split in one direction per timestep; if the puff requires splitting in more than one direction, then the direction which most strongly satisfies the splitting criterion is chosen.

When the puff is split in the x-direction, say, we replace it by three puffs of equal mass each with a new σ_x which is half the original σ_x. The central puff remains in the same position as the original puff, while the other two are symmetrically displaced in the x-direction so as to conserve the second moment in this direction; all other moments are trivially conserved.

Two methods are used to limit the exponential growth of the number of puffs from the splitting process. Firstly, any puffs which can be within the same grid-box are merged together into a single puff with conservation of the moments. Secondly, a minimum mass is specified, below which puffs are no longer allowed to split.

In LSO it was demonstrated that more than 20,000 particles are required to track three orders of magnitude dilution of a puff in a constant shear. The same constant shear test applied to ADPIC in Figs. 13 and 14 of LSO are applied to SPLITPUFF in Fig. 7.3. Results with similar levels of accuracy as that obtained by ADPIC with 5,000 particles may be obtained with SPLITPUFF with less than 100 puffs. The calculation in Fig. 7.3 for ADPIC required approximately 25 minutes on our VAX 11/780 computer in comparison to 2.2 minutes for the SPLITPUFF code on the same machine. Algorithms equivalent to those used to parameterize the diffusion velocity of the particles caused by atmospheric turbulence have been used to determine the spread of the puffs as they are transported by the wind. This test is intended to show that it should be possible to generate a puff model which can represent dispersion more efficiently than relying on many particles to represent the dispersing medium.

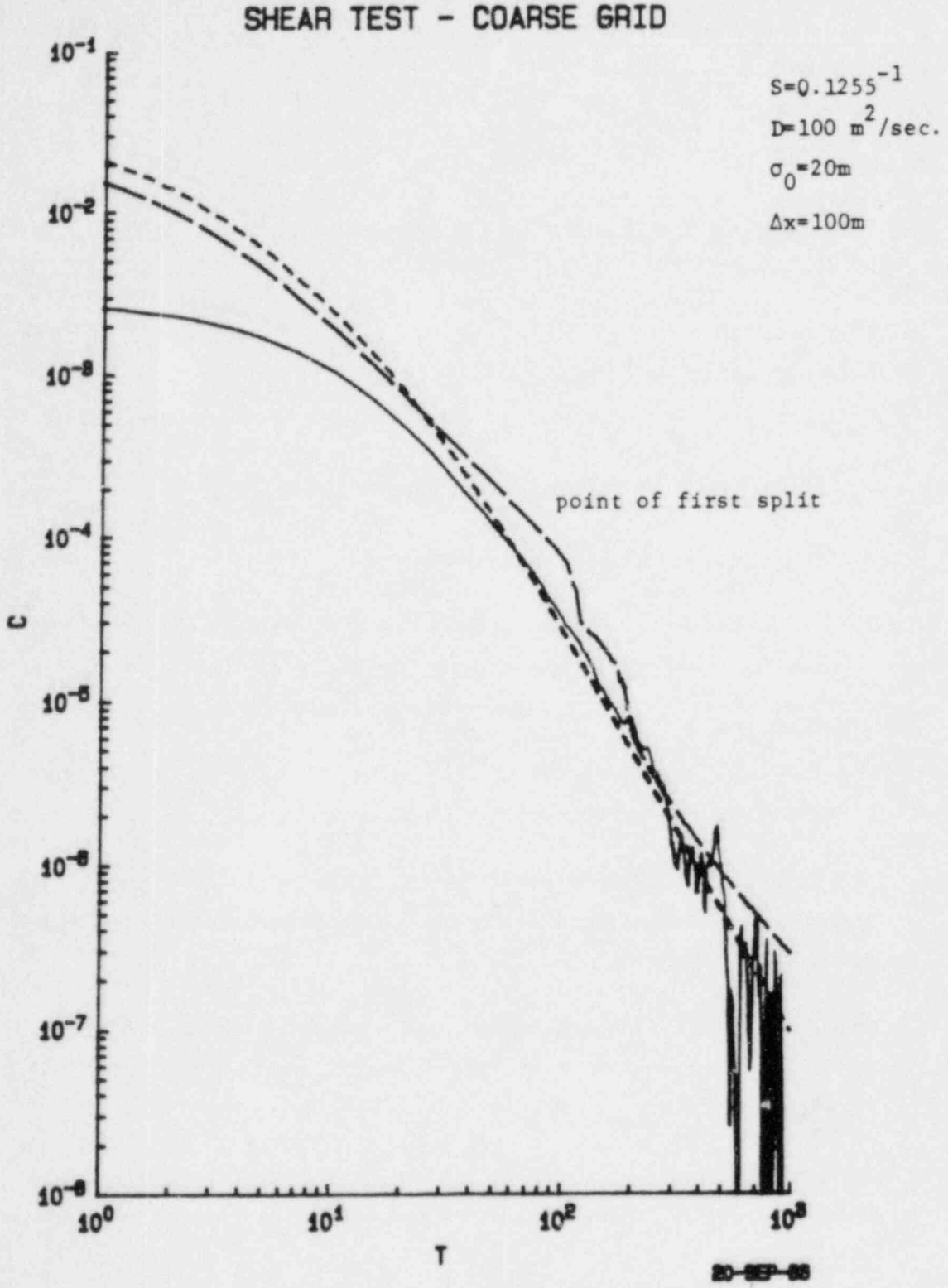

Figure 7.3 - Concentration at the center of 3-D puff in a uniform shear flow as a function of time. ---- analytic solution, ____ ADPIC result with 5,000 particles requiring 25 minutes computing time, __ __ Splitpuff results with from 1-80 puffs requring 2.2 minutes.

7.6 Advantages and Disadvantages of Transport and Diffusion Models based on Mass Continuity

ADVANTAGES

1. They can be terrain specific and should provide for terrain steering of the winds.

2. They are capable of handling the influence of wind shear much better than available puff models.

DISADVANTAGES

1. Require substantial computing resources.

2. Require substantial input data to yield accurate transport results, i.e., data must be adequate to define such features as thermal drainage flow if the influence of such features is to be included.

3. Due to the long computation times necessary, they will be hard pressed to provide timely information.

4. All turbulent diffusion parameters must be determined from empirical scaling relationships which tend to be extrapolated far beyond the range of the original data.

5. Model evaluation tests have not yet demonstrated any statistically significant superiority of these models over the simpler models of Chapter 6.

6. Do not include any estimate of the expected variance from the predicted value of the expected mean concentration.

CHAPTER 8

PRIMITIVE EQUATION MODELS

8.1 General Features

The wind-field models considered in Chapter 7 have been based almost entirely on mass continuity. They apply continuity of the air mass to adjust interpolations of the wind data. Models which attempt to go beyond this and include some form of the conservation of momentum in the simulation of the wind are often called primitive equation models. As we have seen in the previous chapters, one of the most important variables determining the concentrations reaching any particular point is the mean wind direction and the spatial and temporal extent of the angular fluctuations about that mean. The mass adjustment procedures followed by some of the wind models in the last chapter allow some of the influence of terrain to be incorporated, but thermal variations are often more important than terrain variation. Although some attempt has been made to incorporate such influences within the mass adjustment procedure of a model like MATHEW by including thermal vorticity sources (Yocke and Liu, 1980); in general it requires appeal to the momentum equation.

The difficulties with primitive equation models can be divided into three classes. These are: 1) the numerical complexities of dealing with a fully three-dimensional, unsteady flow; 2) the adequate description of the turbulent transport of momentum; and 3) the difficulty of providing adequate initial and boundary conditions to properly constrain the model. Of these, the last is likely to prove the most difficult. The numerical complexities can be handled by using a sufficiently large computer, although it may be difficult to provide a 15-minute response. Turbulent transport theory has progressed to the point that it is no longer likely to be the limiting factor. Thus, the problem of supplying boundary conditions with adequate resolution in time and space to drive the model appears to be a key problem.

In models of laboratory flow, it is generally possible to rigidly prescribe either the boundary values or gradient conditions for the velocity, temperature, pressure, and any other variables of interest at the edges of the model domain. When dealing with a regional model, for a region on the order of 100 km square, this is not often the case. It is nearly impossible to have a measurement network which would provide for the continuous prescription of the flow parameters entering this domain. Further, even if this were possible, it would not be possible to extrapolate these values into the future to provide the boundary conditions necessary to use the model in a forecast mode. For the forecast problem, it appears that the boundary conditions must come from a larger mesoscale weather forecast. However, this larger scale forecast necessarily includes little information on its subgrid scale which would be needed to completely prescribe boundary conditions for the regional model. This problem of nesting grids has been discussed by several authors (e.g., Haltiner and Williams, 1980). It appears the solution can only be partial, at best. When the regional scale flow features generated within the domain are dominant over any similar scale features advected into the computational region, such a nested grid scheme should provide for a valid forecast. This dictates a careful selection of the natural boundary conditions to avoid situations where significant mesoscale features may be convected into the computational domain.

These primitive equation meteorological models fall into the range of mesoscale forecast models. Mesoscale is a term applied to features varying from a scale of 10 km to a scale of 2500 km. For the present purpose of emergency advisory models of dispersion, we are only interested in the lower end of this range, up to approximately 100 km. However, the difficulty with properly prescribing boundary conditions means that a sharp cutoff in the scale of the models of interest is not possible. Mesoscale modeling is an active area of relatively intense current research for the purpose of improved local weather forecasts. We will only consider models which have been run with a grid mesh size of 10 km or smaller. This eliminates such models as the National Weather Services' Limited-area Fine Mesh (LFM) Model; Ross and Orlanski's (1982) model of a cold front; and Long and Shaffer's (1975)

boundary-layer model which uses a 100 km grid spacing.

If one is willing to rely on persistence for short term forecast, the variational approach of Sasaki (1970) could be used to extend a model like MATHEW to incorporate the momentum equation as well as mass continuity. Although this appears to be a quite reasonable approach, as far as we are aware, no results of any attempts to follow this approach have appeared in the literature. The summary report from the SRL Dispersion Model Workshop concluded that this was an area of much needed development.

In the following sections we consider the relative capabilities of three of the available primitive equation models. It is our opinion that none of these models should be considered as "off-the-shelf" candidates for use as a real-time dispersion model at the present time. However, it is possible that one of these or a similar model can be developed into a viable candidate for a Class B model in the near future. In looking at the individual models herein, we are attempting to assess this potential. In Section 8.6 we will also consider the prospect of adding the momentum constraint to an objective analysis model like MATHEW.

8.2 University of Virginia Mesoscale Model

This model is an outgrowth of the sea breeze modeling of Pielke (1974). It is a fully three-dimensional, hydrostatic, primitive equation model which incorporates the boundary layer parameterization of Deardorff (1974). Details of the model are available in a number of different publications, e.g., Mahrer and Pielke, 1975, 1977, 1978; Pielke and Mahrer, 1975, 1978; and a program listing of the version of the program installed on the NCAR CRAY.1 computer is available in a report by McCumber, et al., 1978. In a typical application, (Lyons, Schub and McCumber, 1979); it requires approximately 60 minutes of CRAY-1 CPU to simulate ≤2 hours on a version with 40x30x11 grid points and a horizontal grid spacing of 10 km. It is able to account for flow modifications associated with complex terrain as well as those associated with the air-water temperature interface.

Published verification analyses have demonstrated that the model is, at least, capable of producing correct qualitative features of the sea breeze circulation and upslope-downslope valley conditions. Reasonable skill has been claimed in a number of verification tests for surface meteorological fields over Barbados (Mahrer and Pielke, 1976), over south Florida (Pielke and Mahrer, 1978), over central Israel (Mahrer and Segal, 1979), over Chesapeake Bay (Segal, McNider, McDougal, and Pielke, 1980, and Segal and Pielke, 1981), and over Lake Michigan (Lyons, Shub, and McCumber, 1979). What is meant by "reasonable skill" is exemplified by the comparison in Figure 8.1 between observed and predicted surface winds at a number of different locations at four different times during the simulated day over Chesapeake Bay. The winds tend to agree within approximately 30°, although at Langley at 1800 they show almost a 180° discrepancy. All of the discrepancies in Figure 8.1 are not necessarily caused by the model. Some of the difficulty may be attributed to winds measured at a point being unrepresentative of the 10 km square area simulated by the model grid point. Also, the wind anemometer threshold speed at the synoptic stations may be too high to properly record relatively low wind speeds. This study should provide a fair indication of the results which may be anticipated from such a mesoscale model. It represented a scenario where the meteorology was expected to be dominated by the local sea-breeze circulation, so that uncertainties in the boundary conditions should not dominate.

This model is designed to simulate features in the middle of the range. On the small scale end, it is limited by the fact that it uses the hydrostatic approximation, which is only appropriate when the horizontal scale is much larger than the vertical scale. The limits on the large scale end are somewhat more nebulous, depending upon the parameterization of the subgrid processes. Three specific features which tend to limit the large-scale range of the model are; the neglect of any dynamical influence of clouds, the neglect of any tropopause dynamics, and the neglect of any subgrid scale terrain forcing, the range of scales of most interest to the present application is 1-100 km.

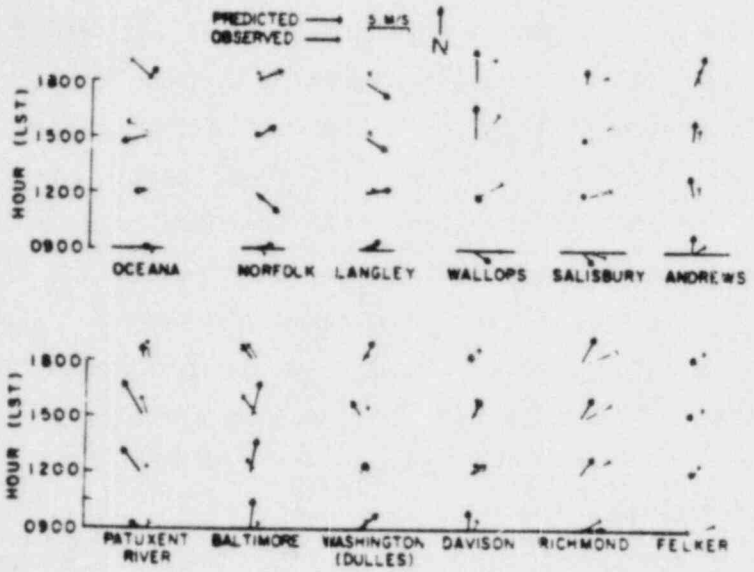

FIGURE 8.1 - Observed surface wind velocities and predicted wind velocities at 12 selected sites (dark circles indicate calm observed wind). (Segal, et.al. 1982)

At the lower end of the range of present interest, the hydrostatic approximation is not rigorously valid, and may be expected to yield some under estimation of the strength of vertical velocities in small scale features such as the sea-breeze front, which may not exceed 1-2 km in width. As long as the horizontal grid spacing is held at 5 km or greater, as it is designed to be in this model, the hydrostatic approximation remains reasonably valid. However, averaging a feature such as a sea-breeze front over a minimum of two grid spaces results in poor resolution and a significant underestimate in vertical velocity. In the Lyons, Shub, and McCumber (1979) study the 10 km grid spacing resulted in a predicted maximum updraft velocity approaching 12 cm/sec, while estimates based on tetroon tracking suggested values as high as 50 cm/sec (and even this is probably a low estimate of the maximum updraft velocity). This is just to emphasize that the model should not be expected to accurately resolve any horizontal features on a scale less than 5 km, in spite of some recent claims to the contrary. Based on comparisons between hydrostatic and nonhydrostatic simulations of a 2-D sea breeze circulation, Martin and Pielke, (1983) conclude that grid increments of 1.5 km or smaller are appropriate for hydrostatic atmospheric models. We believe that their comparison inadvertently favored the hydrostatic model by not supplying sufficient resolution in the region of the sea breeze front to accurately simulate the nonhydrostatic result. Even if a horizontal grid increment as low as 1.5 km is accepted the meteorological flow in many regions of complex terrain cannot be simulated until some means of parameterizing subgrid terrain forcing is derived. Subgrid scale terrain height variance is only small in comparison with grid resolvable terrain variance if horizontal grid spacings are no more than 100m in parts of Colorado (Young and Pielke, 1983) and no more than 1 km in western Virginia (Pielke and Kennedy, 1980). Thus in such complex terrain regions either the hydrostatic approximation should be abandoned or subgrid terrain forcing should be parameterized.

McNider (1981) has added parameterization to the model to represent dispersion from a point source. He attempts to predict turbulent dispersion using the Langrangian-particle, Markov process suggested by Smith (1968) which follows particle trajectories using velocities which have an exponential

autocorrelation in time. In principal, this approach should allow a description of the initial meander phase of the plume with a smooth transition to the later diffusive growth of the plume. Although not attempted by McNider, the method may also be extended to give a prediction of the concentration variance discussed in Chapter 4 by releasing particle pairs and specifying a spatial correlation between the two particles velocities (Durbin, 1980). This approach requires the specification of the turbulence intensities and length scales which McNider parameterized in a manner similar to that used in the boundary layer formulation of the basic model. Due to the critical dependence on turbulent parameterization and due to a nonphysical tendency of particles to congregate in the presence of gradients of the turbulent energy (McNider, 1983) this method requires a good deal of research before it can be used with confidence in real flows.

There are several formidable problems which need to be overcome before this model would appear to be a viable candidate for real-time emergency advisory use. First, a convenient means of inputting boundary conditions and initial value data is required so that results may be obtained in a timely fashion. The question of accuracy with which this may be done will be returned to in Section 8.5, when objective analysis is discussed. Second, the model needs some reprogramming to make it more transportable to other computers. Third, this model needs to address the issue of predictability discussed in Chapter 3. Certainly if the extra time and expense to obtain the data needed to drive this model is to be invested, then the user deserves some indication of the expected variance in the predicted dispersion. Finally, and perhaps most importantly, tests are needed to demonstrate that predictions from such a model would be significantly more accurate than results from one of the simpler models presented in previous Chapters. The additional physical constraints which a primitive equation model can bring to bear on the problem provides the potential for a significant improvement. However, it should be recognized that since it is currently impossible for a transport and diffusion model to represent the complete physical description, it is possible for a more complete model to actually yield a poorer result because the more complete physical description may not be adequately supported by either the

input data or the remaining parameterization.

8.3 Penn State-NCAR Mesoscale Model

This model is an outgrowth of the Anthes (1972) model of a hurricane. It is designed to be a general, hydrostatic meteorological model for forecasting flows with characteristic horizontal scales from approximately 10-2500 km. In particular, it is designed to "model perturbations to the synoptic flow induced by terrain variations, land-water contrasts, convective systems such as squall lines and clusters of cumulonimbi, frontal systems, and propagating upper level disturbances such as jet streaks." (Anthes and Warner, 1978).

Since this model is designed to extend to the sub-synoptic scale, it was developed with map coordinates for the horizontal scale and a pressure coordinate, σ, for the vertical scale:

$$\sigma = \frac{p - p_{top}}{p_{surface} - p_{top}}$$

The model consists of the equations of conservation of momentum, energy, and specific humidity programmed in these coordinates. The horizontal grid mesh typically varies from 30 to 50 points in each direction and approximately 6-12 in the vertical. The execution time is listed as 5000 sec on a CDC 7600 for a 12 hour simulation of a 290 km square region using a 30x30x12 grid (Warner, Anthes, McNab, 1978). The model provides for either a bulk type parameterization of the vertical transport within the planetary boundary layer (PBL), or the explicit resolution of the PBL, by including several computational levels within the boundary layer (Bush, Chang and Anthes, 1976). A number of different simulation experiments have been performed with the model, and these have demonstrated that the model physics are sufficient to allow the model, at least, to provide qualitative insight into a variety of mesoscale processes. The model has been shown to be capable of providing air parcel trajectories which compare favorably with observed tetroon data (Warner, 1981). Seaman (1982) has used the model in a nested grid

configuration with fine mesh grid increments as small as 1 km. This permits a detailed investigation of a small portion of the mesoscale domain. However, none of these studies have been adequate to say that the model has been quantitatively validated.

The difficulties with using this model as a viable candidate for real-time emergency advisory use are similar to those just discussed for Pielke's model.

8.4 Yamada's Mesoscale Model

Yamada's three-dimensional mesoscale atmospheric model is a descendent of a one-dimensional, turbulent transport model for the planetary boundary layer (Mellor and Yamada, 1974). The most substantial difference from the previous two mesoscale models is that it involves a more sophisticated parameterization of vertical turbulent transport. However, in spite of its use of horizontal grid spacings as small as a few hundred meters, it still uses the hydrostatic approximation (Yamada, 1983). This approximation undoubtedly results in larger errors for the small scale features for which this model is designed than it does in the previously discussed mesoscale models.

This model should provide a more accurate description of density driven slope flows, since these flows depend critically upon turbulent transport of heat, momentum and moisture from or to the surface. It uses a turbulent parameterization based on a second-order closure description of turbulent transport. A turbulence kinetic energy equation and a turbulence length-scale equation (Mellor and Yamada, 1977) are solved prognostically. The vertical turbulent fluxes $\overline{uw}$, $\overline{vw}$, $\overline{w\theta_\ell}$ and $\overline{wq_w}$ are then obtained from a set of diagnostic equations derived (Yamada, 1978a, b, and 1979) by assuming a local equilibrium in the one-dimensional set of second-moment turbulence closure equations. This one-dimensional approximation is compatible with the hydrostatic approximation. That is, both are appropriate as long as the horizontal length scales are much bigger than the vertical length scale.

Since this model carries second-order turbulent correlations, it should be possible to add an equation for the concentration variance in order to obtain an estimate of variability following the procedure outlined in Appendix B. As far as we are aware this has not yet been attempted by Yamada.

This model has not yet been released by its author for other people to use. This would be a necessary step before the model could be a serious candidate for the present application.

8.5 A.R.A.P. Second-Order Closure Model

At ARAP we have developed a model for the turbulent transport of mass, momentum, and energy in the atmospheric boundary layer which has been applied to a number of problems as reviewed by Lewellen (1981). This model is similar to that discussed in the last section except in most applications we carry equations for the full set of second-order correlations rather than the reduced set used by Yamada. In return for the added physics carried in the model, our numerical implementation of the model has been limited to two-dimensional problems. Currently, it is strictly a research model and not available as a viable candidate for a real-time dispersion model under general site conditions. We discuss it here because of its potential for the future, and because of its connection with the variability predictions discussed in Chapter 4.

The recent test of our second-order closure model as a part of the Electric Power Research Institute's Plume Model Validation and Development Project (Lewellen, et.al., 1983) did not demonstrate a clear superiority of this type model over simpler models. A major problem with the exercise was the model's limitation to two-dimensional, steady-state conditions which restricted us to either afternoon or nocturnal runs. The nocturnal runs have little interaction with the ground so only limited remote sensor data was available for comparison. On the other hand, the afternoon case, where there are ample surface data to compare with, was the time the model predicts the largest variance in the data close to the stack so that hourly means need not

agree well with the ensemble mean (see Figure 5 Appendix B). Under such conditions of large natural variability, it is difficult to discriminate between model error and data scatter. However, there appeared to be a general overprediction of the plume impact within a few kilometers of the stack, caused by some combination of an underprediction in the initial plume rise and an overprediction of the early downwind diffusion of the plume. How much of this error is attributable to the approximate nature of the integral model used for the initial plume rise phase of the plume dispersal and how much to the model closure is not clear from these results.

The relatively disappointing performance of the second-order closure model on this test has led to a complete review of the model formulation. This review plus the acquisition of recent high quality laboratory data for direct model comparisons has yielded some model modifications which we believe should substantially improve the model's accuracy. These model developments and comparison with the laboratory data are described in detail in Appendix C.

The principal model changes were a change in the modeling of the turbulent diffusion of $\overline{u_i' c_i'}$, the turbulent flux of a given species, and a different formulation for the length scale in the dissipation of the species variance. As may be seen in Appendix C, these modifications were adequate to permit the model results to give a very good representation of both the mean and the variance of the laboratory concentration data. We believe this forms a solid foundation for further model development.

A significant advantage of the second-order closure model is that the variance of the concentration fluctuations may be carried as a natural part of the formulation. This predicted variance provides a logical basis for estimating the natural turbulent variability in any time averaged sample of the concentration, as detailed in Appendix B. We believe the simple integrated form of the variance equation discussed there can supply an important complement to even Gaussian plume models of the type discussed in Chapter 5.

8.6 Objective Analysis

A common problem for any mesoscale model is that of initial conditions and boundary conditions. These conditions must be derived from some combination of output from a larger synoptic scale model and relatively sparse available data in the domain of interest. The input to the mesoscale model is obtained by space and time interpolations of this "data", where the larger scale model is included as part of the data if desired. In view of the general arbitrariness in any such interpolation procedure, it would be desirable to have the model be relatively insensitive to these input conditions, by expanding the region to apply boundary conditions further away from the region of interest and by starting the model earlier than the time of interest, but this exercise is self-defeating to a certain extent. Except for ideal problems where a locally generated mesoscale feature dominates the flow, these input conditions are likely to have a strong influence on the resulting model flow. Therefore, the success of a general mesoscale model in forecasting meteorological conditions after any given emergency is likely to be strongly influenced by the input data interpolation routines.

The two general procedures for accomplishing this interpolation are: 1) to use the model itself by including terms which tend to force the model results towards the available data, or 2) to use an objective analysis procedure on the data which incorporates some smoothness conditions and some physical constraints into the interpolation procedure. We will consider the second of these here because it is independent of the subsequent model, and because any objective analysis routine, when combined with persistence as a forecast, becomes a candidate model for the meteorological part of a real time dispersion model. In fact, the windfield models considered in Chapter 7 are all such models.

The variational analysis approach suggested by Sasaki (1970) provides a framework for applying general physical constraints while simultaneously minimizing discrepancies between prescribed data values and analyzed values. MATHEW, NOABL and IMPACT use this procedure to constrain the analyzed field to satisfy mass continuity. A practical numerical algorithm for adding a

momentum constraint to this procedure would appear highly desirable.

In the variational approach of Sasaki, a momentum constraint may be added as either a strong or weak constraint. By a strong constraint we mean the resulting field is required to exactly satisfy the prescribed momentum equation within the applicable numerical accuracy. While a weak constraint only requires the departures from the momentum equation to be included in the integral which is minimized. Since all the body forces acting on the atmosphere are unlikely to be precisely known, it appears more consistent to apply momentum as a weak rather than a strong constraint. If the momentum equation is symbolized as:

$$M(\bar{u}) = 0 \tag{8.1}$$

then the integral which should be minimized in the variational calculation may be written as

$$I = \int (\bar{u}-\bar{u}_o)^2 \, dv + \mu_1 \int M^2(\bar{u}) \, dv + \int \lambda(x) \nabla \cdot \bar{u} \, dv \tag{8.2}$$

where $\bar{u}_o$ represents the given data field, λ is a Lagrange multiplier to be determined by the variational calculation, and $\mu_1(x)$ is a prescribed weighting function which determines the relative strength of the momentum constraint. The integral I is a minimum with respect to u and λ if the following equations are satisfied.

$$2(\vec{u} - \vec{u}_o) - \nabla\lambda - \mu_1 \vec{M}(u) \cdot \frac{\delta \vec{M}}{\delta \vec{u}(x)} = 0 \tag{8.3}$$

$$\nabla \cdot \vec{u} = 0 \tag{8.4}$$

When $\mu_1=0$ this set of equations reduces to the set satisfied by MATHEW. For $\mu_1\neq 0$ the set is considerably more difficult to solve with the difficulty depending upon the terms included in the momentum operator M.

A similar result may be accomplished by defining a u_m which satisfies the momentum constraint, i.e., $M(u_m)=0$, and defining

$$I = \int [(u-u_o)^2 + \mu_1(u-u_m)^2 + \lambda\nabla\cdot u] \quad dx \tag{8.5}$$

The integral I is now a minimum with respect to u and λ whenever

$$\vec{u} - \frac{\vec{u}_o+\mu_1\vec{u}_m}{1+\mu_1} + \frac{1}{2}\nabla\lambda = 0 \tag{8.6}$$

and

$$\nabla\cdot\vec{u} = 0 \tag{8.7}$$

This appears to provide a relatively straightforward technique for generalizing a model like MATHEW to incorporate a weak momentum constraint. Any desired form of the momentum equation and numerical technique for solving it may be used to determine $\vec{u}_m$. This momentum model velocity is then combined with the available data to obtain the preliminary velocity flowfield which is adjusted by MATHEW to be fully consistent with continuity and the boundary conditions. This is an attractive area for further research.

8.7 Advantages and Disadvantages of Primitive Equation Models

ADVANTAGES

1. They can provide simulations of flows dominated by mesoscale forcing even when little data is present.

2. They can be structured to use all of the available data in providing a best-guess simulation.

DISADVANTAGES

1. Require very large computing resources.
2. Further development work will be required to reduce response time, which must include time for set-up, computation, and interpretation, short enough to provide timely information.
3. With the exception of models which include some turbulent transport theory, the diffusion parameterization used in these models tend to be empirical relationships extrapolated beyond the range of the original data.
4. The data required to provide adequate boundary conditions and initial conditions will be difficult to obtain.
5. No statistical evaluation tests have been carried out to demonstrate a significant superiority of these models over the simpler models of Chapter 6.

CHAPTER 9

COMPARISON OF MODEL RESULTS WITH INEL 1977 TEST DATA

Most existing dispersion data have been aimed at examining diffusion parameterization. Attempts have generally been made to keep transport as simple as possible so as not to compound the complexities of turbulent diffusion. A test of this type was carried out at INEL in April 1977. Tracers were released at ground level during a persistent southwest wind and sampled on arcs at 3.2, 50 and 90 km downwind of the source. Details of the release and sampling techniques and of the meteorological measurements are given by Clements (1979). This data has not been used in the parameterization of any of the models discussed in this report, and thus should represent an unbiased data set for use in evaluating these models. As will be demonstrated, this is not wholly true since the straightline persistent winds tend to show the simplest models in a more favorable light than would be the case for more typical meteorological conditions. Nevertheless, we believe this is a useful baseline test of the models. Any model must necessarily perform reasonably in this simple test to be considered as a viable candidate for emergency response use. But this is only a necessary condition, not a sufficient condition for its consideration as a viable candidate.

The results of the pattern test comparisons between four of the individual model calculations representing the range of model types and the data observations on the 50 and 90 km arcs are given in Figures 9.1 to 9.4. As expected, all the models do reasonably well in this simple test.

Even the simplest gaussian plume model does quite well as demonstrated in Figure 9.1. Approximately 56% of the data points are predicted within a factor of 2 before any shift of the pattern calculated by the EPA model and all of the data points are covered within a factor of 2 by the model calculations when a shift of $\pm$ 16^{o} is permitted.

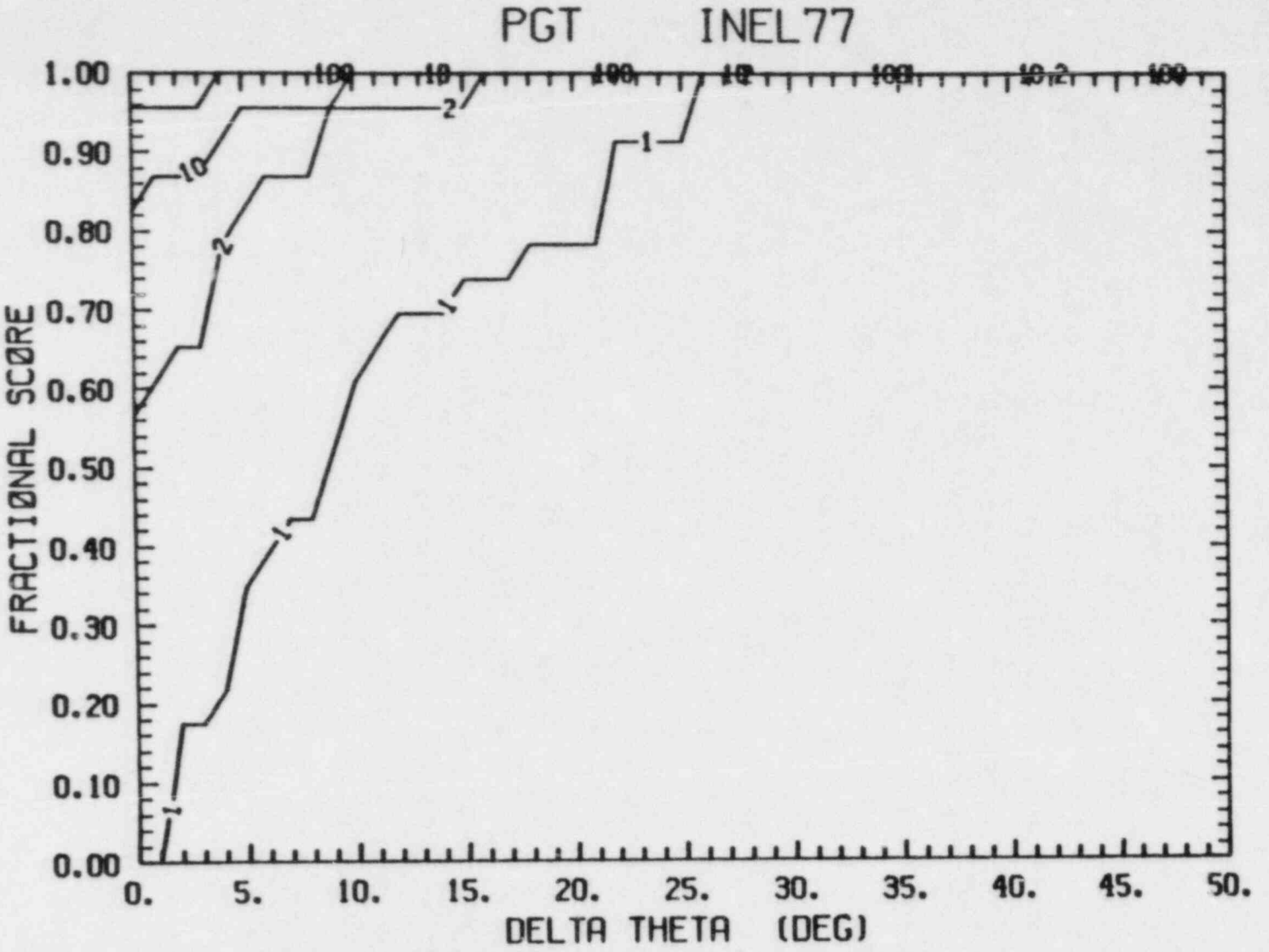

FIGURE 9.1 - Fraction of Data Points Covered Within the Indicated Factor by the Calculated Pattern for the PGT Guassian Plume Model Expanded through an Angle $\Delta\theta$.

Results for the ARL puff model pattern tests are given in Figures 9.2; this model also does well. The fact that this model does not show significantly better results than the steady state plume model is a reflection of how steady the meteorology was for this test. In the limiting case of steady flow, the puff models are designed to reproduce the steady plume results.

The results of two transport and diffusion class models are given in Figures 9.3 and 9.4. As expected, these models also do well. A summary plot comparing the results of the different models is given in Figure 9.5. The largest error factor is plotted as a function of tne angular shift of each model. This is a cross plot of the angular shifts at which the factor lines reach 1.0 on the individual model plots of Figures 9.1-9.4. This may be interpreted as a plot of concentration uncertainty as a function of position uncertainty. That is, the concentration is predicted within an order of magnitude within a band of position uncertainty of approximately 10° to 15° for all of the models. A closer estimate of concentration entails a larger spread in position or a tighter restriction on position leads to some sample points being missed by a larger factor.

Another comparison of the model results which gives less weight to largest error sample points is given in Figure 9.6. This is a cross plot of the previous individual model results at the fixed angular uncertainty of 10°. This shows somewhat larger variations between the models than does Figure 9.5. However, if a choice of models were to be made from this test alone, the favorites would be the simplest models, since the more complex models do not show sufficient improvement in accuracy to justify the added data requirements. The more appropriate conclusion is that the simple meteorology of this test case is unable to provide a meaningful discrimination between the various candidates. The crucial question which still must be answered is whether the added data requirements will prove warranted under more typical meteorological conditions. This is not likely to be answered by the existing data banks of observations taken to characterize diffusion under straightline transport conditions. Only those data bases which span a more representative

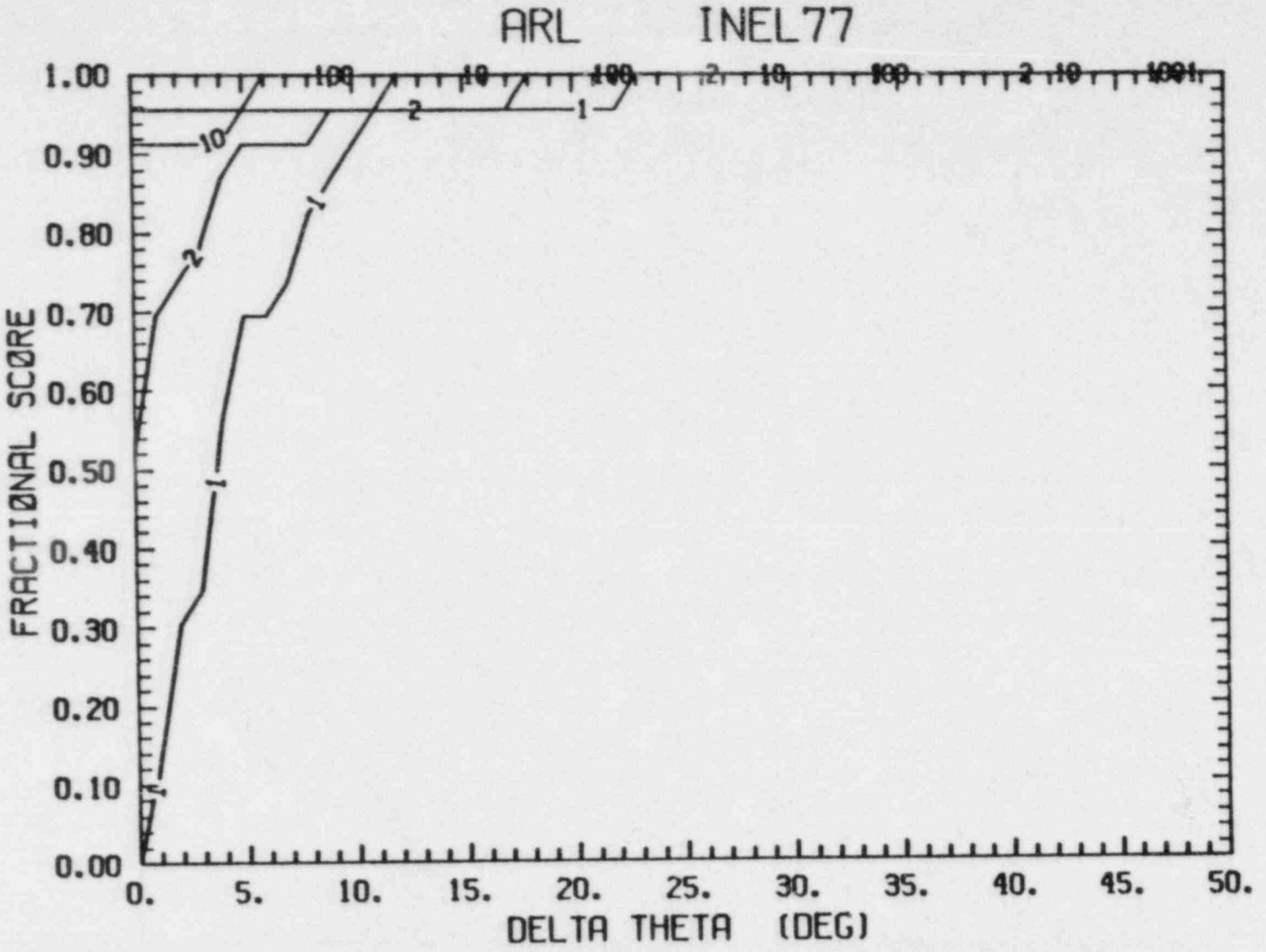

Figure 9.2 - Fraction of Data Points Covered Within the Indicated Factor by the Calculated Pattern for the ARL Model Expanded Through an Angle Δθ.

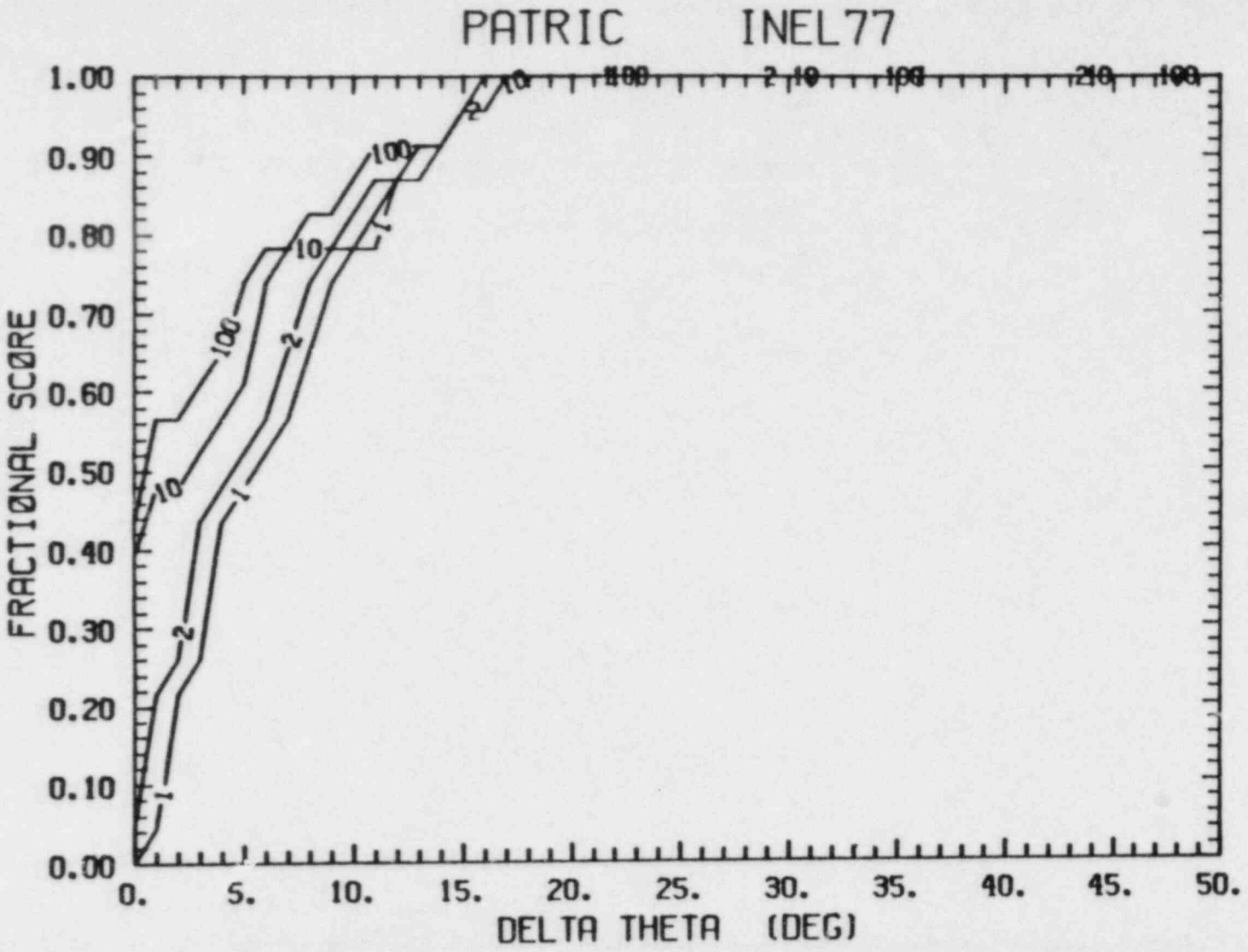

figure 9.3 - Fraction of Data Points Covered Within the Indicated Factor by the Calculated Pattern for the PATRIC Model Expanded Through an Angle Δθ.

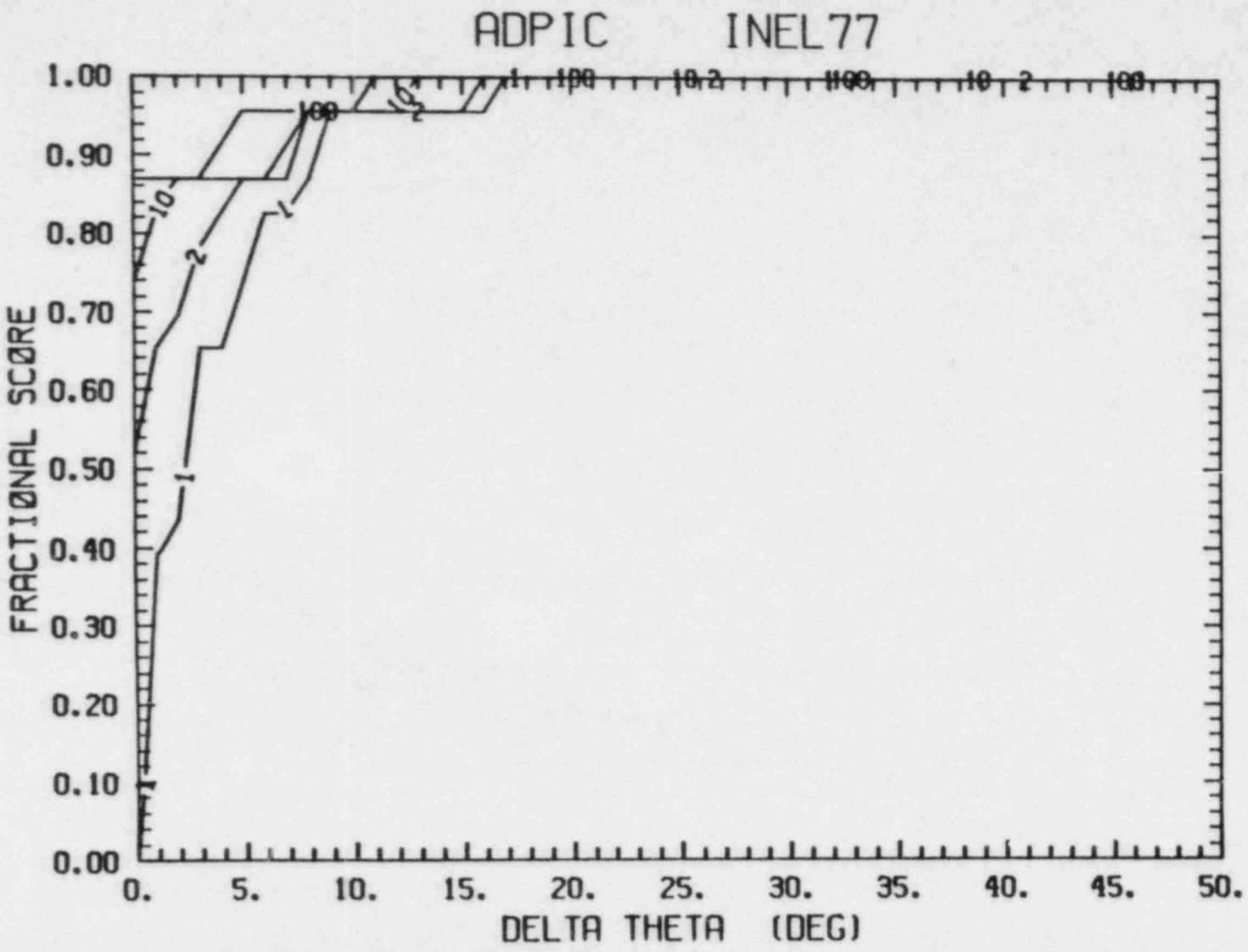

Figure 9.4 - Fraction of Data Points Covered Within the Indicated Factor by the Calculated Pattern for the ADPIC Model Expanded Through an Angle $\Delta\theta$.

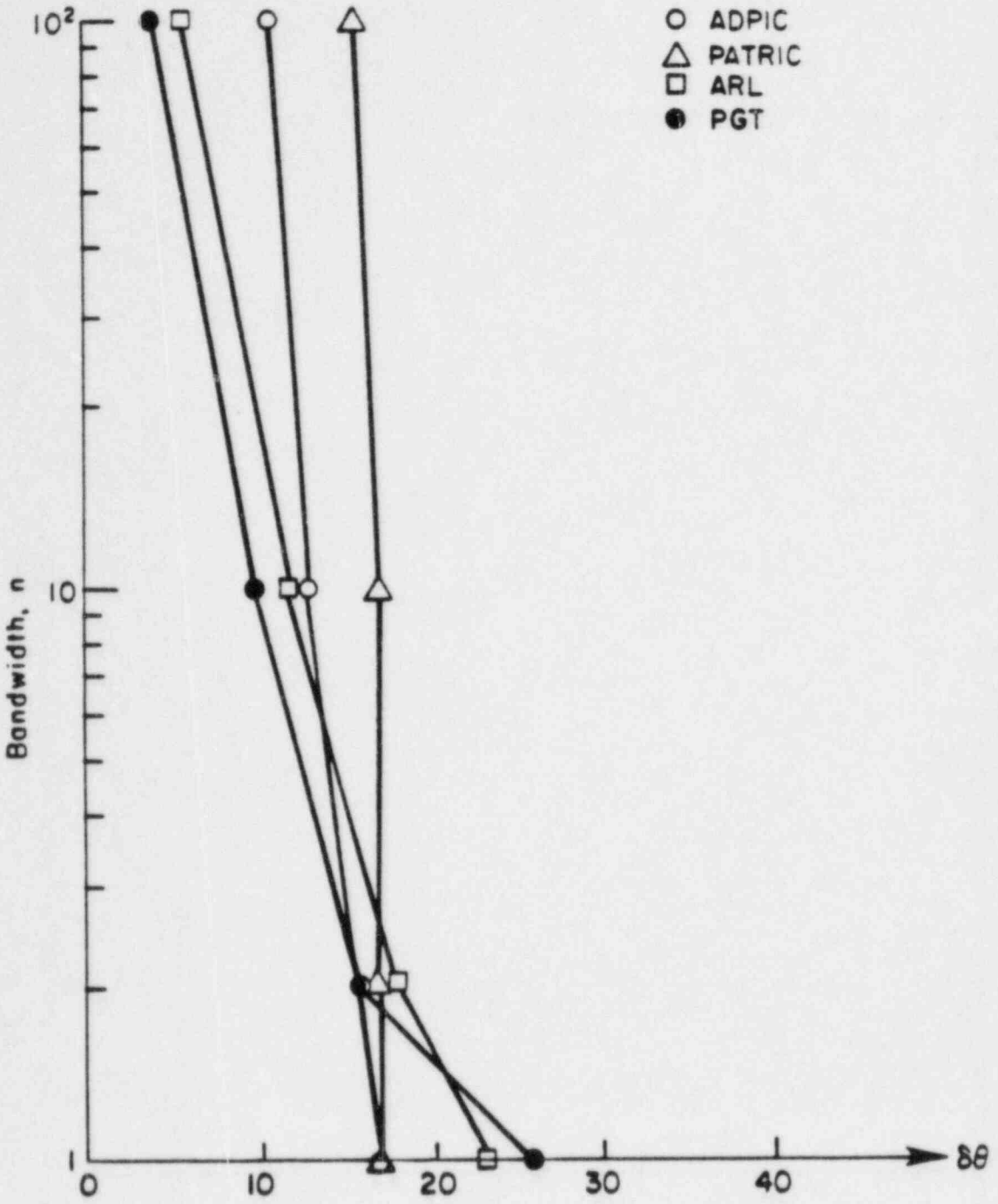

Figure 9.5 - Summary of Pattern Test Results for Various Models with 1977 Inel Data. Angle Required to Cover Data Within Given Bandwidth for the Different Models.

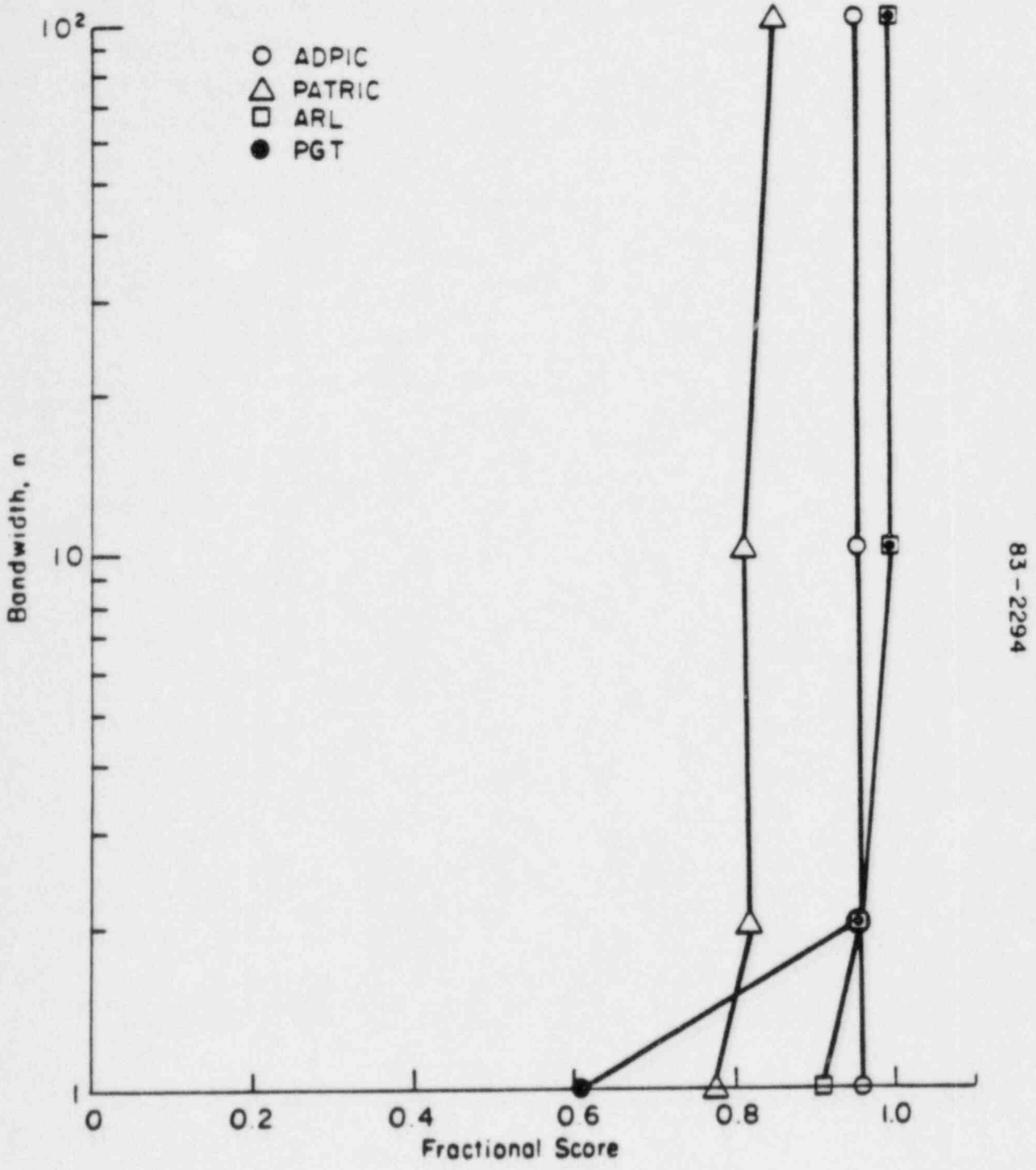

Figure 9.6 - Fraction of Data Points Covered Within the Indicated Factor by the Different Models when a 10 Degree Shift is Permitted.

sample of the meteorological conditions at a given site are likely to provide the information needed for a definitive discrimination between models. Results taken at INEL over a three week period in July 1981 are used to test the models in a companion report. The data collection for this series of tests was specifically designed to obtain surface patterns out to 50 km for whatever meteorological conditions happen to occur during the test period.

CHAPTER 10
CONCLUSIONS

The scientific analysis of the different types of dispersion mdoels available as advisory models for emergency response show that it is possible to incorporate more physical constraints as the complexity of the model increases. But it is not clear at which point the incremental improvement in accuracy is insufficient to justify the added expense required for the additional input data and the additional computer requirements. Detailed field testing of the different types of models discussed herein is desirable to aid in answering this question. Results of a test program designed for this purpose are provided in a companion report.

The randomness inherent in atmospheric turbulence imposes a natural limit on plume predictability which provides an upper bound on model accuracy as a function of available data. This variability is not simply a function of the model chosen, but is rather a complicated function of the meteorological conditions and the nature of the emissions. Under certain strongly convective conditions, even a perfect simulation of the mean concentration distribution can provide a poor estimate of the hourly concentration distributions observed. The usefulness of a real-time dispersion model is thus dependent on a complementary estimate of the variability expected about the mean dispersion. We recommend that any model adapted for real-time emergency use be supplemented by, at least, a simple model of the concentration variance expected under the conditions at that time. A relatively simple model of the mean concentration together with a compatible model of its variance should be more useful than a sophisticated model which even provides a better estimate of the mean if the latter includes no estimate of the variability expected.

Based on our analysis of the different models, we believe that some version of a puff model is likely to prove most efficient for this application. Such a model can be used as either a Class A or Class B model. It can be run with no more input requirements than that required for the simplest gaussian plume models, but permits the accuracy to be improved when

additional data on the temporal and spatial variation of the wind and stability is available. We believe that a number of modifications to the standard puff models can be made to strengthen this apparent advantage. If MESOI is taken as a reference model, we believe it can be substantially improved by:

1. Complementing it with a compatible estimate of the concentration variance over the time period of most interest.

2. Permitting an elevated release for the source.

3. Substituting diffusion algorithms which depend on direct measurements of wind variance rather than depending on stability categories.

4. Allowing puffs to split when they are spread out sufficiently for wind shear to be an important dispersion mechanism.

5. Incorporating wet and dry deposition into the model. Deposition models are discussed in a companion report.

Such an upgraded puff model would remain simpler than the transport and diffusion class models, while sacrificing little accuracy at the level of data input likely to be available for most applications.

The truth of the preceeding paragraph must be established by detailed field testing of the models. Such tests are currently being carried out using the field data collected at INEL last July by an NRC sponsored group (Dickson and Start, 1981).

REFERENCES

Akins, R. E., H. W. Church and M. S. Tierney (1977); "Simulated Atmospheric Dispersion of Radioactive Material Released in an Urban Area," SAND-77-0854C, 4 pp.

American Meteorological Society (1978); "Accuracy of Dispersion Models," Bulletin American Meteorological Society, 59, pp. 1025-1026.

Anthes, R. A. (1972); "The Development of Asymmetrics in a Three- Dimensional Numerical Model of the Tropical Cyclone," Monthly Weather Review, 100, pp. 461-476.

Anthes, R. A. and T. T. Warner (1978); "Development of Hydrodynamic Models Suitable for Air Pollution and Other Mesometeorological Studies," Monthly Weather Review, 106, pp. 1045-1078.

Bander, T.J. (1982); "PAVAN: An Atmospheric Dispersion Program for Evaluating Design Basis Accidental Releases of Radioactive Materials from Nuclear Power Stations," NUREG/CR-2858.

Bass, A. (1980); "Modeling Long Range Transport and Diffusion," Proceedings of Second Joint Conference on Applications of Air Pollution Meteorology, New Orleans, Am. Meteorol. Soc., Boston, MA.

Bass, A. and D. G. Smith, (1981); "Atmospheric Dispersion Modeling for emergency Preparedness," Atomic Industrial Forum/National Environmental Studies Project-022.

Begovich, C. L., B. D. Murphy and C. J. Nappo Jr. (1978); "RETADD: A Regional Trajectory and Diffusion-Deposition Model," ORNL/TM-5859.

Benkley, C. W. and A. Bass (1979a), "Development of Mesoscale Air Quality Simulation Models," Vol. 2, User's Guide to MESOPLUME (Mesoscale Plume Segment) Model EPA 600/7-79-XXX, Environmental Protection Agency, Research Triangle Park, N.C., 141 pp.

Benkley, C. W. and A. Bass (1979); "Development of Mesoscale Air Quality Simulation Models, Vol.3b, User's Guide to MESOPUFF (Mesoscale Puff) Model," EPA 600/7-79-XXX,

Bjorklund, J. R. and R. K. Dumbauld (1978); "User's Instructions for the NASA/MSFC Cloud-Rise Preprocessor Program - Version 6, and the NASA/MSFC Multilayer Diffusion Program - Version 6," NASA CR-2945, H.E.Cramer Co.

Bowne, N. E., R. J. Londergan, D. H. Minott and D. R. Murray (1981); "Preliminary Results from the EPRI Plume Model Validation Project - Plains Site," EPRI Report EA-1788.

Bowne, N. E., R. J. Londergan, D. R. Murray, and H. S. Borenstein (1983); "Overview, Results, and Conclusions for the EPRI Plume Model Validation and Development Project: Plains Site," EPRI Report EA-3074.

Buckner, M. R. (1981); Proceedings of the First SRL Model Validation Workshop. Savannah River Lab., Report DP-1597 CONF-8011132.

Briggs, G. A. (1975); "Plume Rise Predictions," Chapter 3 in Lectures on Air Pollution and Environmental Impact Analysis, D. A. Haugen, Ed., Am. Meteorol. Soc., Boston, MA, pp. 59-111.

Busch, N. E., S. W. Chang and R. A. Anthesu (1976); "A Multi-level Model of the Planetary Boundary Layer Suitable for Use with Mesoscale Dynamic Models," J. Appl. Meteor., 15, pp. 909-919.

Chan, H. and I. Tombach, (1978); "AVACTA: Air Pollution Model for Complex Terrain Applications," Aero Vironment Inc., Pasadena, CA, Report AV-M-8213.

Chnristiansen, J. H. (1976); User's Guide to the Texas Episodic, Model (TEM) Texas Air Control Board, Austin, Texas.

Clark, T. L. and R. E. Eskridge (1977); "Non-divergent Wind Algorithm for the St. Louis RAPS Network," Environmental Protection Agency, EPA 600/4-77-048, Research Triangle Park, N.C.

Clements, W. E. (1979); "Experimental Design and Data of the April 1977 Multitracer Atmospheric Experiment at the Idaho National Engineering Laboratory," Los Alamos Scientific Laboratory, LA-7795-MS.

Csanady, G. T. (1973); Turbulent Diffusion in the Environment, Reidel Publishing Company.

Culkowski, W. M. and M. R. Paterson (1976); "A Comprehensive Atmospheric Transport and Diffusion Model," ORNL/NSF/EATC-17, 117 pp.

Dames and Moore (1980); "Summary Report of the NCAO Atmospheric Dispersion Modeling Panel," 1 - Recommendations, NTIS PB80-174964.

Deardorff, J. W. (1974); "Three-dimensional Study of the Height and the Mean Structure of Heated Planatary Boundary Layer," Bound. Layer Meteor., 7, pp. 81-106.

Dickerson, M. H. and R. C. Orphan (1975-6); "Atmospheric Release Advisory Capability (ARAC)," Lawrence Livermore Laboratory Report UCRL-77200 Preprint, Rev. 1 (1975); published in Nuclear Safety, 17, No. 3, May-June (1976).

Dickerson, M. H. (Ed.) (1980); "A Collection of Papers Based on Drainage Wind Studies in the Geysers Area of Northern California," USPOE Report ASCOT-80-7, Lawrence Livermore Laboratory, Livermore Company.

Dickson, C. R., G. E. Start and J. H. Cate (1981); "1981 Idaho Field Experiment," (April 1981 Draft report to Nuclear Regulatory Commission).

Dieterle, D. A. and A. G. Tingle (1976); "A Numerical Study of Mesoscale Transport of Air Pollutants in Sea Breeze Circulations," Third Symposium on Atmospheric Turbulence, Diffusion and Air Quality, Amer. Meteor. Soc., October 1976, Boston, MA.

Donaldson, C. duP. (1973); "Atmospheric Turbulence and the Dispersal of Atmospheric Pollutants," Amer. Meteor. Soc. Workshop on (D. A. Haugen, Ed.), Science Press, Boston, pp. 313-390.

Drake, R. L. and S. M. Barrager (1979); "Mathematical Models for Atmospheric Pollutants," Electric Power Research Institute, EPRI EA-1131.

Draxler, R. R. (1979); "Modeling the Results of Two Recent Mesoscale Dispersion Experiments," J. Atm. Env. 13, pp. 1523-1533.

Draxler, R. R. (1980); "An Improved Gaussian Model for Long-Term Average Rain Concentration Estimates," J. Atm. Env. 14, pp. 597-601.

Durbin, P.A. (1980); "A Stochastic Model of Two-Particle Dispersion and Concentration Fluctuations in Homogeneous Turbulence," J. Fluid Mechanics, 100, pp. 279-302.

Environmental Protection Agency (1977); "User's Manual for Single- Source (CRSTER) Model. U.S. EPA-450/2-77-0L3, Office of Air Quality Planning and Standards, Research Triangle Park, NC.

Fabrick, A., R. Sklarew and T. Wilson (1977); "Point Source Model Evaluation and Development Study," Science Applications, Inc., Westlake Village, CA.

Fields, D. E. and C. W. Miller (1980); User's Manual for DWNWND: An Interactive Gaussian Plume Atmospheric Transport Model with Eighth Dispersion Parameter Options, Oak Ridge National Lab., TN., ONRL/TM-6874, 39 pp.

Fox, D. G. (1981); "Judging Air Quality Model Performance - Summary of The AMS Woods Hole Workshop," Bulletin of the American Meteorological Society, 62, pp. 599-615.

Garret, A. J. and C. E. Murphy, Jr. (1981); "A Puff-Plume Atmospheric Deposition Model for use at SRP in Emergency Response Situations," SRL Tech Report DP-1595.

Gerrity, J. F. Jr. (1976); "The LFM Model-1976: A Documentation," NOAA Technical Memorandum, NWS NMC 60.

Gifford, F. A. (1961); "Use of Routine Meteorological Observations for Estimating Atmospheric Diffusion," Nuclear Safety, 2:47.

Gifford, F. A. (1973); Proceedings of the 4th Meeting of the Expert Panel on Air Pollution Modeling. NATC-COCMS. Pub. No. 30, Ch. XVI.

Gifford, F. A. (1976); "Turbulent Diffusion Typing Schemes - A Review," Nuclear Safety, 17, pp. 68-86.

Glahn, H. R. and D. A. Lowry (1972); "The Use of Model Output Statistics (MOS) in Objective Weather Forecasting," Journal of Applied Meteorology, 11, pp. 1203-1211.

Goodin, W. R. and G. J. McRoe (1980); "A Procedure for Wind Field Construction from Measured Data which Utilizes Local Surface Roughness," Proceedings of the Second Conference on Coastal Meteorology, Los Angeles, CA, Jan. 31-Feb. 2, pp. 233-239.

Gresko, P. M., R. L. Lee and R. I. Sani (1978); "Modeling the Planetary Boundary Layer Using the Galerkin Finite-Element Method," UCRL-78120.

Hales, J. M., D. C. Powel and T. D. Fox (1977); "STRAM - An Air Pollution Model Incorporating Non-Linear Chemistry, Variable Trajectories and Plume Segment Diffusion," Environmental Protection Agency, EPA 450/3-77-012.

Haltiner, G. J. and R. T. Williams (1980); Numerical Prediction and Dynamic Meteorology, Second Edition, John Wiley and Sons.

Hanna, S. R. (1981); "Handbook on Atmospheric Diffusion Models," Atmospheric Turbulence and Diffusion Laboratory, Oak Ridge, TN, ATDL No. 81/5.

Hanna, S. R,. G. A. Briggs, J. Deardorff, B. A. Egan, F. A. Gifford and F. Pasquill (1977); "Summary of Recommendations on Stability Classification Schemes and Sigma Curves," Bulletin American Meteorological Society, 12, pp. 1305-1309.

Heffter, J. L. (1980); "Air Resources Laboratories' Atmospheric Transport and Diffusion Model," NOAA Technical Memorandum, ERL-ARL-81, Air Resources Laboratories, Silver Spring, MD.

Hilsmeier, W. F. and F. A. Gifford (1962); Graphs for Estimating Atmospheric Dispersion, USAEC Report ORO-545, Weather Bureau, Oak Ridge, TN.

Hilst, G. R. (1978); "Plume Model Validation," Electric Power Research Institute, EPRI EA-917-SY, October 1978.

Hilyer, M. J., et al. (1979); "Procedures for Evaluating the Performance of Air Quality Simulation Models," Systems Applications, Inc., EPA/450/4-79-033, October 1979.

Horst, T. W., J. C. Doran and P. W. Nickola (1979); Evaluation of Emperical Diffusion Data, Pacific Northwest Laboratory, NUREG/CR-0798, Richland, Washington.

Huang, J. C. (1980); "Evaluation of Modified Gaussian Plume Model for Travel Distances 25-150 Km," Second Joint Conference on Applications of Air Pollution Meteorology, March 22-24, 1980, New Orleans, LA.

Hutcheson, M. R. (19__); "Analysis of Ensemble Averaged Concentrations and Fluxes in a Tracer Puff," PB-292-4891/2ST.

Illinois Environmental Protection Agency (1976); "Air Quality Short-Term Model," Springfield, IL.

Irwin, J. S. (1979); "Estimating Plume Dispersion - A Recommended Generalized Scheme," AMS 4th Symposium on Turbulence and Diffusion, Reno, Nevada.

Irwin, J. S. (1983); "Estimating Plume Dispersion - A Comparison of Several Sigma Schemes," J. of Applied Meteorology, 22, 92-114.

Kern, C. D. (1977); "SRL Savannah River Laboratory Environmental Transport and Effects Research," DP-1489. Annual Report.

Kreitzberg, C. W. and M. J. Leach (1978); "Diagnosis and Prediction of Tropospheric Trajectories and Cleansing," Proceedings of the 85th National Meeting, American Institute of Chemical Engineering, Philadelphia, PA, June 4-8, 1978.

Lamb, R. G. (1978); "A Numerical Simulation of Dispersion from an Elevated Point Source in the Convective Boundary Layer," J. Atm. Env., 12, pp. 1297-1304.

Lange, R. (1978); "PATRIC - A Three-Dimensional Particle-in-Cell Sequential Puff Code for Modeling the Transport and Diffusion of Atmospheric Pollutants," Lawrence Livermore Laboratory Report UCID-17701, 8 pp.

Lange, R. (1978); "ADPIC - A Three-Dimensional Transport-Diffusion Model for the Dispersal of Atmospheric Pollutants and Its Validation Against Regional Tracer Studies," Journal of Applied Meteorology, 17, pp. 320-329.

Lavery, T. F., R. L. Baskett, J. W. Thrasher, N. J. Lordi, A. C. Lloyd and G. M. Hidy (1980); "Development and Validation of a Regional Model to Simulate Atmospheric Concentrations of SO_2 and Sulfate," Proceedings of the AMS/APCA Second Joint Conference on Application of Air Pollution Meteorology, Boston, MA.

Lee, H. N. and S. K. Kao (1979); "Finite Element Numerical Modeling of Atmospheric Turbulent Boundary Layer," Journal of Applied Meteorology, 18, pp. 1287-1295.

Lewellen, W. S. (1981); "Modeling the Lowest 1 Km of the Atmosphere," AGARD ograph 267, North Atlantic Treaty Organization, Available from NTIS.

Lewellen, W. S., R. I. Sykes and D. Oliver (1982); "The Evaluation of MATHEW/ADPIC as a Real-Time Dispersion Model," NUREG/CR-2199.

Lewellen, W. S., R. I. Sykes, S. F. Parker, and A. K. Varma (1983); "Second-Order Closure Model Exercise for the Kincaid Power Plant Plume," EPRI EA-3079, Electric Power Research Insti .e.

Liu, M. Ko, Durran, D., Munchkur, P., Yocke, M. A., and Ames, J. (1976); "The Chemistry, Dispersion and Transport of Air Pollutants Emitted from Fossil Fuel Power Plants in California: Data Analysis and Emission Impact Model," EF76-18R, Systems Applications, Inc., San Rafad, CA, PB-264822.

Liu, M. K., D. A. Stewart and P. M. Roth (1978); "A Study of the DEPICT Model," EF 77-100R, Systems Applications, Inc., San Rafael, CA.

Liu, M. K. and D. Durran (1977); "The Development of a Regional Air Pollution Model and its Application to the Northern Great Plains," EPA-908/1-77-001. Systems Applications, Inc., San Rafael, CA.

Liu, M. K. and M. A. Yocke (1978); "Modeling Wind Distributions over Complex Terrain," SAI No. EF 78-78.

Londergan, R. J., J. J. Mangano, N. E. Bowne, D.R . Murray, and N. Borenstein (1980; "An Evaluation of Short-term air Quality Models Using Tracer Study Data," American Petroleum Institute. Report 4333, Vols. I and II.

Long, P. E. and W. A. Shaffer (1975); "Some Physical and Numerical Aspects of Boundary Layer Modeling," NOAA Tech Memo NWS TDL-56.

Long, P. E., W. A. Shaffer and F. E. Kemper (1978); NOAA Technical Memorandum, NWS TDL-66.

Ludwig, F. L. and W. F. Dabberdt (1972); "Evaluation of the APRAC-1A Urban Diffusion Model for Carbon Monoxide," Final Report, Contract CAPA-3-68 (1-69), SRI International.

Ludwig, F. L. ad S. Obinata (1974); "APRAC2 Air Pollution Dispersion Model EPA,"Air and Hazardous Materials Division, San Francisco, CA, PB-283 263/2ST.

Luna, R. E. and H. W. Church (1969); "DIFOUT: A Model for Computation of Aerosol Transport and Diffusion in the Atmosphere," Sandia Laboratories, SC-RR-68-555.

Lyons, W. A. (1977); "Mesoscale Air Pollution Transport in Southeast Wisconsin," EPA-600/4-77-010.

Lyons, W. A., E. R. Sawdey, J. A. Schuh, R. H. Calby and C. S. Keen (1981);"An Updated and Expanded Coastal Fumigation Model," Air Pollution-Control Association paper 81-314.

Lyons, W. A., J. A. Schuh and M. McCumber (1979); "Comparison of Observed Mesoscale Lake Breeze Wind Fields to Computations using the University of Virginia Mesoscale Model," Fourth Symposium on Turbulence Diffusion and Air Pollution, Jan. 15-18, 1979, Reno, NV, Amer. Meteor. Soc., Boston, MA.

McCumber, M. C., et al. (1978); "The University of Virginia Mesoscale Model," Report No. UVA-ENV SCI-MESO-1978-1.

McNider, R. T. (1981); "Investigation of the Impact of Topographic Circulations on the Transport and Dispersion of Air Pollutants," Ph.D. Dissertation, Dept. of Environmental Sciences, U. of VA, 210 pp.

McNider, R. T. and R. A. Pielke (1980); "Nocturnal Jet Development Over Sloping Terrain and Implications for Pollutant Transport," Proceedings of Symposium on Intermediate Range Atmospheric Transport Processes and Technology Assessment, Union Carbide, CONF-801064.

Mahrer, Y. and R. A. Pielke (1975); "A Numerical Study of the Air Flow over Mountains using the Two-Dimensional Version of the University of Virginia Mesoscale Model," J. Atmos. Sci., 32, pp. 2144-2155.

Mahrer, Y. and R. A. Pielke (1977); "The Effects of Topography on Sea and Land Breezes in a Two-Dimensional Numerical Model," Monthly Weather Review, 105, pp. 1151-1162.

Mahrer, Y. and R. A. Pielke (1978); "A Test of an Upstream Spline Interpolation Technique for the Advective Terms in a Numerical Mesoscale Model," Monthly Weather Review, 106, pp. 818-830.

Mahrer, Y. and R. A. Pielke (1976); "Numerical Simulations of the Airflow over Barbados," Monthly Weather Review, 104, pp. 1392-1402.

Mahrer, Y. and M. Segal (1979); "A Numerical Study of the Air Flow over Israel Using a Two-Dimensional Mesoscale Model," Fourth Conference on Numerical Weather Predictions, Amer. Meteor. Soc., pp. 259-258.

Martin, C. L. and R. A. Pielke (1983); "The Adequacy of the Hydrostatic Assumption in Sea Breeze Modeling over Flat Terrain." J. Atmos. Sci., 40, 1471-1481.

Mellor, G. L. and T. Yamada (1974); "A Hierarchy of Turbulence- Closure Models for Planetary Boundary Layer," J. Atmos. Sci., 31, pp. 1791-1806.

Mellor, G. L. and T. Yamada (1977); Turbulent Shear Flows, Pennsylvania State University State College, PA, 6.1-6.14.

Mills, M. T. et al. (1981); "Evaluation of Point Source Dispersion Models," EPA-450/4-81-032, TEKNEKRON Research Inc., 274 pp.

Moore, R. E. (1977); "The Airdos-II Computer Code for Estimating Radiation Dose to Man from Airborne Radionuclides in Areas Surrounding Nuclear Facilities," ORNL-5245, ORNL, Oak Ridge, TN, 159 pp.

Morris, C. S., C. W. Benkley and A. Bass (1979); "Development of Mesoscale Air Quality Simulation Models, Vol. 4, User's Guide to Mesogrid (Mesoscale Grid) Model. Environmental Protection Agency, EPA 600/7-79-XXX. Research Triangle Park, N.C., 118 pp.

Murphy, B.D., J. H. Novak, and D. B. Turner (1976); "An Efficient Gaussian-Plume Multiple Source Air Quality Algorithm," Journal of the Air Pollution Control Association, 26 (6), pp. 570-575.

Ott, W. R. (Ed.); Proceedings of the EPA Conference on Environment Modeling and Simulation, 1976, EPA 600/7-76-016.

Otter, J. M. and D. K. Chung (1977); "Comradex 4: Evaluator of Potential Radiological Doses in the Near (< 10 km) Environment of Radioactive Release," ORNL, RSIC Report CCC-332.

Pasquill, F. (1961); "The Estimation of the Dispersion of Windborne Material," Met. Mag., 90, pp. 33.

Pasquill, F. (1974); Atmospheric Diffusion, Second Edition, Halstead Press, John Wiley and Sons, New York.

Pasquill, F. (1976); "Atmospheric Dispersion Parameters in Gaussian Plume Modeling. Part II. Possible Requirements for Change in the Turner Workbook Values," Environmental Protection Agency, EPA-600/4-76-030b.

Patnaik, P. C. (1978); "A Preliminary User's Guide for SIGMET Mesoscale Meteorological Code," SAI Report No. SAI-78-703-LJ, Dept. of Energy Report RLO/244-77/9.

Pepper, D. W. and A. J. Baker (1979); "A Simple One-Dimensional Finite Element Algorithm with Multi-Dimensional Capabilities," Num. Heat Transfer 2, pp. 81-95.

Pepper, D. W. and A. J. Baker (1980); "A High-Order Accurate Numerical Algorithm for Three-Dimensional Transport Prediction," Computers and Fluids, 8, pp. 371-390.

Pepper, D. W., C. D. Kern and P. E. Long, Jr. (1976); "Modeling the Dispersion of Atmospheric Pollution Using Cubic Splines and Chapeau Functions," DP-MS-76-83. J. Atm. Env., 13, pp. 223-237.

Pepper, D. W. (1981); "Results from the Savannah River Laboratory Model Validation Workshop, 19-21 November 1980," Fifth Symposium on Turbulence, Diffusion, and Air Pollution, Amer. Meteor. Soc., March 1981.

Phillips, G. T. (1978); "A Preliminary User's Guide for the NOABL Objective Analysis' Code," SAI Report No. SAI-78-769-LJ, RLO/2440-77/10.

Pielke, R. A. (1974); "A Three-Dimensional Numerical Model of the Sea Breezes," Monthly Weather Review, 102, pp. 115-139.

Pielke, R. A. and Y. Mahrer (1975); "Representation of the Heated Planetary Boundary Layer in Mesoscale Models with Coarse Vertical Resolution," J. Atmos. Sci., 32:12, pp. 2288-2308.

Pielke, R. A. and Y. Mahrer (1978); "Verification Analysis of the University of Virginia Three-Dimensional Mesoscale Model Prediction over South Florida for July 1, 1973," Monthly Weather Review, 106:11.

Pielke, R. A. and E. Kennedy (1980). "Mesoscale Terrain Features" Reps. UVA-ENV SCI-MESO - 1980-1, University of Virginia.

Powell, D. C., D. J. McNaughton, L. L. Wendell and R. L. Drek (1979); "A Variable Trajectory Model for Regional Assessments of Air Pollution from Sulfur Compounds," PNL-2734. Battelle, Pacific Northwest Laboratory, Richland, VA.

Powell, D. C. et al. (1979); "Mesodiff-II: A Variable Trajectory Plume Segment Model to Assess Ground-level Air Concentrations and Deposition of Effluent Releases from Nuclear Power Facilities," NUREG/CR-0523, PNL-2419.

Ramsdell, J. V. and G. F. Athey (1981); "MESOI: An Interactive Lagrangian Trajectory Puff Diffusion Model," Battelle Pacific Northwest Lab., PNL-3998.

Rao, K. S. (1981); "Analytical Solutions of a Gradient Transfer Model for Plume Deposition and Sedimentation, ATDL Report 81/4, NOAA Atmospheric Transport and Diffusion Laboratory, Oak Ridge, TN.

Riley, F. F., et al. (1979); "A Numerical and Experimental Study of Stably Stratified Flow around Complex Terrain," PB-262, 540/8ST.

Ross, B. B. and I. Orlanski (1982); "The Evolution of an Observed Cold Front. Part I: Numerical Simulation," J. Atmos. Sci., 39, pp. 296-327.

Ruff, R. E., H. S. Javitz and J. S. Irwin (1979); "Development and Application of a Statistical Methodology to Evaluate the Realtime Air Quality Model (RAM), AMS/APCA Second Joint Conference on Applications of Air Pollution Meteorology, 1980; (also see 4 volume SRI report on Project 6868, "Evaluation of the Real-Time Air-Quality Model using the RAPS Data Base," April 1979).

Runchal, A. K., W. R. Goodin, and K. J. Richmond (1979); "Development and Validation of a Lagrangian, Random-Walk Model for Atmospheric Dispersion," TN-LA-38, Dames and Moore, Advanced Technology Group. Los Angeles, CA.

Sagendorf, J. F. and J. T. Goll (1977); "XOQDOQ Program for the Meteorological Evaluation of Routine Effluent Releases at Nuclear Power Stations," NUREG-0324, Sept. 1977, Nuclear Regulatory Commission, Washington, DC.

Sasaki, Y. (1970); "Some Basic Formalisms in Numerical Variational Analysis," Monthly Weather Review, 98, pp. 875-898.

Sedefian, L. and E. Bennett (1980); "A Comparison of Turbulence Classification Schemes," Atmospheric Environment, 14, pp. 741-750.

Segal, M., R. T. McNider, D. S. McDougal and R. A. Pielke (1982); "A Numerical Model Study of the Regional Air Pollution Meteorology of the Greater Chesapeake Bay Area - Summer Day Case Study," Atmospheric Environment 16, 1381-1397.

Segal, M. and R. A. Pielke (1981); "Numerical Model Simulation of Biometeorological Heat and Conditions--Summer Day Case Study for the Chesapeake Bay Area," Journal of Applied Meteorology 20(7), pp. 735-749.

Shannon, J. D. (1981); "A Model of Regional Long Term Average Sulfur Atmospheric Pollution, Surface Removal and Net Horizontal Flux," Atmospheric Environment, 15, pp. 689-701.

Sherman, C. A. (1978); "A Mass Consistent Model for Wind Fields over Complex Terrain," Journal of Applied Meteorology, 17 (3), pp. 312-319.

Sklarew, R. H., A. J. Fabrick and J. E. Prager (1971); "A Particle-in-Cell Method for Numerical Solution of the Atmospheric Diffusion Equation, and Applications to Air Pollution Problems, Systems, Science and Software," La Jolla, CA., SSR-844.

Slade, D. H. (Ed.), (1968); "Meteorology and Atomic Energy," U.S. Atomic Energy Commission, Div. Tech. Inf.

Smith, F. B. (1968); "Conditioned Particle Motion in a Homogeneous Turbulent Field," Atmospheric Environment, 2, pp. 491-508.

Start, G. E. and L. L. Wendell (1974); "Regional Effluent Dispersion Calculations Considering Spatial and Temporal Meteorological Variations," NOAA Tech Memo, ERLARL-44.

Strenge, D. L., E. C. Watson and J. C. Droppo (1976); "Review of Calculational Models and Computer Codes for Environmental Dose Assessment of Radioactive Releases," Battelle, Pacific Northwest Laboratory, Richland, WA, BNWL-B-454.

Tapp, M.C. and P. W. White (1976);"A Nonhydrostatic Meso-Scale Model," QJRMS 102, pp. 277-296.

Tran, K. T. and C. Y. Liu (1981); "Development of a Predictive Dispersion Modeling System for Realtime Emergency Applications," 5th Symposium on Turbulence, Diffusion and Air Pollution, Amer. Meteor. Soc., March 9-13, 1981, Atlanta, GA. Extended Abstracts.

Tran, K. T. and R. C. Sklarew (1979); "User's Guide to IMPACT: An Integrated Model for Plumes and Atmospheric Chemistry in Complex Terrain," Form and Substance, Inc. 875 Westlake Blvd., Suite 212, Westlake Village, CA 91361.

Turner, D. B. (1970 revised); "Workbook of Atmospheric Dispersion Estimates," U.S.D.H.E.W., Environmental Health Service.

Turner, D. B. (1979); "Atmospheric Dispersion Modeling-A Critical Review," Journal of the Air Pollution Control Association, 29, pp. 502-519.

Warner, T. T. (1981); "Verification of a Three-Dimensional Transport Model Using Tetroon Data from Project STATE," Atmospheric Environment, 15, pp. 2219-2222.

Warner, T. T., R. A. Anthes and A. L. McNab (1978); "Numerical Simulations with a Three-Dimensional Mesoscale Model," Monthly Weather Review, 106, pp. 1079-1099.

Weber, A. H., M. R. Buckner (1982), J. H. Weber; "Statistical Performance of Several Mesoscale Atmospheric Dispersion Models", Journal of Applied Meteorology, 20, 1633-1644.

Webster, R. D., R. L. Welsh and P. K. Terkonda (1978); "AIRMOD - A General Program for the Rapid Assessment of Airborne Pollutants," Construction Engineering Research Laboratory, Champaign, Ill., U.S. Army, AD-A058-569/5ST.

Wilkie, W. and S. Garry (1981); "Emergency Data Management System User's Manual," Radiological Assessment Systems for Nuclear Power (RAS/NUC), Roswell, GA.

Woodard, K. (1975); "Real Time Operating Plant Meteorological Data Processing and Dose Assessment Using a Minicomputer," Transaction of the American Nuclear Society, 1975 Winter Meeting, Vol. 22.

Yamada, T. (1978a); "Three-Dimensional, Second Order Closure Numerical Model of Mesoscale Circulation in the Lower Atmosphere: Description of the Basic Model and an Application to the Simulation of the Environmental Effects of a Large Cooling Pond," ANL/RER-78-1.

Yamada, T. (1978b); "A Three-Dimensional Second Order Closure Numerical Model of Mesoscale Circulation in the Lower Atmosphere," Report ANL/RER-78-1, ANL, Argonne, IL.

Yamada, T. (1979); "An Application of a Three-Dimensional Simplified Second-Moment Closure Model to Study Atmospheric Effects of a Large Cooling-Pond," Atmospheric Environment, Vol. 13, pp. 693-704.

Yanskey, G. R., E. H. Markee and A. P. Richter (1966); Climatography of the National Reactor Testing Station. IDO-12048.

Yocke, M. A. and M. K. Liu (1978); "Modeling Wind Distributions over Complex Terrain," Systems Applications, Inc., San Rafael, CA, EF 78-78.

Young, G. S. and R. A. Pielke (1983). Application of Terrain Height Variance Spectra to Mesoscale Modeling. J. Atmospheric Science, 40, 2555-2560.

Zannetti, P. (1980); "A New Gaussian Puff Algorithm for Non-Homogeneous Non-Stationary Dispersion in Complex Terrain," NATO/CCMS Meeting, Amsterdam, November 1980.

Appendix A

THE INFLUENCE OF MESOSCALE WIND FLUCTUATIONS ON ATMOSPHERIC DISPERSION

I. Introduction

Most existing models of atmosphere dispersion implicitly assume that transport by some mean wind can be clearly separated from diffusion by turbulence. This is based on an assumed spectral gap between high frequency wind fluctuations which induce diffusion and the low frequency variations of the transporting wind. Although there is evidence of reduced wind energy in the frequency range of a few cycles per hour, exhibited by Van der Hoven (1957), there seldom is a complete absence of energy in this mesoscale range. In fact, in the presence of mesoscale forcing such as convective cloud activity or specific terrain features this range may be expected to be quite active. Under certain conditions wind fluctuations in this midrange may contribute to either diffusion or transport, but often they will contribute more to an unpredictability of plume dispersion. In this Appendix we will discuss qualitatively the different interactions wind fluctuations may have with a plume. By reference to actual wind spectra we will demonstrate that the uncertainty introduced into concentration samples over time periods as long as an hour may be quite significant. This provides an upper bound on the accuracy which may be achieved by real-time dispersion models.

We first discuss the difference between an ensemble average and a time average because of the key role this distinction has in determining predictability. We can then make the distinction between diffusion in ensemble space and diffusion in real space. These ideas are then used to superimpose different plume interaction boundaries on a real wind spectrum.

II. The Distinction between Ensemble Average and Time Average

The atmospheric fluxes of mass, momentum and energy are at least partially composed of motions that are too small to ever hope to be resolved in urban or mesoscale models. These turbulent fluxes control the interaction of the atmosphere with the surface and the dispersal of anything released within the atmosphere. Such mesoscale phenomena as the sea-breeze circulation, mountain-valley circulations, and the moisture build-up in the boundary layer necessary to drive convective clouds are all dominated by turbulent interactions with the surface. This is perhaps most evident in the simulations of the dispersal of passive tracers in the atmosphere where almost all the motions responsible for dispersion are unresolvable in any meteorological model of the region of interest.

In addition to the question of what scale of motion can be resolved by a feasible grid system, there is the question of how much of the motion we wish to resolve. Flow in the atmospheric boundary layer inherently contains a turbulent stochastic component. Even if one were able to accurately simulate all of the scales of motion in time and space for one particular realization, this would not provide a precise prediction of the motion in time and space for any other particular realization. In general, what we would like to simulate is the ensemble mean flow distribution in time and space. We would also like to gain some information about the variability of particular realizations from this mean. Model simulations either involve ensemble averaging of the equations or averaging of the simulations realized. For nonhomogeneous, nonstationary problems the choice of scales to average over is an important part of the problem. The larger the scales over which the equations are averaged the more uncertainty introduced by the closure approximations, but the smaller the scales the larger the computational requirements and the more averaging which must be done after the simulation to provide proper interpretation of the results.

The ensemble of flows of interest are all the possible flows which satisfy the prescribed input data. In ideal problems this input data may be sufficient to relatively tightly constrain this ensemble of flows, but in attempts to simulate dispersion in local meteorological flows which occur at a specific time and place the input data is unlikely to provide tight constraints. Such simulations must be able to deal with relatively large variances from the resulting ensemble mean solution.

The standard ensemble average concentration may be defined as

$$\langle C(\underline{x},t)\rangle = \int_{\Omega} C_{\alpha}(\underline{x},t)p(\alpha)d\alpha \qquad (A.1)$$

where Ω is the set of all fields which satisfy the prescribed input conditions and $p(\alpha)$ is the probability density function of any particular field indicated by α.

We can also define a time average as

$$\overline{C_{\alpha}(\underline{x},t)}^{T} = \frac{1}{T}\int_{t-T/2}^{t+T/2} C_{\alpha}(\underline{x},t)dt \qquad (A.2)$$

which can be different for each realization. The expected deviation σ_c between $\langle C\rangle$ and $\overline{C}^T$ can be written as

$$\sigma_c^2 = \int_{\Omega}\left(\frac{1}{T}\int_{t-T/2}^{t+T/2} C_{\alpha}(\underline{x},t)dt - \langle C(\underline{x},t)\rangle\right)^2 p(\alpha)d\alpha \qquad (A.3)$$

The time average of the ensemble average is

$$\langle\overline{C}\rangle^{T} = \frac{1}{T}\int_{t-T/2}^{t+T/2}\int_{\Omega} C_{\alpha}(\underline{x},t)p(\alpha)d\alpha dt \qquad (A.4)$$

which is also equal to the ensemble average of the time average since these two operations commute.

As discussed by Venkatram (1979) the ratio of $\sigma_c/\langle\overline{C}\rangle^T$ provides a good measure of the predictability of any particular time-averaged sample. Venkatram attempted to estimate this measure under conditions for which the mesoscale gap in the spectral distribution of wind fluctuations remains valid. His estimate under these ideal conditions is

$$\frac{\sigma_c}{\langle\overline{C}\rangle^T} = \left[\frac{2(\Gamma-1)\ell}{uT}\right]^{1/2} \qquad (A.5)$$

where Γ is the ratio of the ensemble average instantaneous peak concentration of $\langle\overline{C}\rangle^T$, ℓ is the dominant turbulent eddy scale in the stream-wise direction, and u is the mean wind speed at some appropriate height. His subsequent numerical estimates were based on Gifford's (1959, 1970) observations of Γ. Even under his ideal conditions, he estimates that less than half of the hourly averaged concentrations resulting from a tall stack emitting into a convective boundary layer may be expected to lie within a factor-of-two of the ensemble mean value. The assumed 5 minute time scale of the turbulence is not sufficiently smaller than the 1 hour sampling time to average out the randomness of the flow. This problem is compounded when wind fluctuations of a lower frequency exists which cannot be incorporated in the transporting winds.

III. The Range of Interactions between a Plume and Wind Fluctuations

The velocity variance determines the dispersion of a passive tracer in the flow. It is generally recognized that the high frequency velocity motions are responsible for the diffusion of a tracer as a puff of tracer material is transported by the low frequency velocity motions. What is not so well recognized is that intermediate range motions may either diffuse the puff or introduce an uncertainty in the transport of the puff. All of the variance

serves to spread the puff in ensemble space but only the motions of a scale less than the scale of the puff serve to diffuse the instantaneous puff. The rest of the ensemble spread manifests itself as a meander of the plume.

The contributions of these meanders to the diffusions of a time-averaged puff are determined by the relative time scale of the meanders and the sampling time. A mesoscale gap in the wind energy spectrum, often evoked as justification for a distinct division between mean, transporting winds, and fluctuating, diffusing winds, is generally not as pronounced as theoreticians would desire. The wind energy spectrum from the 100m level of a tower at the Kincaid power plant site in Illinois is given in Fig. A.1 for three 3-week periods in 1980-1981 as taken from Lewellen, Sykes, and Parker (1983). Some interaction boundaries have been sketched on the spectrum to indicate what part of the spectrum may be expected to contribute to different effects.

Line A is intended to represent the bound of motions included in the mean transport of the plume. The motions at frequencies less than this bound must be adequately resolved so that the transport of a plume element may be tracked. There must be a consistency between the time for which the plume is tracked and the spatial resolution of the wind motion. In Figure A.1 the transition between transport and turbulence has been arbitrarily placed at f_t=0.5 cycle/hour. This would permit a 4 m/s mean wind to transport the plume approximately 30 km before spatial correlation between the transporting wind at the tower and at the plume is lost. The shape of line A is symbolic of the fact that there is not a discontinuous break at this bound, but rather there is a transition range of frequencies over which the ability to include the wind energy into the mean transport is lost.

Line B represents the lower frequency bound of the energy which can be included as part of the ensemble turbulence. B should complement A in such a way as to assure that there is no source or sink of wind kinetic energy in this transition from mean transport winds to turbulent winds.

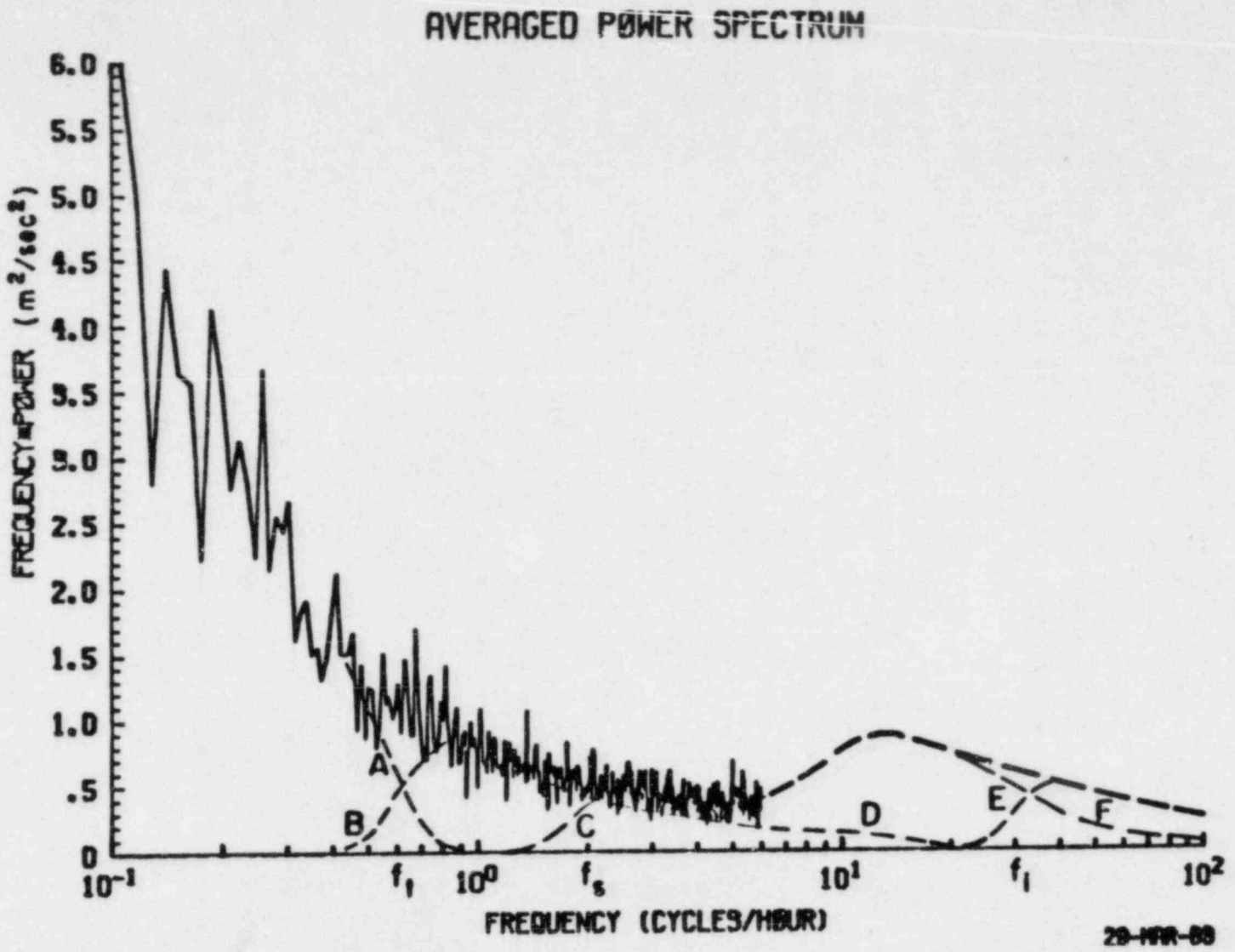

FIGURE A.1 - Spectrum of the horizontal wind fluctuations at the Kincaid site (from Lewellen et.al.,1983) with the dashed lines, A, B, C, D, E, and F indicating the boundaries of different interactions between the plume and the atmospheric motions. These interactions are discussed in the text.

At the high frequency end of the spectrum, line E represents the lower bound of motions which contribute directly to the diffusion of the instantaneous plume. Line F represents the upper bound on motions which contribute to the total ensemble variance of the concentration. Higher frequencies contribute to the dissipation of the variance rather than its production. The larger the spatial spread of the instantaneous plume, the lower the frequency which can contribute either to the diffusion of this instantaneous plume or the dissipation of the concentration variance. Thus, lines E and F will move to the left to lower frequencies as the plume spreads downstream. The turbulent kinetic energy between B and E is responsible for the meander of the instantaneous plume. If the plume is tracked sufficiently far downwind of the stack then E may move to the left of B. If the additional spatial information is available so that the A-B boundary still correctly represents the transition from transport to turbulence, then when E crosses to the left of B it means that part of the resolvable transport motion is now contributing to the "diffusion" of the instantaneous plume.

The meander of the plume driven by the energy between boundaries B and E can contribute to either the time-averaged diffusion of the plume or to the uncertainty in the position of the time-averaged plume. The location of these boundaries C and D on Figure A.1 are determined by the sampling time period. The position of C and D sketched is arbitrarily set at a sampling frequency of twice per hour. Line C represents the bound on energy affecting the concentration level of the time-averaged sample. Motions represented by energy to the left of boundary C move the time-averaged plume around as a coherent entity rather than contributing to its diffusion. Boundary D represents the boundary between the motions which contribute to the time-averaged variance of the concentration and that which contribute to the time-averaged diffusion. Energy to the right of D contributes only to the time-averaged diffusion of the plume. We expect the contribution of energy in frequencies greater than f_s to the time-averaged variance to fall off as (f_s/f) approximately; this determines the shape of D. The shape C is harder to set but is determined by the enhanced diffusion resulting from the interaction of the small scale inner plume turbulence with the distortions of

the plume forced by the large scale motion. As sampling time is reduced lines C and D approach lines E and F, respectively.

IV. Concluding Remarks

Our purpose here is not to precisely define the shape of all the boundaries on fig. A.1, but to argue that such boundaries exist and qualitatively note the type of influence the energy bounded by the different lines has on the plume. This breakdown of the interactions of different scales of motions illustrates that some level of uncertainty is an inherent part of any plume dispersion model. Improved models will not be able to eliminate this uncertainty but should be able to provide an estimate of variability along with their predictions of the mean concentration distributions. A framework for such a model is given in Appendix B.

References

1. Gifford, F.A., (1959); "Statistical Properties of a Fluctuating Plume Dispersion Model," Atmospheric Diffusion and Air Pollution, Adv. Geophys. 6, F. Frenkiel and P.A. Sheppard, Eds., Academic Press, New York.

2. Gifford, F.A., (1970); "Peak to Mean Concentration Ratios According to a 'Top-Hat' Fluctuating Plume Model," ATDL Contribution No. 45, Air Resources Atmospheric Turbulence and Diffusion Laboratory, Oak Ridge, Tennessee.

3. Lewellen, W.S., R.I. Sykes and S.F. Parker, (1983); "Analysis of Plume Variability Based on Select Periods of the Kincaid Data Set," A.R.A.P. Report No. 495, for Electric Power Research Inst., Palo Alto, CA.

4. Venkatram, A., (1979); "A Note on the Measurement and Modeling of Pollutant Concentrations Associated with Point Source," Boundary-Layer Meteorology, 17, pp. 523-536.

APPENDIX B

ON THE USE OF CONCENTRATION VARIANCE PREDICTIONS AS A MEASURE OF NATURAL UNCERTAINTY IN OBSERVED CONCENTRATION SAMPLES

W.S. Lewellen and R.I. Sykes
Aeronautical Research Associates of Princeton, Inc.
Princeton, New Jersey

1. INTRODUCTION

In the early stages of plume dispersal by the atmosphere, the spread of the plume is often less than the length scale of the turbulence in the atmosphere. The resultant plume meander accounts for much of the plume dispersal during this stage of evolution. This meander not only contributes to the time integrated plume spread, but also produces a large statistical uncertainty in the value of a time-averaged sample, unless the sampling time is much longer than the turbulent time scale producing the meander. Since wind spectra often contain significant kinetic energy on time scales in excess of 10 minutes, we believe that surface observations sampled on the basis of hourly or shorter averages should consequently be subject to considerable scatter. This is particularly important for model evaluation studies since this phenomenon will establish a lower bound on the errors expected from any prediction of measured concentration. Under such conditions, even a model with a perfect prediction of the expected mean concentration will exhibit scatter on a plot of predicted versus measured concentrations.

We approach this question of predictability by attempting to predict the ensemble variance of the concentration, $\overline{c'^2}$, as well as the ensemble mean concentration, $\overline{C}$. This approach involves three steps: 1) the interpretation of the time-averaged variance as a measure of the expected uncertainty in sample observations, 2) the determination of the relationship between the ensemble variance and the variance in a particular time-averaged sample; and 3) the ensemble prediction of $\overline{c'^2}/\overline{C}^2$. This paper will deal with all three of the above steps. Some sample predictions of $\overline{c'^2}/\overline{C}^2$ are given both for laboratory conditions and for some meteorological conditions simulating conditions found during EPRI's Plume Model Validation Program at the Kincaid Power Plant in 1980 and 1981. Emphasis here will be placed on the actual predictions rather than on the development of the second-order closure model.

2. INTERPRETATIONS OF THE TIME-AVERAGED VARIANCE AS A MEASURE OF NATURAL UNCERTAINTY

Atmospheric motions cover a range of scales from small dissipative eddies on the order of 10^{-3} meters, to the large synoptic weather features of the order of 10^{6} meters. It is somewhat arbitrary where the break between resolved wind features and unresolved turbulent motion is placed. It is essential to average over, at least, the lower end of this spectrum of scales, particularly since the smallest scale motions tend to be random in character, and thus most susceptible to statistical analyses. These unresolved turbulent motions will induce some essentially random variation in the plume. That is, even if it were possible to introduce two separate plumes into the same resolved wind field, there would be some variance in the dynamics of the two plumes due to the unresolved turbulence. It is intuitively recognized that the stronger the ratio of turbulence to mean wind, the more uncertainty will be involved in predicting plume dispersal. This sometimes shows up in models as a lower bound on wind speed below which the model should not be used.

In order to make the estimate of the uncertainty more quantitative, it is necessary to assume some form for the concentration probability distribution function (pdf). We consider two different distributions, a clipped normal distribution and a log normal. Csanady (1973) argues persuasively that within a continuous plume, i.e., ignoring intermittency, the log of the concentration should follow a normal distribution. Hanna (1982) reported that most of the hourly concentration samples in the RAPS St. Louis data appeared to follow such a log normal distribution. The other distribution considered here is that for which the concentration itself is normally distributed, but with all of the potentially negative values replaced by a zero. This form permits a highly intermittent plume. It appears to provide a reasonable fit to the measurements by Fackrell and Robins (1982b) of the pdf obtained for concentration fluctuations in a laboratory turbulent boundary layer. These two concentration probability distributions are used to plot Figures 1 and 2, where the probability of an individual measured concentration being within a factor F of the mean value is plotted as a function of the ratio of the standard deviation of the distribution to the mean for different values of F. From Figure 1, it may be seen that if $(\overline{c'^2})^{1/2}/\overline{C} = \sigma_c/\overline{C} = 1$, then there is only a 25% chance of finding an individually measured $\overline{C}$ within a factor of 1.5 of the modeled $\overline{C}$, even if the model is perfect. For the same conditions, the chance of being within a factor of 2 is approximately 50% and the chance of being within a factor of 5 is greater than 95%. Figure 2 shows that these probabilities are smaller for the same value of $\sigma_c/\overline{C}$ when the clipped normal distribution is used. The difference is largest when the variance in the concentration is larger and when a larger factor of agreement is considered. This appears to be

To be presented at the AMS 6th Symposium on Turbulence and Diffusion, Boston, MA, March 22-25, 1983.

a result of the intermittency permitted in the distribution used to obtain Figure 2.

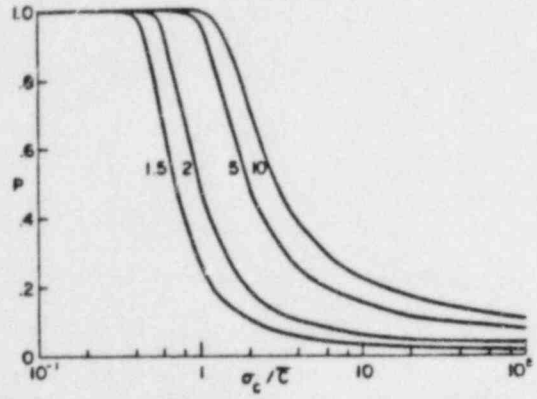

Figure 1. Probability P of finding a concentration sample within a factor F of its true mean value as a function of $\sigma_c/\bar{C}$ for a log normal probability distribution function.

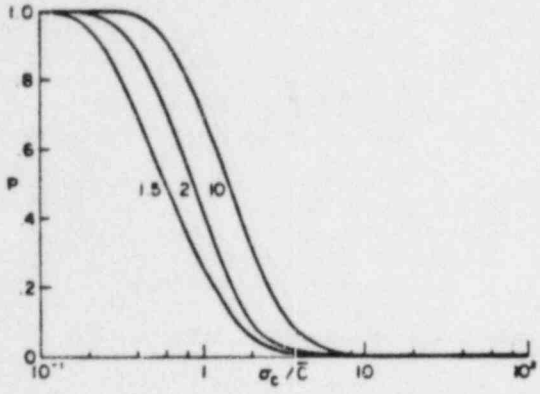

Figure 2. Probability P of finding a concentration sample within a factor F of its true mean value as a function of $\sigma_c/\bar{C}$ for a clipped normal probability distribution function.

3. RELATIONSHIP BETWEEN TIME-AVERAGED VARIANCE AND ENSEMBLE VARIANCE

The two averaging times important to the problem are the sampling time for the concentration and the sampling time for the meteorology. These two need not be the same, and have opposing effects on the concentration variance. Increasing the meteorological averaging time incorporates more of the atmospheric motion into the turbulent motion by reducing the time resolution of the "mean" wind. On the other hand, increasing the concentration sampling time allows more of the concentration fluctuations to be averaged over, thus reducing the concentration variance for the same level of turbulence. The quantitative analysis of either effect depends upon the spectrum of the turbulent velocity fluctuations.

If we make the ideal assumption of an aut- -rrelation function which varies exponent. with time, then

$$(\overline{c'^2})_\tau/\overline{c'^2} = 2\frac{T_i}{\tau}\left[1 - \frac{T_i}{\tau}(1-e^{-\tau/T_i})\right] \quad (1)$$

with τ the sampling time and T_i the integral time scale of the turbulence. Under the same assumptions

$$\sigma_{v\tau}^2/\sigma_{v_\infty}^2 = 1 - \frac{T_i}{\tau}(1-e^{-\tau/T_i}) \quad (2)$$

This ideal assumption does not cover the full range of velocity spectra expected in the atmospheric boundary layer, but it does provide a rough guide for the influence of sampling time. For small sampling times the concentration variance approaches its ensemble value while the velocity variance increases linearly with τ. At large sampling times the concentration variance is inversely proportional to τ while the velocity variance approaches its ensemble value. We will assume a sufficiently long averaging time for the meteorological measurements so that the velocity variances are essentially equal to their ensemble values and (1) can be used to relate the time-averaged concentration variance to the ensemble concentration variance.

4. AN APPROXIMATE EQUATION FOR CONCENTRATION FLUCTUATION VARIANCE

The ensemble variance of the concentration, $\overline{c'^2}$, is a variable included naturally as part of any second-order closure calculation of plume dispersal. The equation for the fluctuation variance is obtained from the diffusion equation as

$$\frac{D}{Dt}\overline{c'^2} = -2\,\overline{u_i'c'}\,\frac{\partial C}{\partial x_i} - \frac{\partial}{\partial x_i}(\overline{u_i'c'^2}) - \varepsilon_c \quad (3)$$

where u_i' is the velocity fluctuation, and $\varepsilon_c = 2\kappa(\overline{\partial c'/\partial x_i})^2 - \kappa\nabla^2\overline{c'^2}$ is the dissipation of $\overline{c'^2}$ (κ is the molecular diffusivity for C).

The second-order closure model for plume dispersal presented by Lewellen and Teske (1976) combines (3) with the mean concentration equation

$$\frac{D\bar{C}}{Dt} = -\frac{\partial}{\partial x_i}\overline{u_i'c'} \quad (4)$$

and equations for $\overline{u_i'c'}$ to close the system. In such a system it is necessary to model the last 2 terms in Eq. (3) as well as some of the terms in the equation for $\overline{u_i'c'}$. We will not present the full set of modeled equations here, but refer to Lewellen (1981) for a recent review of these equations and some of the alternative modeling choices. Instead, we present a relatively simple integral version of (3) which can be used in conjunction with a standard Gaussian plume solution to (4) to estimate the variance.

We assume a steady-state plume, and employ the parabolic equations which neglect streamwise gradients except in the mean advection term. We then combine (3) and (4) and integrate in the plane transverse to the plume to obtain

$$U\frac{\partial}{\partial x}(\langle\overline{c'^2}\rangle + \langle\bar{C}^2\rangle) = -\langle\varepsilon_c\rangle \quad (5)$$

where angular brackets denote the cross-plane integral. If we now assume that $\overline{c'^2}$ and $\overline{C}$ both have a Gaussian profile in cross-section with spread σ in the horizontal and vertical directions, we obtain

$$U \frac{\partial}{\partial x} \left[\sigma^2 \left(\hat{c}^2 + \frac{C_m^2}{2}\right)\right] = \frac{\langle \varepsilon_c \rangle}{2\pi} = -\sigma^2 \frac{\hat{c}^2}{\tau_c} \tag{6}$$

where $\hat{c}^2$ and C_m are the maximum values of $\overline{c'^2}$ and $\overline{C}$ and the dissipation is modeled as inversely proportional to τ_c, the dissipation time scale for $\overline{c'^2}$. For this integral model, we will use the recent laboratory study of concentration fluctuations by Fackrell and Robins (1982 a,b) to aid in estimating τ_c.

Fackrell and Robins (1982a) (FR) show that the early stages of plume growth from a small source are dominated by the meandering of the plume. Using the fluctuating plume model of Gifford (1959), FR obtain good predictions of concentration variance in comparison with data. Giffords' model requires prediction of inner and outer scales for the plume; these are the instantaneous and time-averaged plume width, and FR use the velocity spectrum integral formulations of Hay and Pasquill (1959) and Smith and Hay (1961) for the outer and inner scales, respectively.

The outer plume scale can be identified with σ in the foregoing analysis, and we will assume that σ is determined from an independent equation such as Hay and Pasquill (1959) or, in the results presented below, from a second-order closure approximation (Lewellen, Sykes, Varma & Parker (1982)). We still need to calculate σ_i, since $\overline{c'^2}$ occurs on this inner scale and therefore the dissipation time scale should be obtained from σ_i in the early stages. In keeping with our attempts to devise a simple equation for $\overline{c'^2}$, we replace the Smith and Hay equation for σ_i by

$$\frac{U d\sigma_i}{dX} = q_i = \alpha q_o \left(\frac{\sigma_i}{\Lambda_o}\right)^{1/3} \tag{7}$$

where q_o^2 is the total tu bulent energy, Λ_o is the length scale of the turbulence, and α is a constant. Essentially, q_i is a measure of the turbulent velocity fluctuations on the scale σ_i, and the one third power law scaling arises from the assumption that σ_i lies in the inertial range of the turbulent energy spectrum. This equation gives the same qualitative features as the spectral integral, i.e., linear initial growth followed by a range proportional to $x^{3/2}$. Thus, σ_i will be smaller than σ in the early stages, then will grow more quickly and finally exceed σ. When σ_i exceeds σ, the inner scale is set equal to the outer scale, and the plume meander phase is ended.

The dissipation time scale τ_c is set equal to $\beta\sigma_i/q_i$ where β is a constant to be determined, but q_i is limited to be less than q_o. Figure 3 shows that the choice of α=0.28 and β=0.39 permits the present mo l to compare favorably with the experimental observations of FR for different initial plume sizes introduced into their turbulent boundary layer.

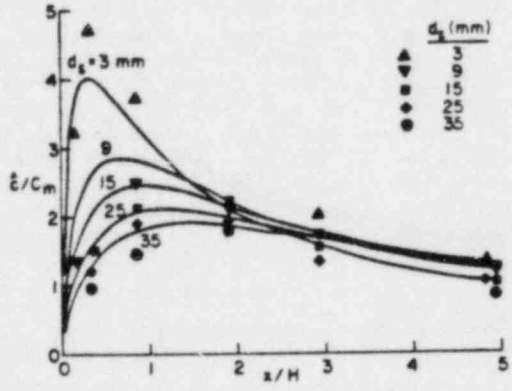

Figure 3. Comparison of model predictions with the observations of Fackrell and Robins (1982b) for the relative intensity of concentration fluctuations for an elevated source of various diameters, d_s, within a laboratory turbulent boundary layer as a function of normalized downstream distance.

5. SAMPLE PREDICTION OF THE NATURAL VARIABILITY FOUND DURING EPRI'S PLUME MODEL VALIDATION PROGRAM

As a part of EPRI's Plume Model Validation Program (Hilst (1978)), we have simulated plumes dispersed by a number of different meteorological conditions found at the Kincaid Power Plant in 1980 and 1981 using our full second-order closure model. Complete results of this study will be discussed elsewhere (Lewellen et al. 1982). Here we wish to discuss only one case, a case of light winds and unstable convective conditions, using the simple model developed in the last section.

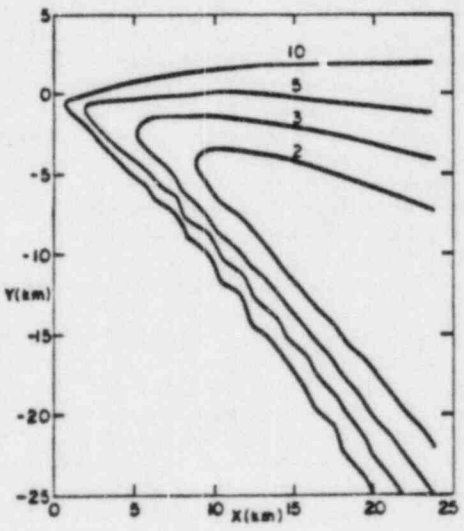

Figure 4. Prediction of surface contours of the ensemble value of $\sigma_c/\overline{C}$ downwind of the Kincaid Power Plant on 7/24/80 (1000-1400).

Figure 4 presents the surface contours of $\sigma_c/\overline{C}$ obtained from this model when it is used to simulate a quasi-steady 4 hour period of the plume from 1000 to 1400 on July 24, 1980. Large values of $\sigma_c/\overline{C}$ are predicted. This is particularly true close to the stack and in the edges of the plume. Even with a relatively large reduction due to time averaging over a period significantly larger than the time scale of the fluctuations, this still suggests regions of large natural variability.

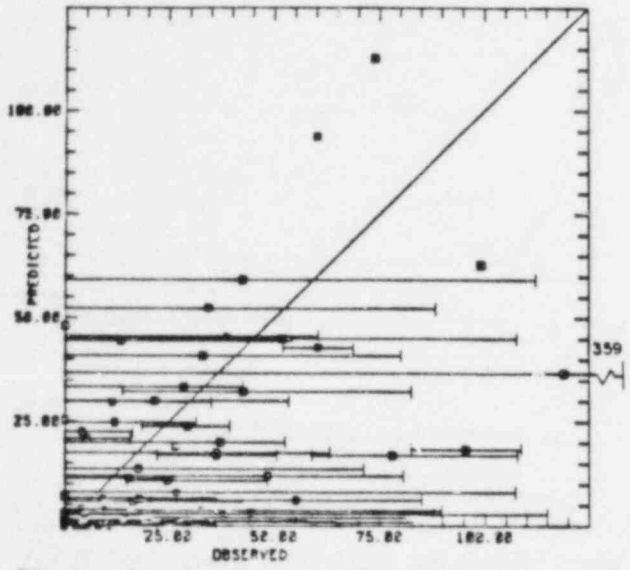

Figure 5. Comparison of prediction and observations of the average value of SF_6 at a number of surface samplers for the period 1000-1400, 7/24/80. Bars attached to the data represent the spread between the lowest and highest hour observations during this period. Predictions are taken from Lewellen et al. 1982.

Figure 5 is a scatter plot of predictions versus observations for 1 hour samples of a tracer, SF6, released from the stack during this period. The surface samplers are scattered out to approximately 20 km from the stack with the observed maximum occurring 7 km from the stack. The spread bars on the observations represent the spread between the highest hourly value and the lowest hourly value during that period. Samples without spread bars represent stations where only one hourly reading was available for the 4 hour period.

There is qualitative agreement between the data scatter observed in Figure 5 and the natural variability implied by Figure 4. A more quantitative comparison requires both an estimate of the correlation time to be used in Equation 1 and an estimate of the appropriate probability distribution function. The simplest estimate of T_1 is to take it as equal to the longitudinal integral time scale of the horizontal velocity fluctuations which for this time should be approximately 5 minutes. According to Figure 3, this should result in the hour averaged σ_c being approximately 15% of the ensemble value predicted by Figure 4. This still leaves values of $\sigma_c/\overline{C}$ sufficiently large that either of the pdfs represented by Figure 1 or 2 should produce scatter approaching that given in Figure 5. However, the spread bars in Figure 5 which extend from zero to values of 100 or more are hard to explain in terms of a 5 minute time scale. There appear to be more of these than could be expected on the basis of each 5 minute average being independent of the other. There is the strong suggestion of significant contributions to the spectrum of concentration fluctuations from a longer time scale such as would occur if the large scale convective eddies are aligned with the wind to form longitudinal vortices as often occurs.

6. CONCLUDING REMARKS

We have presented an analytical framework for estimating expected natural uncertainty for plume dispersal. Although considerable work will be involved in improving the quantitative precision of the 3 separate steps involved, even the present crude estimates should provide a valuable input into current model validation programs.

7. ACKNOWLEDGEMENTS

This work was supported by NRC with R.F. Abbey as project manager and by EPRI with G.R. Hilst as project manager. We also thank Systems Applications, Inc. for preparation of Figure 5.

8. REFERENCES

Csanady, G. T., 1973: Turbulent Diffusion in the Environment. D. Reidel Publishing Co. 248 pp.

Fackrell, J. E., and A. G. Robins, 1982: The effects of source size on concentration fluctuations in plumes. Boundary-Layer Met., 22, 335-350.

_____, 1982b: Concentration fluctuations and fluxes in plumes from point sources in a turbulent boundary layer. J. Fluid Mech., 117, 1-26.

Gifford, F. A., 1959: Statistical properties of a fluctuating plume dispersion model. Adv. Geophys., 6, 117-137.

Hanna, S. R., 1982: Natural variability of observed hourly SO_2 and CO concentrations in St. Louis. Atmospheric Environment, 16, 1435-1440.

Hay, J. S., and F. Pasquill, 1959: Diffusion from a continuous source in relation to the spectrum and scale of turbulence. Adv. Geophys., 6, 345-365.

Hilst, G. R., 1978: Plume model validation. EPRI EA-917-SY, Workshop WS-78-99, Summary Report.

Lewellen, W. S., 1981: Modeling the lowest 1 Km of the atmosphere. AGARDograph No. 267, North Atlantic Treaty Organization.

_____, and M. Teske, 1976: Second-order closure modeling of diffusion in the atmospheric boundary layer. Boundary Layer Met., 10, 69-90.

_____, R. I. Sykes, S. Parker, and A. Varma, 1982: Second-order closure model exercise for the kincaid power plant plume. Report No. 473, Aeronautical Research Associates of Princeton, Inc.

Smith, F. B., and J. S. Hay, 1961: The expansion of clusters of particles in the atmosphere. Quart. J. Roy. Meteorol. Soc., 87, 89-91.

J. Fluid Mech. (1984), *vol.* 139, *pp.* 193–218
Printed in Great Britain

A turbulent-transport model for concentration fluctuations and fluxes

By R. I. SYKES, W. S. LEWELLEN AND S. F. PARKER

Aeronautical Research Associates of Princeton, Inc., 50 Washington Road, P.O. Box 2229, Princeton, New Jersey 08540

(Received 31 March 1983)

A second-order closure model describing the diffusion of a passive scalar from a small source is presented. The model improves upon the earlier work of Lewellen & Teske (1976) by ensuring the early stage of the release, the so-called meander phase, is accurately described. In addition to the mean concentration and scalar fluxes, a model equation for the evolution of the scalar variance is proposed. The latter introduces a new lengthscale which represents the scale of the concentration fluctuations. The model predictions are compared with the recent experimental data of Fackrell & Robins (1982*a*, *b*).

1. Introduction

The problem of predicting the dispersal of a pollutant in a turbulent flow is of enormous importance, and has received considerable attention from researchers. Although there is an extensive literature on the subject, practical prediction methods have not progressed much beyond the Gaussian plume formulae or the eddy-diffusivity models. There is, however, a broad basis of more fundamental research on turbulent diffusion of a scalar field, both experimental and theoretical, which can be used to provide the necessary insight to develop an improved prediction method. Most of the more fundamental theoretical methods present very severe problems in their extension to non homogeneous or time-dependent turbulent fields, so that some intermediate level is required. The second-order closure framework provides such a level, in that more of the physical processes are contained within the equations than with eddy-diffusivity models, but the equations are still considerably simpler than a spectral closure (see e.g. Leslie 1973).

A further advantage of closure at second order is the inclusion of fluctuating scalar concentration variance, since this is a second-order correlation. Given the scalar variance, and an integral timescale for the concentration fluctuations, it is possible to estimate the uncertainty in likely measured values for different averaging times. This natural variability, which should be considered for proper evaluation of atmospheric dispersion models, may be important for sampling times as long as one hour under some conditions. Knowledge of the higher-order moments of the probability density function for the scalar field can be particularly valuable in situations where instantaneous or very short time averages are important, for example in the dispersion of toxic or flammable gases, or in assessing the problem of detectable odours. In these cases, the ensemble-mean concentration may be well below the threshold value, but the locally measured value can still exceed the limit for short times and cause problems.

The application of second-order closure models to the diffusion of a scalar has

received less attention than that of the transport of momentum and heat (e.g. Lewellen 1977; Launder, Reece & Rodi, 1975; Lumley & Khajeh-Nouri 1974). The development of such a model for dispersion in the atmosphere was first given by Donaldson (1973). Lewellen & Teske (1976) presented the results of a simple second-order closure model for dispersion in the atmospheric boundary layer. Their model was able to describe the two stages of diffusion from a small source, namely the initial or meander plume where the plume dimensions grow linearly and the late phase where the plume spreads with a constant diffusivity; this behaviour is consistent with Taylor's (1921) diffusion theory. Lewellen & Teske (LT) showed how the transition between the two stages was accomplished in the model by a change in balance in the scalar flux equation. Deardorff (1978) elucidated the model dynamics by presenting an exact solution for an exponential autocorrelation in homogeneous turbulence and showing that the second-order closure model could reproduce the result. The study of El Tahry, Gosman & Launder (1981) also demonstrates the ability of second-order closure to describe scalar dispersion, but is limited in its application, since it uses an algebraic model for the fluxes, which cannot describe the early evolution from a small source.

The objective of this paper is to improve the LT second-order closure model for the mean concentration and to develop a model for the concentration variance in a non-homogeneous flow. We shall use analytical and experimental results in designing the modelled terms wherever possible, and our principal comparison with laboratory data will be the recent experiment by Fackrell & Robins (1982*a*), who measured turbulent correlations in a plume diffusing in a wind-tunnel boundary layer. We shall first discuss diffusion in homogeneous turbulence to help clarify the basic timescales of the problem. Recent experimental work by Warhaft & Lumley (1978) on the decay of homogeneous scalar variance, has shown that the scalar field introduces its own lengthscale into the dynamics. The presence of more than one timescale is also emphasized in the theoretical descriptions using spectral closure (Newman & Herring 1979), large-eddy simulation (Antonopoulos-Domis 1981), second-order closure (Newman, Launder & Lumley 1981) and random-walk simulation (Durbin 1982). Having determined the appropriate timescales and turbulence model, we shall then proceed to the non-homogeneous boundary-layer studies by Fackrell & Robins (1982*a*).

2. Diffusion in homogeneous turbulence

2.1. *Mean concentration*

We consider the diffusion of a passive scalar in a homogeneous turbulent field in the limit of large Péclet and Reynolds numbers. Let $c(x,t)$ denote the scalar field, and let the overbar represent an ensemble average. Then

$$\frac{\mathrm{D}\bar{c}}{\mathrm{D}t} = -\frac{\partial}{\partial x_i}\overline{u_i' c'}, \tag{2.1}$$

where

$$\frac{\mathrm{D}}{\mathrm{D}t} \equiv \frac{\partial}{\partial t} + \bar{u}_j \frac{\partial}{\partial x_j},$$

and a prime denotes a fluctuating quantity, e.g. $c' = c - \bar{c}$; u_i is the velocity component in the coordinate direction x_i.

The equation for the turbulent concentration flux is

$$\frac{\mathrm{D}}{\mathrm{D}t}\overline{u_i'c'} = -\overline{u_i'u_j'}\frac{\partial \bar{c}}{\partial x_j} - \overline{u_j'c'}\frac{\partial \bar{u}_i}{\partial x_j} - \frac{\partial}{\partial x_j}\overline{u_i'u_j'c'} - \frac{1}{\bar{\rho}}c'\overline{\frac{\partial p'}{\partial x_i}}, \tag{2.2}$$

where p' is the pressure fluctuation and $\bar{\rho}$ the mean density. We have assumed that the molecular dissipation term is isotropic, and therefore vanishes in (2.2).

In this section we consider the source term to consist of an instantaneous line release of zero dimension, so that at $t = 0$

$$\bar{c}(y, z, t = 0) = Q\delta(y)\,\delta(z),$$

where δ is the Dirac delta function, Q is the mass released per unit length in the x_1 direction, and we have identified y and z with the x_2 and x_3 coordinates respectively.

Deardorff (1978) shows that the exact solution should be expected to be Gaussian with a spread in the y-direction given by

$$\sigma_y^2 = 2\overline{v'^2}\tau^2\left\{\frac{t}{\tau} - 1 + \exp\left(\frac{-t}{\tau}\right)\right\}, \tag{2.3}$$

where $\sigma_y^2 = (1/Q)\int\int y^2\bar{c}(y, z, t)\,\mathrm{d}y\,\mathrm{d}z$. A similar equation holds for σ_z^2, with $\overline{w'^2}$ replacing $\overline{v'^2}$ in (2.3). The timescale τ in (2.3) is the integral timescale of the Lagrangian velocity autocorrelation function, which was assumed to be exponential. In fact, Deardorff only considered the one-dimensional diffusion problem, but it is easily extended to two dimensions with the assumption that $\overline{v'w'} \equiv 0$. The latter can always be assured by a rotation of the (y, z)-coordinate axes.

We first note that the triple-moment term does not affect the calculation of σ_y^2 or σ_z^2, as shown by Lewellen (1981), provided that the triple is modelled as a gradient term. Thus the only modelled term affecting the development of the plume lengthscales is the pressure correlation. Deardorff shows that this term needs to be modelled as

$$\frac{1}{\bar{\rho}}c'\overline{\frac{\partial p'}{\partial x_i}} = \frac{\overline{u_i'c'}}{\tau}.$$

In accordance with earlier work (Lewellen 1977), we model this term as $A(q/\Lambda)\,\overline{u_i'c'}$, where $q^2 = \overline{u_i'u_i'}$, and Λ is a turbulent lengthscale defined so that the dissipation of turbulent kinetic energy is $q^2/8\Lambda$. A is a numerical constant, which takes a value of 0.75. Note that this model is closer to that originally proposed by Donaldson (1973) than to the LT model, which used a timescale corresponding to the turbulent timescale in the region of the spectrum defined by the plume scale. The longer timescale Λ/Aq now seems more appropriate in the light of Deardorff's result. We can interpret this physically as saying that, even when the plume is very small, the diffusion is effected by large-scale meandering of the plume, so that the flux is carried by the ambient energy-containing eddies on the lengthscale Λ, having a timescale of order Λ/q. The latter ambient turbulent timescale is therefore the appropriate timescale for the pressure correlation term in the scalar flux equation, although other terms in the equations will depend on plume turbulent timescales.

The triple moment in (2.2) determines the shape of the mean-concentration profile in the early stages of the dispersion. Deardorff shows that the triple-moment term can be modelled as

$$\frac{\partial}{\partial x_j}\overline{u_i'u_j'c'} = \frac{\partial}{\partial x_j}\left(K_{jm}\frac{\partial}{\partial x_m}\overline{u_i'c'}\right). \tag{2.4}$$

where K_{jm} has to take a certain time-dependent form to ensure a Gaussian profile. In fact, the requirement can be stated more clearly when one notes that the Gaussian profile is a self-similar profile, so that all moments and correlations are diffusing at the same rate and thus preserve the shape. This means that, when we close the equations and model a diffusive term empirically, we must ensure that all the correlations are diffusing at the same rate to obtain a self-similar solution. For closure at second order, (2.4) is thus the appropriate closure with K_{jm} obtained from the diffusion of the mean concentration. In order to keep the model as simple as possible, bearing in mind our desire to extend it to more complex flows, we choose to estimate K_{jm} as

$$K_{jm} = \frac{1}{Q}\int\int (x_j \overline{u_m' c'} + x_m \overline{u_j' c'})\,\mathrm{d}y\,\mathrm{d}z. \tag{2.5}$$

This will correspond exactly to Deardorff's value in the case of homogeneous turbulence at short time, and will provide a robust estimate for more complex situations. Using this closure model, it follows from Deardorff's analysis that the equations do predict a Gaussian mean profile with the correct spread rate. This model is also different from LT, so that the latter does not predict Gaussian profiles.

At late times, LT show that the balance in equation (2.2) is between production and pressure scrambling, i.e.

$$-\overline{u_i' u_j'}\frac{\partial \bar{c}}{\partial x_j} - \frac{Aq}{\Lambda}\overline{u_i' c'} = 0,$$

so that we have gradient diffusion with an effective viscosity $K_{jm} = \overline{u_j' u_m'}\,\Lambda/Aq$. In this late-time limit the diffusivities calculated from (2.5) will yield this same value.

Our model for the mean concentration and its fluxes is therefore

$$\frac{\mathrm{D}\bar{c}}{\mathrm{D}t} = -\frac{\partial}{\partial x_i}\overline{u_i' c'},$$

$$\frac{\mathrm{D}}{\mathrm{D}t}\overline{u_i' c'} = -\overline{u_i' u_j'}\frac{\partial \bar{c}}{\partial x_j} - \overline{u_j' c'}\frac{\partial \bar{u}_i}{\partial x_j} + \frac{\partial}{\partial x_j}\left(K_{jm}\frac{\partial}{\partial x_m}\overline{u_i' c'}\right) - \frac{Aq}{\Lambda}\overline{u_i' c'}, \tag{2.6}$$

where

$$K_{jm} = \frac{\langle x_j \overline{u_m' c'} + x_m \overline{u_j' c'}\rangle}{\langle \bar{c}\rangle}$$

and $\langle \phi \rangle = \int\int \phi\,\mathrm{d}y\,\mathrm{d}z$.

Deardorff criticizes the LT model on the grounds that K_{jm} is a function of time since release. We have removed the explicit dependence on time in K_{jm}, and replaced it with a value that depends on the local state of the plume; this permits individual plumes to be treated separately. Thus the second-order closure model possesses several advantages over first-order closure. First, the diffusion process is described in terms of the more fundamental turbulence quantities rather than an empirical eddy diffusivity. Note that we have avoided the necessity to specify such an eddy diffusivity for the second-order quantities by using (2.5), which is the effective diffusivity predicted by the closure model itself. Secondly, the second-order closure provides a definite framework for extending the model to non-homogeneous or buoyancy-driven flows. Finally, a prediction of scalar variance is a natural part of the second-order closure model, so that we obtain significantly more information about the concentration distribution. As we shall demonstrate, modelling the scalar variance introduces a new lengthscale which represents the scale of the concentration fluctuations; this scale grows as the plume grows, so that the time since release is dynamically significant.

2.2. *Concentration-fluctuation variance*

There have been a number of studies, both theoretical and experimental, of the variance of concentration fluctuations. Gifford (1959) proposed a relatively simple phenomenological model for the early or meander stage of a plume in terms of two plume lengthscales but did not prescribe a method for predicting the scales themselves. Chatwin & Sullivan (1979*a*, *b*, 1980) investigated theoretically the relative diffusion of a cloud of marked particles and demonstrated that the variance depends on source size, so that it is meaningless to consider a point source. They did not include molecular dissipative effects rigorously, however, and comparison with any second-order closure result is further precluded by their examination of the relative diffusion as opposed to the ensemble average. Unfortunately, the latter is also true of their measured data, and also the data of Murthy & Csanady (1971).

Durbin (1980) used a two-particle random walk model to predict the concentration variance. His model includes the effect of small molecular diffusivity by averaging the fluctuations over a small volume. Functional forms for the one- and two-particle time and space correlations are chosen to be consistent with an inertial range at small separation, and exponential in time. Several predictions are made by homogeneous turbulence, but there is no quantitative comparison with data.

There have been a number of studies of the decay of homogeneous scalar variance, as mentioned in the introduction, but we shall concentrate on the diffusion from a small source since our main interest lies in this direction.

Fackrell & Robins (1982*b*) have recently completed Gifford's fluctuating plume model and used it to predict concentration variance $\overline{c'^2}$, which is compared with laboratory data for an elevated source in a wind-tunnel boundary layer. Gifford's model requires prediction of the outer scale of the plume, i.e. the scale over which the plume meanders, and the inner or instantaneous plume scale, i.e. the relative spread of the plume. Fackrell & Robins used the statistical formulations of Hay & Pasquill (1959) and Smith & Hay (1961) to predict these scales in terms of the measured Eulerian velocity spectra. The Smith–Hay model has been criticized by Sawford (1982) for slow growth during part of the range for a very small source, but the formulation is consistent with other approximations over most of the range. Fackrell & Robins demonstrate reasonable agreement with the observations using this simple model, indicating that the model probably contains the correct basic physics. We wish to include these processes within a second-order closure framework, and we shall therefore draw on this model to assist in the determination of closure assumptions.

The Reynolds-averaged equations for the concentration variance is

$$\frac{\mathrm{D}}{\mathrm{D}t}\overline{c'^2} = -2\overline{u_i'c'}\frac{\partial \mathscr{C}}{\partial x_i} - \frac{\partial}{\partial x_i}\overline{u_i'c'^2} - \epsilon_c, \tag{2.7}$$

where ϵ_c represents the dissipation of $\overline{c'^2}$ by molecular diffusion. Since $\overline{c'^2}$ should diffuse with the turbulent correlations, we model the triple-correlation term as in the flux equations. Thus we set

$$-\frac{\partial}{\partial x_i}\overline{u_i'c'^2} = \frac{\partial}{\partial x_j}\left(K_{ij}\frac{\partial}{\partial x_i}\overline{c'^2}\right),$$

where K_{ij} is given by (2.5).

In earlier work (LT, Lewellen 1977), ϵ_c has been modelled as $0.45\,\overline{c'^2}/\tau_c$, where τ_c is a dissipation timescale, calculated from the turbulence timescale in the region of the ambient turbulent spectrum defined by the plume scales σ_y and σ_z. This formulation is not correct, because σ_y and σ_z are the outer or meander scales, which

Fackrell & Robins show become rapidly independent of the source, while the total $\overline{c'^2}$ is largely a result of the disparity between the inner and outer scales, and the inner scale remembers its initial condition for much longer. We therefore require an inner scale, Λ_c, which we shall then use to determine τ_c.

The basis of the Smith–Hay model for the inner scale is a selective filter on the velocity spectrum, which states in effect that the inner scale will grow at a rate proportional to the scale of the velocity fluctuations in the part of the spectrum corresponding to the inner scale itself. We can derive a much simpler equation for Λ_c by assuming that the turbulent energy decays in a manner consistent with an inertial range for scales much less than the turbulent lengthscale Λ. In practical situations, some such assumption will be necessary, since turbulent spectra will not generally be available. We therefore set

$$q_c = q\left(\frac{\Lambda_c}{\Lambda}\right)^{\frac{1}{2}} \quad (\Lambda_c \ll \Lambda) \tag{2.8}$$

and

$$\frac{\mathrm{d}\Lambda_c}{\mathrm{d}t} = \alpha_1 q_c, \tag{2.9}$$

where α_1 is an $O(1)$ constant, to be determined from comparison with data. Note that (2.8) and (2.9) give the expected initially linear growth with t, followed by a region with $\Lambda_c \propto t^{\frac{3}{2}}$ (see e.g. Sawford 1982). The dissipation timescale τ_c is then constructed from q_c and Λ_c, so that our model for ϵ_c is

$$\epsilon_c = \alpha_2 \frac{q_c}{\Lambda_c} \overline{c'^2}, \tag{2.10}$$

where α_2 is a second constant.

Note that our dissipation model depends entirely upon inertial properties of the velocity field, i.e. explicit molecular-diffusivity effects are absent. This means that our model is only applicable for high-Péclet-number flows, i.e. flows in which $\Lambda_c \gg \eta_c$, where η_c is the dissipation scale $\kappa_c^{\frac{3}{4}} \epsilon^{-\frac{1}{4}}$; κ_c is the molecular diffusivity of the scalar, and ϵ is the turbulent energy dissipation rate. Λ_c must also be much larger than the Kolmogorov scale $\nu^{\frac{3}{4}} \epsilon^{-\frac{1}{4}}$, where ν is the kinematic viscosity. In the experiment of Fackrell & Robins (1981), the dissipation scales are roughly 0.1 mm, while the smallest source diameter is 3 mm.

An analytic solution for the early-time behaviour is obtained in Appendix A, and we summarize the results here. We denote by δ the source-scale to turbulence-scale ratio, i.e. $\sigma_0/\Lambda = \delta$, and define Λ/q as the unit time. Then, the production of $\overline{c'^2}$ is important only for $t < O(\delta)$; the maximum value of $\hat{c}^2/C_\mathrm{m}$ is $O(\delta^{-\frac{1}{2}})$, and occurs at $t = O(\delta^{\frac{1}{2}})$. Here $\hat{c}^2$ and C_m are the maximum values of fluctuation variance and mean concentration respectively in the plane transverse to the mean flow. These results are in good agreement with the data of Fackrell & Robins for their elevated release; they suggest that $\overline{c'^2}$ is a maximum at $t = O(\delta)$, while the maximum $\hat{c}^2/C_\mathrm{m}$ is $O(\delta^{-0.4})$ at $t = O(\delta^{0.7})$. Thus our model for the dissipation of $\overline{c'^2}$ contains the correct timescales, and we shall fix α_1 and α_2 to optimize quantitative agreement with the laboratory data of Fackrell & Robins. We emphasize that in this section we are treating the elevated releases as homogeneous turbulence; this is a good approximation for the early part of the release, and we shall show in §3 that a more complete treatment of the effect of the wall does not significantly alter the predictions of $\hat{c}^2/C_\mathrm{m}$.

Before attempting to fix α_1 and α_2, we should recognize that eventually Λ_c will grow

to be as large as Λ, so that (2.8)–(2.10) will be inappropriate. Λ_c will continue to grow, since different parts of the plume will continue to separate. Λ_c is related to Durbin's (1980) particle separation Δ, which grows like $t^{\frac{3}{2}}$ at late times, so a simple model which gives the correct asymptotic behaviour is

$$\frac{\mathrm{d}\Lambda_c}{\mathrm{d}t} = \beta_1 q \frac{\Lambda}{\Lambda_c} \quad (\Lambda_c \gg \Lambda). \tag{2.11}$$

Our philosophy here is to establish various asymptotic limits for modelled terms, and then match smoothly with the simplest type of function. In view of the complexity introduced by the presence of multiple scales, some firm idea of the behaviour in different limits is vital to the development of a physically realistic model. We now need to determine the dissipation timescale for $\overline{c'^2}$ when $\Lambda_c \gg \Lambda$. The timescale in (2.10) for $\Lambda_c \ll \Lambda$ can be derived by an inertial-range argument on the basis of Péclet-number independence, so that the spectral transfer of $\overline{c^2}$ towards large wavenumber depends only on the local values in wavenumber space. A similar argument for $\Lambda_c \gg \Lambda$ would require the knowledge of energy-spectrum decay at small wavenumbers, but it appears that local wavenumber interactions are not the principal mechanism for transfer down the spectrum when $\Lambda_c \gg \Lambda$. Rigorous analysis is, of course, virtually impossible at present, but the Test Field Model of Newman & Herring (1979) is a spectral closure giving some insight into the dynamics. The TFM predicts that in the limit $\Lambda_c \gg \Lambda$ the dominant interactions removing $\overline{c'^2}$ stuff from the Λ_c scale involve the energy-containing eddies on the scale Λ. Thus the timescale for the decay of $\overline{c'^2}$ as obtained from the TFM is $O(\Lambda_c/q)$, i.e. the large scale of the concentration fluctuations with the full turbulence energy. We therefore model the dissipation as

$$\epsilon_c = \beta_2 \frac{q}{\Lambda_c} \quad (\Lambda_c \gg \Lambda). \tag{2.12}$$

At this stage we have fixed asymptotic behaviour at both extremes of Λ_c, and introduced four empirical constants. This is somewhat misleading because Λ_c has not been defined precisely except in terms of the dissipation ϵ_c, so that there are actually only two constants. To make this clearer, and also to fix one of the constants, we consider the dispersion of a plume from a point source in decaying homogeneous turbulence. Gad-el-Hak & Morton (1979) performed such an experiment and obtained a self-similar profile of $(\overline{c'^2})^{\frac{1}{2}}/\bar{c}$ across the plume well downstream of the source. We are unable to model the initial development of the plume, since the scalar was introduced in a jet which causes the initial phase to be non-homogeneous turbulence. However, it is claimed that the jet decays very quickly and we can consider their measured profiles to represent the late stages of dispersion in homogeneous turbulence.

The second-order closure model predicts power-law decay of the turbulence energy (Lewellen 1977) and growth of the lengthscale Λ with exponents $-\frac{6}{7}$ and $\frac{3}{7}$ respectively. If we substitute these quantities into the plume equations, it is possible to obtain a self-similar form for $\overline{c'^2}$. We note that the mean concentration will spread as a Gaussian at the same rate as Λ, with the fluxes proportional to the mean-concentration gradient. The mean concentration has the similarity form

$$\bar{c}(r,t) = \frac{Q_0}{\sigma^2} \exp\left(-\frac{r^2}{\sigma^2}\right), \tag{2.13}$$

where r is the radial distance from the centre of the plume, Q_0 is a constant

proportional to the mass flux in the plume, and σ is the spread of the plume, so that $\sigma \propto t^{\frac{1}{2}}$. If we postulate a similarity form for $\overline{c'^2}$, namely

$$\overline{c'^2}(r,t) = \frac{Q_0^2}{\sigma^3} f(\xi), \tag{2.14}$$

where $\xi = r/\sigma$, we can obtain an equation for f as

$$f'' + \left(\xi + \frac{1}{\xi}\right) f' + (4 - \Gamma) f = -2\xi^2 \mathrm{e}^{-\xi^2}, \tag{2.15}$$

where Γ is a constant which depends on the Λ_c equation. If we use the large-Λ_c equations for Λ_c and ϵ_c, then

$$\Gamma = \beta_2 \left(\frac{40}{3\beta_1}\right)^{\frac{1}{2}}; \tag{2.16}$$

this choice will be justified *a posteriori*. This similarity equation has precisely the same form as that proposed by Csanady (1967), except that Csanady chose his form for ϵ_c so that he obtained the similarity equation for non-decaying turbulence. Our specification predicts no similarity for that case, but the experimental details furnished by Csanady are not sufficient to determine whether there is any real inconsistency with observations. However, the data of Gad-el-Hak & Morton do suggest similarity, and we choose the constant Γ to fit their data. Figure 1 shows the predicted form for $(\overline{c'^2})^{\frac{1}{2}}/\bar{c}$ using $\Gamma = 4.6$ and $\Gamma = 5.2$ together with the data of Gad-el-Hak & Morton. We choose to use $\Gamma = 4.6$, implying $\beta_2/\beta_1^{\frac{1}{2}} = 1.26$; this provides a reasonably good fit for the range of the data with largest errors at the origin.

As we noted earlier, this large-Λ_c formulation only involves one constant, namely $\beta_2/\beta_1^{\frac{1}{2}}$, which we have now fixed at 1.26. The small-Λ_c formulation similarly involves only one constant. There remains the problem of joining the two asymptotic regimes, and we accomplish this by making the simple postulate that the two regimes match at a certain point, say $\Lambda_c = c_0 \Lambda$. Then, from (2.8)–(2.12),

$$\beta_1 = \alpha_1 c_0^{\frac{4}{3}} \tag{2.17}$$

and

$$\beta_2 = \alpha_1 c_0^{\frac{1}{3}}, \tag{2.18}$$

so that we have three relations between the five constants α_1, α_2, β_1, β_2 and c_0 in total. There is still an arbitrary factor in the definition of Λ_c, but this is removed by setting the initial value of Λ_c equal to the initial σ_y of the plume. There are thus two more constants with which to optimize model performance; we fix α_1 and α_2, then the above relations will determine c_0, β_1, β_2.

The elevated release data of Fackrell & Robins (1982*a*) provides the evolution of $\overline{c'^2}$ and $\bar{c}$ for a range of source sizes. The latter part of the measurements are affected by the presence of the wall, but the first half is near-homogeneous flow conditions. In order to fix α_1 and α_2, we set the background turbulence values to the observed values at the source height, and solve the parabolic problem marching in the streamwise direction with the observed mean speed. The plume was initialized as a Gaussian shape $\sigma_y = \sigma_z = \frac{1}{2}d_s$, where d_s is the diameter of the source, and $\overline{c'^2}$ was set to zero initially. Λ_c is also set at $\frac{1}{2}d_s$ initially, and the background turbulence scale Λ is obtained from the empirical formula

$$\frac{1}{\Lambda} = \frac{1}{0.65 z_s} + \frac{1}{0.2H}, \tag{2.19}$$

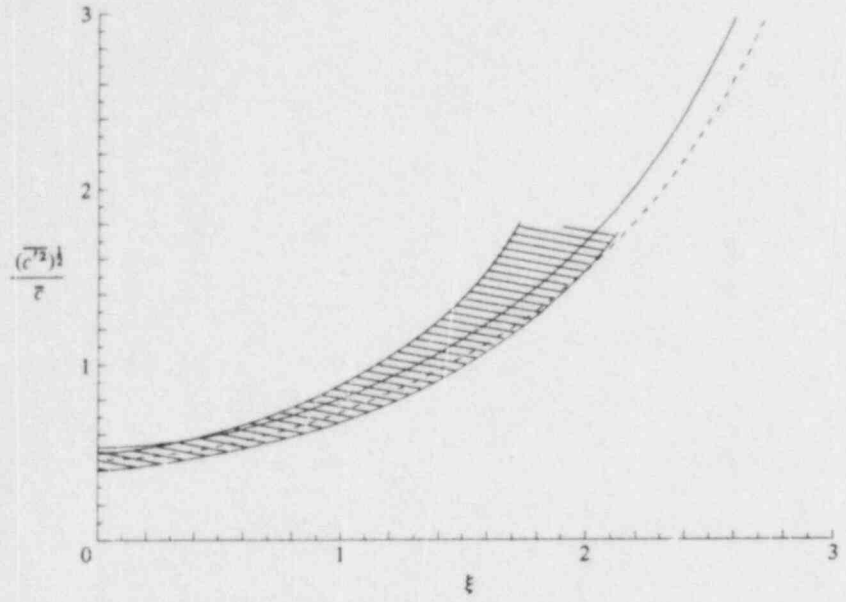

FIGURE 1. Relative intensity of concentration fluctuations $(\overline{c'^2})^{\frac{1}{2}}/\bar{c}$ as a function of dimensionless distance ξ from plume centre, for plume in decaying, isotropic turbulence. Similarity solutions for $\Gamma = 4.6$ (solid line) and $\Gamma = 5.2$ (dashed line) are shown. Shaded region indicates data of Gad-el-Hak & Morton (1979).

where z_s is the height of the source, and H is the depth of the boundary layer. The specification of the turbulence scale is discussed more fully in §3, but it should be noted that the constants α_1, α_2 etc. do have a weak dependence on the value of Λ. The initial value for σ_y is somewhat arbitrary, because the initial development of the plume is affected by such factors as turbulence in the source jet, and jet exit velocity profiles, which are ignored in the model. We are therefore beginning the integration at some effective downstream distance where the plume has grown slightly, and setting $\sigma_y = \frac{1}{2}d_s$ allows an acceptably accurate fit to the data points, as we shall show below. We have not varied this parameter in the optimization procedure, so it is possible that there is a better effective source size for this experiment.

The integrations were made on a finite-difference grid that expands with the plume to maintain similar resolution at all times. Spatial differences were second-order-centred, and the time-differencing scheme utilized the ADI method. Fields were interpolated linearly onto the new grid after expansion, and different grids and expansion rates were tested to ensure that numerical errors were insignificant. The principal comparison was with $\hat{c}/C_m$, where $\hat{c}^2$ is the maximum value of $\overline{c'^2}$, and C_m is the maximum $\bar{c}$ at any x-station. Various combinations of α_1, α_2 were tested, and a good fit to the measurements was obtained with $\alpha_1 = 0.34$, $\alpha_2 = 0.54$. The results for this combination are shown in figure 2, together with the observations of Fackrell & Robins. The model gives a good fit to all the data points; in particular, the variation with source size is accurately described, confirming the correctness of the form for Λ_c and ϵ_c. These values of α_1 and α_2 imply $c_0 = 0.41$, $\beta_1 = 0.10$ and $\beta_2 = 0.40$.

Wilson, Robins & Fackrell (1982) and Wilson, Fackrell & Robins (1982) obtained good fits to this laboratory data also, using a largely empirical model for $\overline{c'^2}$ and

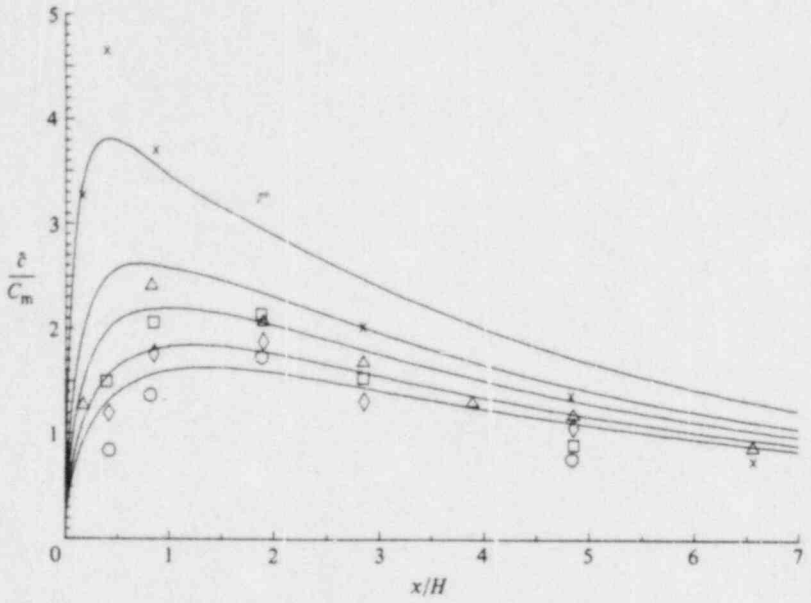

FIGURE 2. Dimensionless fluctuation intensity $\hat{c}/C_m$, for the elevated releases of Fackrell & Robins (1982*a*). Model predictions shown as solid lines for different source sizes. Symbols represent observed data as follows: ×, $d_s = 3$ mm; △, 9 mm; □, 15 mm; ◇, 25 mm; ○, 35 mm.

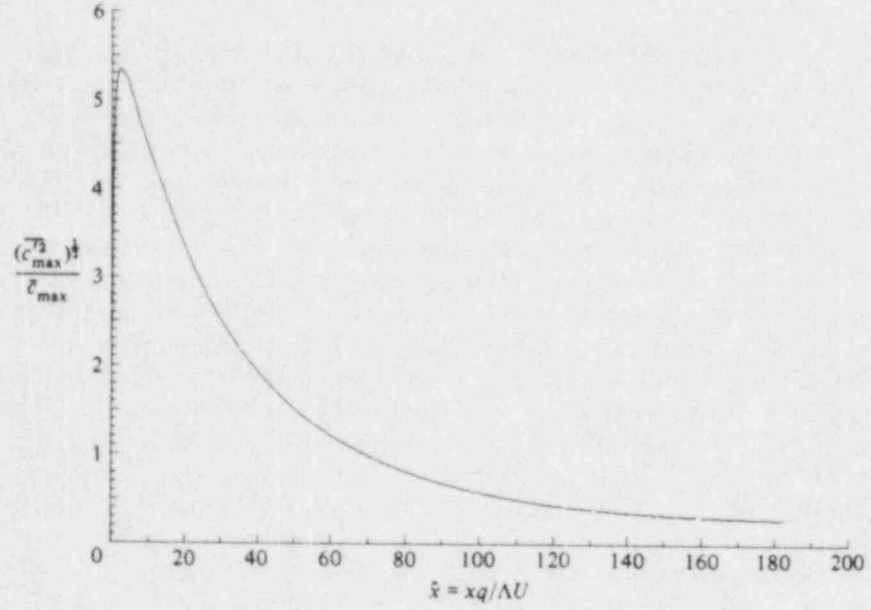

FIGURE 3. $(\overline{c^2_{max}})^{\frac{1}{2}}/\hat{c}_{max}$ versus $xq/\Lambda U$ for release in homogeneous isotropic turbulence; $d_s/\Lambda = 0.01$.

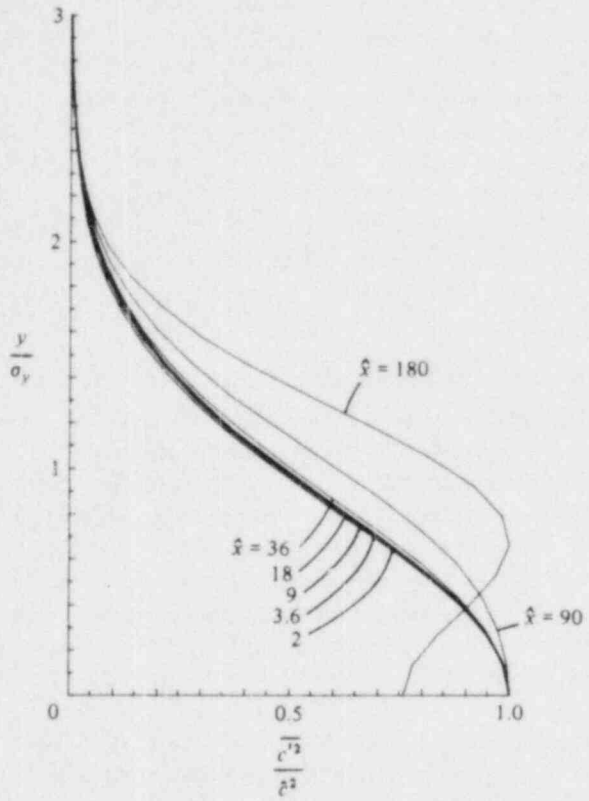

FIGURE 4. Transverse profiles of $\overline{c'^2}/\bar{c}^2$ at various downstream locations for $d_s/\Lambda = 0.01$.

suitably chosen constants. The objective of using a more complicated model here is to increase the generality by including more fundamental physics, so that a wider range of flow conditions and source sizes can be simulated.

In order to provide clearer justification of our assumption that the $\overline{c'^2}$ profile is Gaussian in the early stages, the results from an integration with $d_s/\Lambda = 0.01$ are presented here in detail. The development of $(\overline{c'^2_{\max}})^{\frac{1}{2}}/\bar{c}_{\max}$ (where max denotes the maximum at a downstream location) is shown in figure 3 as a function of dimensionless downstream distance xq/AU. The dimensionless profiles of $\overline{c'^2}$ across the plume are shown in figure 4. It is clear that the early profiles all have the same shape, which is actually Gaussian, but this eventually changes to a profile with a minimum in the centre. Comparison with figure 3 shows that the Gaussian shape begins to change where $(\overline{c'^2_{\max}})^{\frac{1}{2}}/\bar{c}_{\max}$ falls below about 1. This behaviour is consistent with our earlier ideas about the development of $\overline{c'^2}$ where we assumed that $\overline{c'^2}$ would be Gaussian whenever the production could be neglected. The one-half term on the left-hand side of (A 4) in the Appendix represents the production term in the $\overline{c'^2}$ equation, so this should be compared to $(\overline{c'^2_{\max}})^{\frac{1}{2}}/\bar{c}_{\max}$ to determine its importance, and a value of 1 is a reasonable estimate of the point where production is significant. At late times $\Lambda_c \propto t^{\frac{1}{2}}$, so the dissipation timescale is also proportional to $t^{\frac{1}{2}}$. A balance of production and dissipation at late times gives $\overline{c'^2}/\bar{c}^2 \sim t^{-\frac{1}{2}}$, and also gives a profile shaped like the gradient of $\bar{c}$, i.e. zero in the centre and maxima away from the centre. The predicted behaviour of $(\overline{c'^2_{\max}})^{\frac{1}{2}}/\bar{c}_{\max} \sim t^{-\frac{1}{2}}$ is a very slow decay, and is consistent with

the numerical solutions which show both slow decay of the relative intensity of the fluctuations and also a very slow transition toward the asymptotic profile shape.

As a final justification for our model for the late-time behaviours (2.11) and (2.12), Durbin's (1980) random-walk solution for a constant mean scalar gradient in homogeneous non-decaying turbulence gives $\overline{c'^2} \propto t^{\frac{1}{2}}$ at late times. Our model predicts the same dependence since Λ_c will grow like $t^{\frac{1}{2}}$, giving a dissipation timescale proportional to $t^{\frac{1}{2}}$; the scalar flux will be a constant in the presence of a constant gradient, so the production of $\overline{c'^2}$ is constant. The resulting balance between production and dissipation gives $\overline{c'^2} \propto t^{\frac{1}{2}}$. In contrast, the second-order closure model of Newman *et al.* (1981) gives $\overline{c'^2} \propto t$ and $\epsilon_c \to 0$.

3. Diffusion in non-homogeneous turbulence

Since all practical cases of interest involve non-homogeneous turbulence fields, we must consider the extension of our model to cover such cases. In air-pollution studies, the situation is generally a release within a boundary layer, so that we must deal with variations in mean velocity, turbulence energy and also turbulence lengthscales, since the latter tend to zero on the rigid boundary. The laboratory data of Fackrell & Robins (1982*a*, *b*) is very relevant to these studies and extensive comparison with our model predictions will be made. Fackrell & Robins made detailed measurements of turbulent correlations for elevated and ground releases in a wind-tunnel boundary layer, so that the performance of the model can be directly assessed from such comparisons.

In non-homogeneous turbulence, we need to account for spatial variation of variables such as K_{jm}, which were independent of position in the homogeneous case. When the background turbulence is not constant, the global integral of (2.5) needs to be replaced with a local integral so that we use only local similarity to relate the triple moments to the second moments. The appropriate range for such an integral would be the turbulence lengthscale Λ, which represents the size of the energy-containing eddies. Thus a more general definition of the diffusivity is

$$K_{jm}(\boldsymbol{x}) = -\frac{\iint_{D(\boldsymbol{x})} (x'_j - x_j)\,\overline{u'_m c'} + (x'_m - x_m)\,\overline{u'_j c'}\,\mathrm{d}y'\,\mathrm{d}z'}{\iint_{D(\boldsymbol{x})} (x'_j - x_j)\,\dfrac{\partial c}{\partial x_j}\,\mathrm{d}y'\,\mathrm{d}z'}$$

where the domain $D(\boldsymbol{x}) = \{\boldsymbol{x}' : |\boldsymbol{x}' - \boldsymbol{x}| < \Lambda(\boldsymbol{x})\}$. Note that the integral in the denominator has been written in a form that makes a constant background value immaterial.

Unfortunately it is computationally expensive to calculate a local integral of this form at every spatial position at each timestep, and we have therefore used a simpler approximation in our calculations. The major effect of the local average in the boundary-layer flow is to limit K_{jm} near the wall where the lengthscale is small, and the fluxes are in local equilibrium. We have therefore retained the global integral in the definition of K_{jm}, but applied a local limit of the equilibrium value, $K_{jm} \leqslant \overline{u'_j u'_m}\,\Lambda/Aq$.

The concentration-fluctuation lengthscale Λ_c should also be treated as a spatial variable in non-homogeneous flow, and values of turbulence energy and lengthscale appearing in the equations for Λ_c and ϵ_c should probably be approximated by local integrals of the form suggested for $K_{jm}(\boldsymbol{x})$. However, in view of the computational

expense, we shall represent Λ_c as a constant for the entire plume. We calculate it exactly as in the homogeneous case, but whenever a value is required from the background field we use a plume average defined by

$$\phi_p = \frac{\langle \tilde{c}\phi \rangle}{\langle \tilde{c} \rangle},$$

where ϕ is the field to be averaged. Thus (2.8) becomes

$$q_c = (q^2)_p^{\frac{1}{2}} \left(\frac{\Lambda_c}{\Lambda_p}\right)^{\frac{1}{3}} \quad (\Lambda_c \ll \Lambda_p),$$

for example.

A similar philosophy also lies behind our neglect of mean strain and surface-reflection terms in the pressure-gradient correlations appearing in the scalar flux equations. Complicated models exist which claim to model these effects (e.g. Gibson & Launder 1978), but their accuracy and generality have not been proven; we therefore prefer to retain the simplest model until the need for a better representation is demonstrated. We note that the scalar variance equation does not contain any pressure terms, and is thus unaffected by this modelling choice.

There is one further extension which we found necessary but less obvious. This involves the horizontal concentration flux $\overline{v'c'}$ and its behaviour near the boundary wall. If we simply use the local scales for q and Λ in the $\overline{v'c'}$ equation, then the damping timescale will vanish near the wall because $\Lambda \sim 0.65z$ (Lewellen 1977), and therefore $\overline{v'c'}$ will be $O(z)$ because the production term

$$-\overline{v'^2}\frac{\partial \bar{c}}{\partial y}$$

remains finite. Measurements by Fackrell & Robins (1982*a*) show that $\overline{v'c'} = O(\ln z)$ near the wall, as can be seen from their figure 18, which shows $\overline{v'c'}/\bar{U}(z)$ remaining constant as $z \to 0$. Fackrell & Robins' interpretation of this measurement is that the damping timescale for $\overline{v'c'}$ is proportional to $\bar{U}(z)$ near the wall, since they also show that there is a balance between production and damping in this region. They note that the behaviour of $\overline{v'c'}$ is precisely that required to ensure that the plume spreads laterally at the same rate at all heights, the rate being measured as a function of distance x downstream from the source. There seems to be no rationale for a turbulent timescale that varies like $\bar{U}(z)$, and we therefore propose a different physical model for the observed behaviour. Our hypothesis is based on our view of the plume as a coherent entity, so that concentration fluctuations occur on the same lengthscale throughout the plume. We suggest that there are therefore contributions to $\overline{v'c'}$ on the scale Λ_p, i.e. the average turbulence scale over the plume. Note that this is not the fluctuation scale Λ_c, but is the scale of the average turbulent eddies that are diffusing the plume. This scale will be considerably larger than the local scale near the wall if the plume extends significantly upward from the boundary. Such a scale is prohibited in the vertical flux $\overline{w'c'}$, since the proximity of the wall prevents any large scales in the vertical direction. Assuming that there are contributions to $\overline{v'c'}$ on the Λ_p scale, we can then explain the observations by pointing out that the production term

$$-\overline{v'^2}\frac{\partial \bar{c}}{\partial y}$$

occurs on the local scale Λ, because that is the scale of $\overline{v'^2}$. Thus small-scale

contributions to $\overline{v'c'}$ are produced locally, and also removed locally on the short local timescale, giving the observed balance between production and damping. There is, however, very little energy in this small-scale contribution; the main part of $\overline{v'c'}$ near the wall is in the Λ_p scale which is damped on the much slower

$$\frac{\Lambda_p}{(q^2)_p^{\frac{1}{2}}}$$

timescale, and reaches the ground via diffusion from above. Thus vertical coupling of $\overline{v'c'}$ is the factor that ensures that the plume diffuses at the same rate at all heights, and hence produces the observed $\overline{v'c'}$ profiles. We must determine the partition of $\overline{v'c'}$ between the two scales Λ_p and Λ within the model, because the assumption that $\overline{v'c'}$ is all on the Λ_p scale would give $\overline{v'c'}$ tending to a constant value at the wall rather than proportional to $\bar{U}(z)$. We propose a crude but simple estimate based on the local production rate of $\overline{v'c'}$, namely

$$\overline{v'c'_s} = \frac{-\overline{v'^2}\Lambda}{Aq}\frac{\partial \bar{c}}{\partial y}, \tag{3.1}$$

where $\overline{v'c'_s}$ is the small-scale contribution to $\overline{v'c'}$, with the restriction that

$$0 \leqslant \frac{\overline{v'c'_s}}{\overline{v'c'}} \leqslant 1.$$

Equation (3.1) postulates a balance between small-scale production and dissipation whenever possible, but does not allow the small-scale dissipation to exceed the small-scale production. Defining $\overline{v'c'_p} = \overline{v'c'} - \overline{v'c'_s}$, we write the damping term in the $\overline{v'c'}$ equation as

$$-\frac{Aq}{\Lambda}\overline{v'c'_s} - \frac{A(q^2)_p^{\frac{1}{2}}}{\Lambda_p}\overline{v'c'_p}. \tag{3.2}$$

This model implies that when larger values of $\overline{v'c'}$ are present near the ground than could be produced by the local turbulence, presumably by diffusion from aloft, then the additional $\overline{v'c'}$ is dissipated on the longer average plume timescale. We show model results below which indicate that this crude parametrization gives reasonably good predictions of the $\overline{v'c'}$ profiles.

Finally, in accord with the above philosophy, we calculate the horizontal diffusivities in the modelled triple correlation terms using plume-average quantities rather than local values. This is not strictly justified since we have postulated only part of the correlations on the Λ_p scale, but the differences from calculating each part separately do not justify the extra complexity, since diffusion is usually unimportant when the small-scale contribution is dominant.

We are now in a position to compare our model predictions with the data obtained by Fackrell & Robins. In order to ensure that we are evaluating the predictions of the scalar transport equations, we use the measured profiles for the dynamical quantities rather than a model prediction. Unfortunately, the turbulence lengthscale Λ is not easily specified from the measurements. Λ is used to determine several different timescales in the model, with coefficients which have been determined to be consistent with other model predictions. We lose this consistency by using measured values for the Reynolds stress, so that Λ becomes somewhat arbitrary. Rather than use the measured dissipation rate to set Λ, we chose a simple algebraic form which is consistent with earlier model integrations for boundary-layer flows (Lewellen 1977), namely

$$\frac{1}{\Lambda} = \frac{1}{0.65z} + \frac{1}{0.2H}. \tag{3.3}$$

where H is the boundary-layer thickness. The linear relation is appropriate near the wall, while the constant value is a typical value in the outer part of the boundary layer; the latter value is also roughly consistent with the dissipation measurements of Fackrell & Robins for $z/H = 0.5$. We may note that the integrations reported below were also run with a different scale profile between the two limits, namely

$$\Lambda = \min(0.65z, 0.2H), \tag{3.4}$$

and produced results which were in most cases within 15 % of those presented. In making these runs, α_1 and α_2 were set to 0.30 and 0.56 to optimize the fit with the elevated release data using the different value for Λ implied by (3.4).

We have also used $4\overline{u^2}$ in place of q^2 in all the modelled terms, because the observed q^2 implies inconsistent behaviour of the effective diffusivity in the surface layer. This was one of the means for determining model constants (Lewellen 1977), so that consistency here is quite important. We note that the observed profile of $\overline{u^2}$ is very close to the model predictions, and the model surface-layer relationship $q^2 = 4\overline{u^2}$ allows us to make a consistent estimate of q^2 from the observations.

Having defined all the background turbulence fields, and the evolution equations for the scalar quantities, the parabolic equations were integrated in a two-dimensional domain, marching in the streamwise direction, i.e.

$$\frac{\mathrm{D}}{\mathrm{D}t} = \bar{U}(z)\frac{\partial}{\partial x}.$$

At the lower boundary $z = 0$ we specify the appropriate conditions for an impenetrable wall, i.e.

$$\frac{\partial \bar{c}}{\partial z} = \overline{c'w'} = \frac{\partial}{\partial z}\overline{c'v'} = \frac{\partial}{\partial z}\overline{c'^2} = 0. \tag{3.5}$$

All scalar quantities are set to zero on the outer boundaries $z = Z_\mathrm{m}$ and $y = Y_\mathrm{m}$, and we use a plane-of-symmetry condition at $y = 0$ so that only half the domain needs to be considered. The outer boundaries Y_m, Z_m are adjusted during the integration to maintain

$$Y_\mathrm{m} \in [7\sigma_y, 10\sigma_y], \quad Z_\mathrm{m} \in [\bar{z} + 14\sigma_z, \bar{z} + 20\sigma_z],$$

where $\bar{z}$ is the height of the plume centroid, and σ_y and σ_z are the plume spreads.

Integrations were made for all the cases reported by Fackrell & Robins; these constitute five elevated releases and three ground releases. Detailed profiles for the 9 mm elevated release and the 15 mm ground release are reported, while the ratio of concentration fluctuation standard deviation to mean concentration are given for all the releases. We first compare the model predictions for the latter quantities, giving some overall comparison of the model performance on the range of data.

Figure 5 shows the model predictions for the ratio of the maximum value of $(\overline{c'^2})^{\frac{1}{2}}$ $(= \hat{c})$ to the maximum value of $\bar{c}$, denoted by C_m, as a function of x/H. The data of Fackrell & Robins are also displayed in the figure. The elevated releases are little different from the homogeneous results shown in figure 1, as anticipated in §2. The ground releases show reasonable agreement with the measurements also, although they lie somewhat below the virtually constant observed value of 0.6 over the range of release diameters and over the downstream range of the data. Figure 5 demonstrates the ability of the model to predict the independence of the ratio of standard deviation to mean for a wide range of releases.

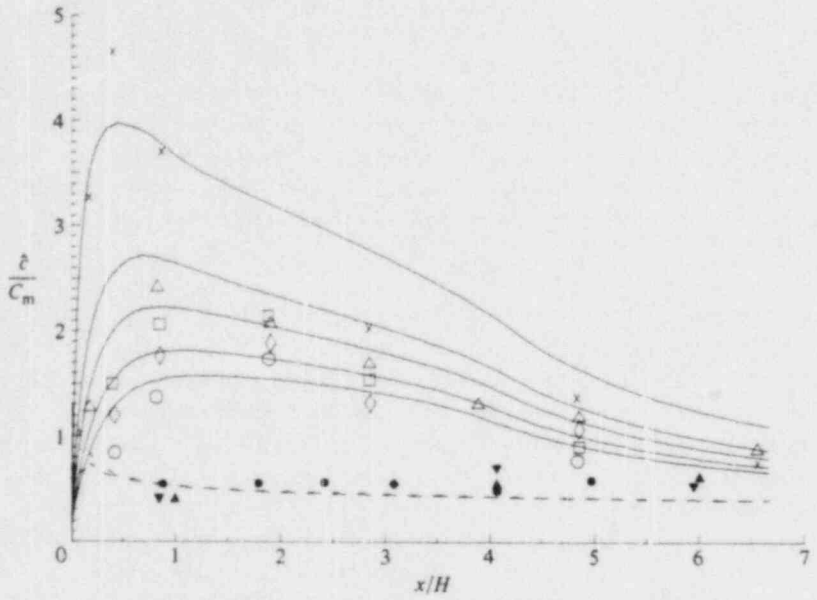

FIGURE 5. Full model predictions for $\hat{c}/C_m$ in elevated and ground releases. Symbols as in figure 2 for elevated releases. Ground-release predictions are shown as dashed lines, data symbols are △, 3 mm; ▽, 9 mm; ○, 15 mm.

It is true that two empirical constants were chosen to optimize the fit for the elevated releases, but the agreement with measurements on the shape and magnitude of the range of data values strongly suggests that the dominant physical processes and timescales have been incorporated into the model. Further support for this view comes from examination of the detailed measurements of the plumes.

Figure 6 shows the evolution of several plume quantities, namely C_m, δ_y and δ_z for the elevated (9 mm) and ground (15 mm) releases. δ_y and δ_z are the plume scales, defined by Fackrell & Robins as the distance over which the concentration falls to half its maximum value. In the y-direction, the plume shapes are very close to Gaussian, so we have plotted $\delta_y = 1.17\sigma_y$, which is the appropriate value. For the ground release the vertical profiles are nearly self-similar, as we shall see below, so that δ_z is defined from the profile at $y = 0$. For the elevated release, however, Fackrell & Robins obtained δ_z by fitting a reflected Gaussian to the measured profile and relating δ_z to the Gaussian spread. Since a Gaussian does not provide a good fit at late times, we have simply plotted $\delta_z = 1.17\sigma_z$, where σ_z is the standard deviation of the entire plume, i.e. no reflections considered. This should agree with the measurements at early times, but is a different measure after the plume has touched the ground, so that the comparison is not useful after $x/H = 3$ in figure 6(*b*). The maximum concentration on the ground is also shown in figure 6(*b*). The predictions of the spread rates and maximum concentrations are generally good for both releases. There is a tendency to underpredict the horizontal spread rate for the ground release by about 20 %, with a consequent 20 % overprediction of the maximum concentration. The elevated release is predicted accurately until it reaches the ground, where the diffusion is too slow. The latter point will be discussed further when we examine the profile shapes.

Comparisons of the shape of the concentration profiles (normalized by the

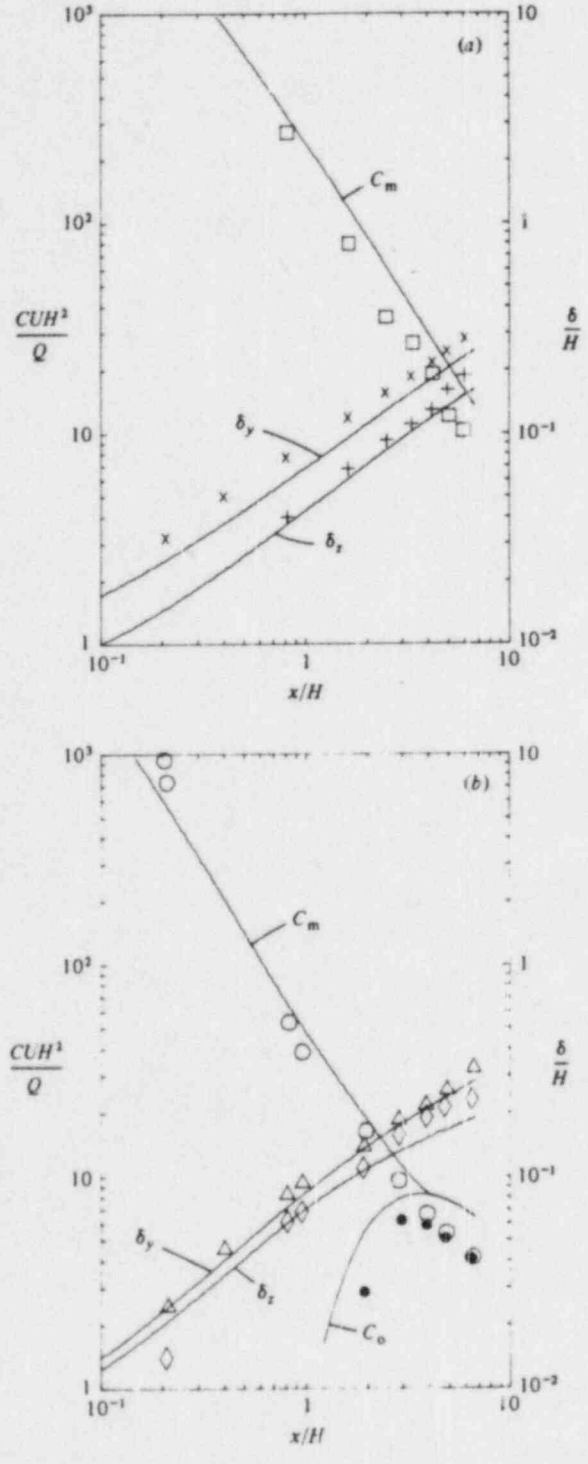

FIGURE 6. Predictions and observations of plume spread and maximum concentrations. Predictions shown as solid lines. (*a*) Ground release; data: □, C_m; +, δ_z; ×, δ_y. (*b*) Elevated release; data: ○, C_m; ■, C_0; ◇, δ_z; △, δ_y (C_0 is the maximum concentration on the surface).

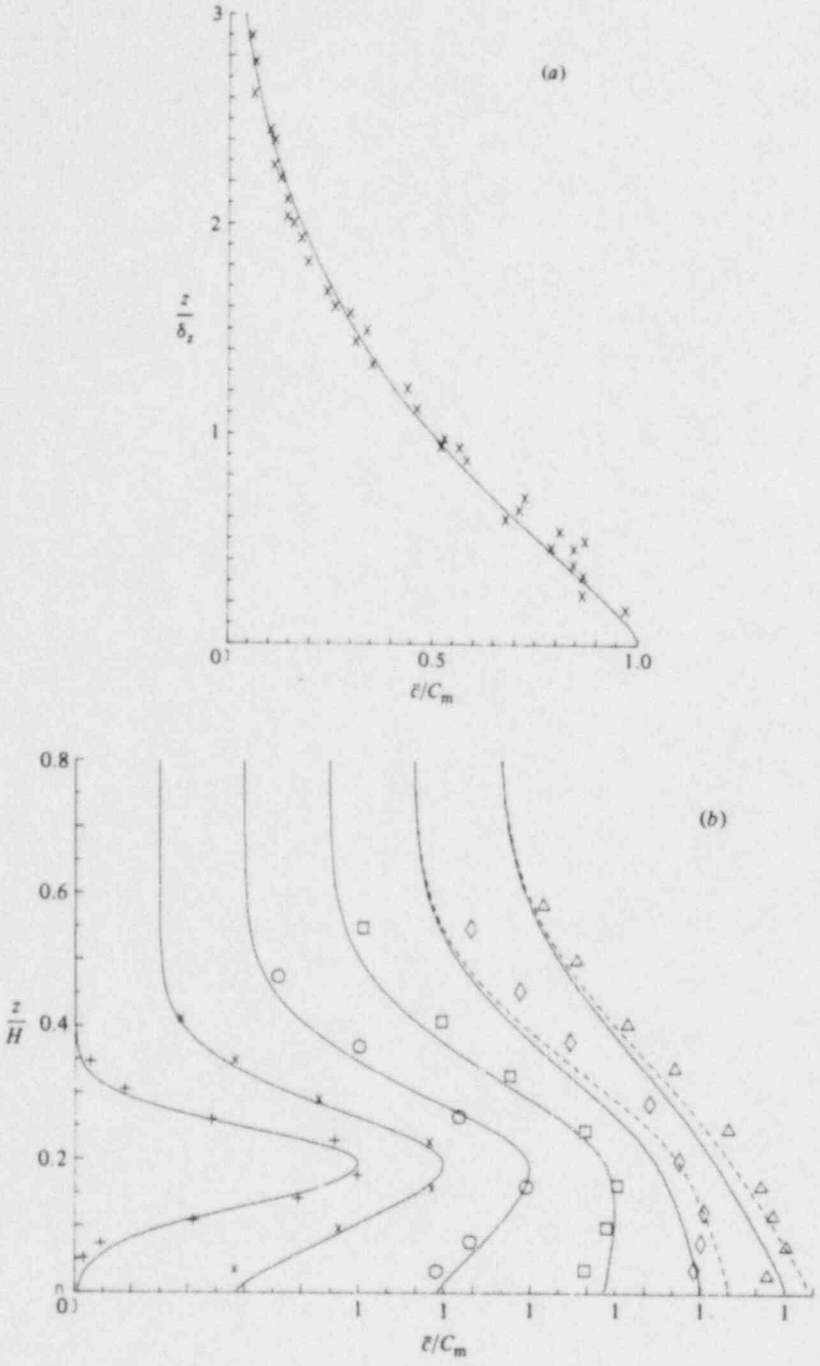

FIGURE 7. Vertical profiles of $\bar{c}/C_m$ at plume centre. (*a*) Ground release. (*b*) Elevated release; data symbols: +, $x/H = 0.96$; ×, 1.92; ○, 2.88; □, 3.83; ◇, 4.79; △, 6.52. Note that origins of consecutive profiles are offset to the right.

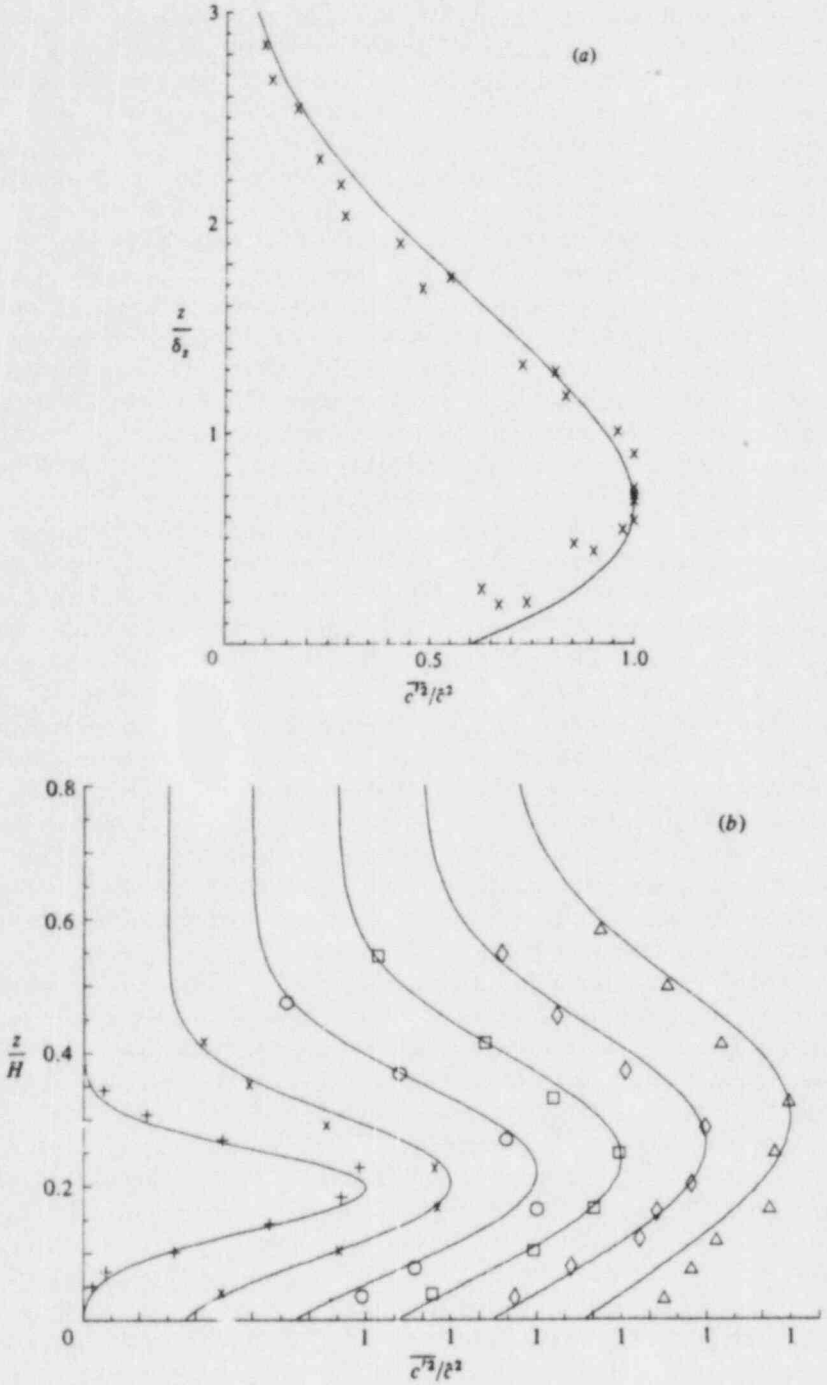

FIGURE 8. Vertical profiles of $\overline{c'^2}/\hat{c}^2$. Symbols as figure 7. (*a*) Ground release. (*b*) Elevated release.

maximum concentration) in the vertical direction are shown in figure 7. The ground-level release profiles collapsed onto a single non-dimensional curve when plotted against z/δ_z. Fackrell & Robins report the same results from their measurements, and the model prediction for the shape of the profile is in excellent agreement with the observations. Good results are also obtained for the elevated release, with profiles closely matching the data, except for the latest station which indicates the model prediction progressing toward the final ground-release shape more quickly than the observations. The discrepancies are only significant very close to the ground, as the dashed lines in figure 7 (*b*) demonstrate. These profiles were obtained by rescaling $\bar{c}$ so that the actual maximum is predicted correctly; those curves are different because the observed maximum is elevated whilst the model predicts the maximum on the ground. It is evident that the upper region of the profile is more accurately predicted. The errors below $z/H = 0.1$ are probably due to underprediction of the horizontal fluxes near the ground, as we shall see later. We note however, that there seems to be some inconsistency in the data near the ground also; figure 6 (*b*) shows the observed maximum to be on the ground at the last station, while figure 7 (*b*) shows the ground value to be significantly lower than the maximum.

The model profiles are the most sensitive to changing the specification of Λ; use of (3.4) causes the elevated release to diffuse downward and develop the features of the ground release more quickly, although the differences are still less than about 25 %.

We also compare the vertical profiles of $\overline{c'^2}$, again normalized by the maximum value in the profile; the results are shown in figure 8. The ground release profiles collapse onto a self-similar curve when plotted against δ_z; this curve shows a maximum value of $\overline{c'^2}$ at about $0.75\delta_z$, with reduction to about half the maximum value at the surface. The model prediction is very close to the measurements again.

For the elevated release (figure 8*b*) there is also good agreement with observation. At early times the $\overline{c'^2}$ profile is close to Gaussian, as discussed in §2 for homogeneous turbulence. As the Gaussian spreads, it eventually reaches the ground plane and ceases to mirror the mean concentration profile. Instead, $\overline{c'^2}$ remains small near the ground, and the elevated maximum begins to move upward, following the region of maximum production where gradients of $\bar{c}$ are significant.

The second-order closure model predicts the observed reduction in $\overline{c'^2}$ near the wall, which Fackrell & Robins suggest arises through increased dissipation by the small eddies in that region. The model, however, does not include such a mechanism because we have assumed that the concentration fluctuations occur principally on the Λ_c scale. There is a slight increase in the dissipation rate near the wall due to the increase in turbulence energy, but this is only a small effect. The main cause of the small $\overline{c'^2}$ seems to be the absence of production terms; we plotted the profile on the centreline, $y = 0$, so that $\overline{v'c'} = 0$ at all heights, and also $\overline{w'c'} = 0$ on the lower boundary. Thus there is no production of $\overline{c'^2}$ at the ground, and the value there is determined by the rate of diffusion. The diffusion rate in the vertical is small near the ground, since the scale of the eddies with significant energy in the vertical component must tend linearly to zero at the wall and we limit the diffusivity using the local equilibrium rate; there is therefore a low value of $\overline{c'^2}$ in this region, the value being determined by the horizontal diffusion rate. The difference between the point on the ground and the point of maximum $\bar{c}$ in the early elevated plume is in the diffusion rate only, both points have no production of $\overline{c'^2}$, but the elevated point has a larger scale for the vertical eddies, and consequently diffuses $\overline{c'^2}$ much faster to fill in the region of low production.

Lateral cross-sections of $\overline{c'^2}$ illustrate the roles of diffusion and production, figure

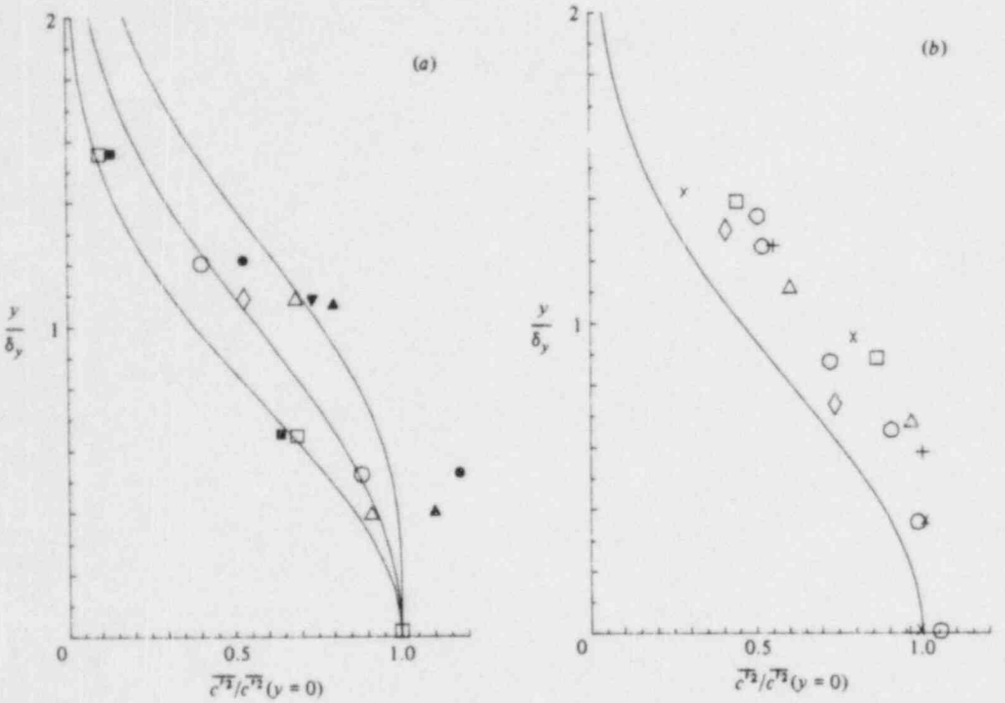

FIGURE 9. Transverse profiles of $\overline{c'^2}$. (*a*) Ground release; solid data symbols are at $z/\delta_z = 0.5$, open symbols at $z/\delta_z = 1.5$. (*b*) Elevated release; all profiles are at the height of maximum c'^2.

9(*a*) shows cross-sections through the ground release at three different heights. The curves are the same at all x-stations when normalized by δ_y and the centreline value. We may note that the mean-concentration profiles are all close to Gaussian in the y-direction, in accord with observations, and the spread measured at various heights is generally within 10% of the mean value obtained for the entire plume. Figure 9(*a*) shows the model predicting a very slight minimum on the centreline at $z = 0$, but a maximum on $y = 0$ at $z = \frac{1}{2}\delta_z$ and $z = \frac{3}{2}\delta_z$. The measured profiles at the two elevated positions show a relatively lower value at $y = 0$, i.e. more tendency toward a minimum on the centreline; the measured profile at $z = \frac{1}{2}\delta_z$ is closer to the predicted profile at $z = 0$. The model has the correct quantitative behaviour, but details of the profile shapes are not precise. We believe that the discrepancies here are due to errors in $\overline{v'c'}$ near the ground, and consequent errors in the production rate for $\overline{c'^2}$; the flux profiles will be discussed in detail below. The profiles for the elevated release at the height of the maximum $\overline{c'^2}$ are shown in figure 9(*b*); these also agree quite well with the observations, but show the same tendency as the ground release to be closer to Gaussian than the observation.

Normalized vertical profiles of the vertical concentration flux $\overline{w'c'}$ are shown in figures 10 and 11. Figure 10 shows ground-release results for two downstream stations, and various positions across the plume. The centreline profile and the inner profile at roughly $y = \frac{1}{2}\delta_y$ from the model prediction collapse together very well, but the outer profile at $y \geqslant \delta_y$ is slightly larger in magnitude, with a sharper maximum. The measured profiles do not really confirm this change in profile, but there are generally higher values in the outer profile. The overall agreement in profile shape

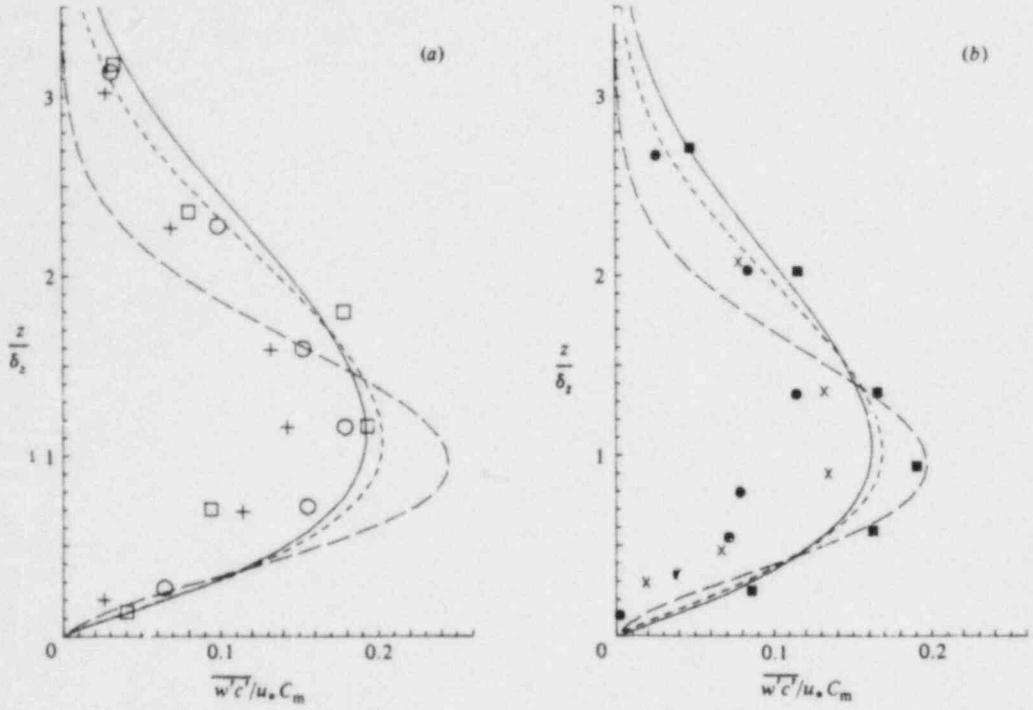

FIGURE 10. Vertical profiles of vertical flux $\overline{w'c'}$ for the ground release.

(a) $x/H = 2.5$:	y/δ_y	Model	Data	(b) $x/H = 5.92$:	y/δ_y	Model	Data
	0	——	+		0	——	×
	0.39	-----	○		0.51	-----	○
	1.07	– – –	□		1.20	– – –	■

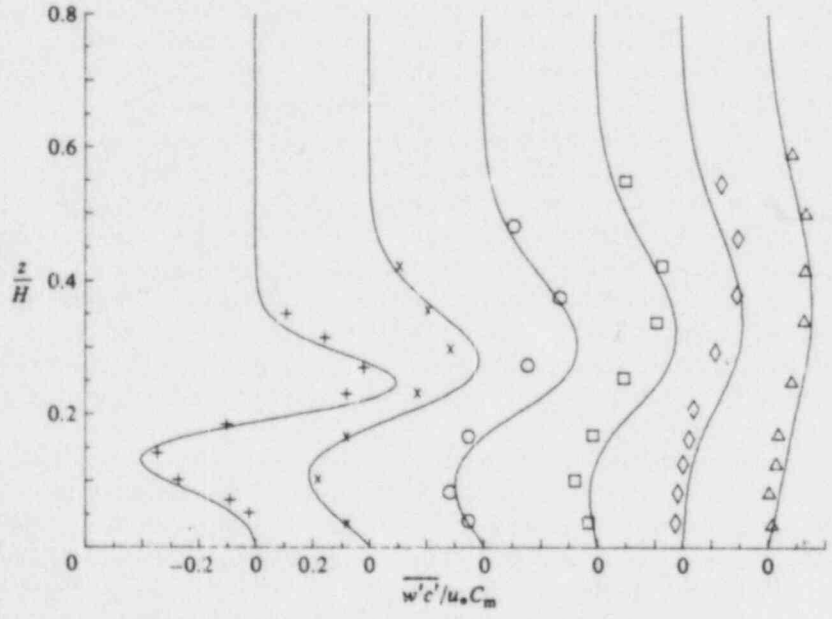

FIGURE 11. Vertical profiles of $\overline{w'c'}$ for the elevated release. Symbols as in figure 7.

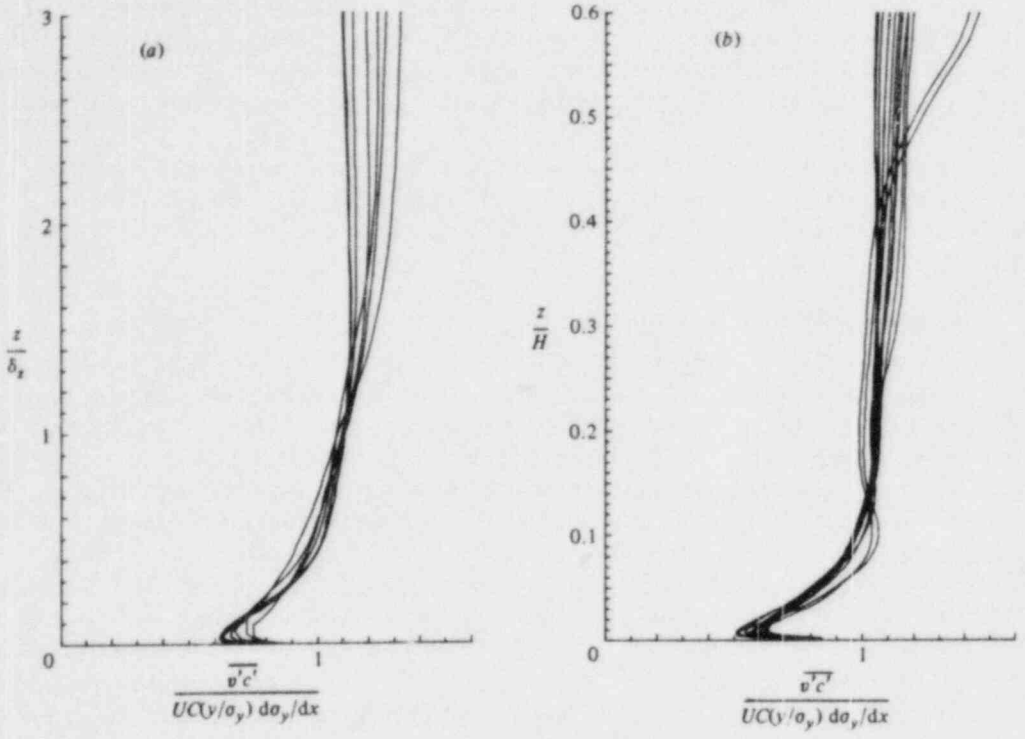

FIGURE 12. Dimensionless profiles of $\overline{v'c'}$ at the range of locations reported by Fackrell & Robins. (*a*) Ground release. (*b*) Elevated release.

is very good. The same is true of the centreline profiles for the elevated release, shown in figure 11; predicted and observed values agree very well.

Vertical profiles of the normalized lateral flux $\overline{v'c'}$ are shown in figure 12 for ground and elevated releases. The graphs are a composite of all the profiles at the positions plotted by Fackrell & Robins, which covers the range of downstream stations and also lateral position within the plume. The normalization includes the mean velocity $\bar{u}(z)$, and is the appropriate scaling (as shown by Fackrell & Robins) if the plume is diffusing laterally at the same rate at all heights. The measurements show a scatter of points within about 20 % of unity, and no evident trend with height or downstream or lateral portion. The model predictions do not show any significant trend with downstream or lateral position, but there is a reduction to a value of 0.5 at the surface, which takes the model results out of the band of the measurement below about $0.4\delta_z$ for the ground release and below $z = 0.07H$ for the elevated release.

The behaviour of $\overline{v'c'}$ near the ground was discussed at the beginning of this section, and used as the basis of a 'two-scale' model, i.e. we considered $\overline{v'c'}$ to be composed of fluctuations on two distinct scales near the ground, namely Λ_p and Λ. Our estimate of the fraction in the small scale Λ is denoted by $\overline{v'c'_s}$ and given in (3.1). We accept that this is a very crude description of the dynamics, but point out that the assumption that all the lateral flux is on one scale, i.e. $\overline{v'c'_s} = 0$ or $\overline{v'c'_s} = \overline{v'c'}$, results in significantly worse predictions of the vertical profile, and also gives a plume which diffuses at a very different rate near the ground. The two-scale description of $\overline{v'c'}$ does introduce considerable potential for complexity, but seems to be necessary to understand the behaviour of the plume. Having accepted the impossibility of

modelling the flow with a single scale, we feel justified in choosing the simplest conceptual model in order to investigate its consequences and possibilities. Although the prediction of $\overline{v'c'}$ is in error close to the ground, the discrepancies are much smaller than the one-scale model, and we have gone some way toward an accurate description of these processes.

As noted earlier, the reduced value of $\overline{v'c'}$ near the surface is probably responsible for the lateral $\overline{c'^2}$ profiles being closer to Gaussian, in that larger values of $\overline{v'c'}$ would give higher production off the centreline, and tend to increase $\overline{c'^2}$ in that region.

4. Summary and conclusions

A second-order closure model for the dispersion of a passive scalar has been presented and tested against laboratory data. The model improves upon the earlier work of Lewellen & Teske (1976) in that attention has been paid to the early stages of the release to ensure that correct behaviour is modelled. Our final model predicts the linear and parabolic regimes of the mean-concentration profile growth without any new empirical constraints, and compares well with experimental data. The main restriction is that each release must be treated separately; this seems to be a fundamental problem with any closure scheme, as shown by Deardorff (1978). However, we have removed any requirement from the specification of time-dependent diffusivities, by allowing all the turbulence correlations to diffuse at the same rate as the mean concentration in the early stages. This closes the system of equations, allowing the closure model to completely determine the solution in terms of the background turbulence parameters.

The new model also includes a prediction of the concentration variance $\overline{c'^2}$; this quantity is known to be dependent on source size, and introduces a new lengthscale into the problem, namely the concentration fluctuation scale Λ_c. A simple equation for Λ_c has been prepared which is based on the behaviour in the limits of very small or very large Λ_c. These limits are obtained by identifying Λ_c with the two-particle separation as discussed by Durbin (1980). Having determined these asymptotic behaviours, empirical coefficients were then chosen to optimize the agreement with the data of Fackrell & Robins (1982*a*). It should be noted that the shape of the $\overline{c'^2}$ evolution, as well as its variation with source size, is predicted, so that agreement does imply that the dynamics are being described correctly.

In conclusion, it has been demonstrated that the dispersion of a passive scalar can be modelled using second-order closure techniques under the idealized laboratory conditions considered in this paper. The main advantage of the closure scheme is that it provides a foundation for considering more complex situations, as well as a framework within which simpler parametrizations can be developed.

This work was partially supported by EPRI with G. R. Hilst as project manager and by NRC with R. F. Abbey as project manager.

Appendix

We examine here the early-stage model predictions for the concentration variance. Recalling that we denote the integral over the plume by angular brackets, we can combine the $\overline{c'^2}$ equation with the $\bar{c}$ equation to obtain

$$\frac{\mathrm{D}}{\mathrm{D}t}(\langle\overline{c'^2}\rangle + \langle\bar{c}^2\rangle) = -\langle\epsilon_c\rangle. \tag{A 1}$$

We know from §2.1 that $\bar{c}$ has a Gaussian profile, with standard deviations σ_y and σ_z given by $(\sigma_0 + (\overline{v^2})^{\frac{1}{2}}t)$ and $(\sigma_0 + (\overline{w^2})^{\frac{1}{2}}t)$ respectively, where σ_0 is the initial (circular) spread of the plume. If we assume that $\overline{c'^2}$ has the same profile shape as $\bar{c}$, then (A 1) will become an equation for the centreline value of $\overline{c'^2}$. This assumption is justified by numerical solution of the full equations (see figure 2.4), but we note here that $\overline{c'^2}$ does mirror the $\bar{c}$-distribution for some time, because the production of $\overline{c'^2}$ occurs very early during the release from a small source. Once the production phase is passed, $\overline{c'^2}$ diffuses at the same rate as $\bar{c}$, by construction, and therefore will adopt the same Gaussian profile.

If $\hat{c}^2$ and C_m are the centreline values of $\overline{c'^2}$ and $\bar{c}$ respectively, then (A 1) can be rewritten as

$$\frac{\mathrm{D}}{\mathrm{D}t}(\sigma_y \sigma_z [\hat{c}^2 + \tfrac{1}{2}C_m^2]) = -\frac{\alpha_2 q_c}{\Lambda_c}\sigma_y \sigma_z \hat{c}^2. \tag{A 2}$$

Equations (2.8) and (2.9) can be solved to give

$$\Lambda_c = [\sigma_0^{\frac{4}{3}} + \tfrac{2}{3}\alpha_1 q t \Lambda^{-\frac{1}{3}}]^{\frac{3}{4}}, \tag{A 3}$$

where we set $\Lambda_c(0) = \sigma_0$. We have the freedom to set this initial condition since we allowed two empirical constants in the earlier equations.

Substituting for σ_y and σ_z, and using the fact that the total flux $C_m \sigma_y \sigma_z$ is conserved, (A 2) becomes

$$\frac{\mathrm{D}}{\mathrm{D}t}\left(\sigma_y^{-1}\sigma_z^{-1}\left[\frac{\hat{c}^2}{C_m^2} + \frac{1}{2}\right]\right) = -\frac{\alpha_2 q}{\sigma_0^{\frac{4}{3}}\Lambda^{\frac{1}{3}} + \frac{2}{3}\alpha_1 q t}\sigma_y^{-1}\sigma_z^{-1}\frac{\hat{c}^2}{C_m^2}, \tag{A 4}$$

where the equation has been written in terms of the variable $\hat{c}/C_m$, which measures the relative intensity of the concentration fluctuations. For a small source ($\sigma_0/\Lambda \ll 1$) $\hat{c}/C_m$ will be large, so the term in square brackets on the left-hand side of (A 4) is approximately $\hat{c}^2/C_m^2$. However, the one-half cannot be neglected in the very early stages, since it represents the production terms. The production can be seen to be important only for $t < \sigma_0/q$, by which time $\hat{c}/C_m$ is $O(1)$; this is a very short time and justifies our Gaussian assumption. Hence for $t > O(\sigma_0/q)$ (A 4) predicts a relatively straightforward decay of $(\sigma_y \sigma_z)^{-1}\hat{c}^2/C_m^2$.

The solution is

$$\frac{\hat{c}^2}{C_m^2} = \frac{A_0}{\sigma_0^2}\sigma_y \sigma_z \left[1 + \tfrac{2}{3}\alpha_1 \frac{qt}{\sigma_0^{\frac{4}{3}}\Lambda^{\frac{1}{3}}}\right]^{-\gamma}, \tag{A 5}$$

where $\gamma = 3\alpha_2/2\alpha_1$, and A_0 is an $O(1)$ constant related to the maximum value of $\hat{c}^2$ attained at the end of the production phase.

Several features can be noted from (A 5). First, $\hat{c}/C_m$ will only maximize within this early-time solution if $\gamma > 2$, since σ_y and σ_z grow linearly with t for t much smaller than the turbulence time Λ/q; this imposes a constraint on the empirical constants α_1 and α_2. Secondly, if $\gamma > 2$ the maximum $\hat{c}/C_m$ occurs at $t = O(\sigma_0^{\frac{4}{3}}\Lambda^{\frac{1}{3}}/q)$ and takes a value $O(\Lambda^{\frac{1}{3}}/\sigma_0^{\frac{1}{3}})$.

REFERENCES

Antonopoulos-Domis, M. 1981 Large-eddy simulation of a passive scalar in isotropic turbulence. *J. Fluid Mech.* **104**, 55–79.

Chatwin, P. C. & Sullivan, P. J. 1979*a* The relative diffusion of a cloud of passive contaminant in incompressible turbulent flow. *J. Fluid Mech.* **91**, 337–355.

Chatwin, P. C. & Sullivan, P. J. 1979*b* Measurements of concentration fluctuations in relative turbulent diffusion. *J. Fluid Mech.* **94**, 83–101.

CHATWIN, P. C. & SULLIVAN, P. J. 1980 Some turbulent diffusion invariants. *J. Fluid Mech.* **97**, 405–416.

CSANADY, G. T. 1967 Concentration fluctuations in turbulent diffusion. *J. Atmos. Sci.* **24**, 21–28.

DEARDORFF, J. W. 1978 Closure of second- and third-moment rate equations for diffusion in homogeneous turbulence. *Phys. Fluids* **21**, 525–530.

DONALDSON, C. DUP. 1973 Atmospheric turbulence and the dispersal of atmospheric pollutants. In *Proc. AMS Workshop on Micrometeorology* (ed. D. A. Haugen). Science Press, Boston.

DURBIN, P. A. 1980 A stochastic model of two particle dispersion and concentration fluctuations in homogeneous turbulence. *J. Fluid Mech.* **100**, 279–302.

DURBIN, P. A. 1982 Analysis of the decay of temperature fluctuations in isotropic turbulence. *Phys. Fluids* **25**, 1328–1332.

EL TAHRY, S., GOSMAN, A. D. & LAUNDER, B. E. 1981 The two- and three-dimensional dispersal of a passive scalar in a turbulent boundary layer. *Intl J. Heat Mass Transfer* **24**, 35–46.

FACKRELL, J. E. & ROBINS, A. G. 1982*a* Concentration fluctuations and fluxes in plumes from point sources in a turbulent boundary layer. *J. Fluid Mech.* **117**, 1–26.

FACKRELL, J. E. & ROBINS, A. G. 1982*b* The effects of source size on concentration fluctuations in plumes. *Boundary-Layer Met.* **22**, 335–350.

GAD-EL-HAK, M. & MORTON, J. B. 1979 Experiments on the diffusion of smoke in isotropic turbulent flow. *AIAA J.* **17**, 558–562.

GIBSON, M. & LAUNDER, B. E. 1978 Ground effects on pressure fluctuations in the atmospheric boundary layer. *J. Fluid Mech.* **67**, 569–581.

GIFFORD, F. 1959 Statistical properties of a fluctuating plume dispersal model. *Adv. Geophys.* **6**, 117–137.

HAY, J. S. & PASQUILL, F. 1959 Diffusion from a continuous source in relation to the spectrum and scale of turbulence. *Adv. Geophys.* **6**, 345–365.

LAUNDER, B. E., REECE, G. J. & RODI, W. 1975 Progress in the development of a Reynolds-stress turbulence closure. *J. Fluid Mech.* **67**, 537–566.

LESLIE, D. C. 1973 *Developments in the Theory of Turbulence*. Oxford University Press.

LEWELLEN, W. S. 1977 Use of invariant modelling. In *Handbook of Turbulence* (ed. W. Frost & T. M. Moulden). Plenum.

LEWELLEN, W. S. 1981 Modelling the lowest 1 km of the atmosphere. *AGARD*-AG-267.

LEWELLEN, W. S. & TESKE, M. E. 1976 Second-order closure modelling of diffusion in the atmospheric boundary layer. *Boundary-Layer Met.* **10**, 69–90.

LUMLEY, J. L. & KHAJEH-NOURI, B. 1974 Computational modelling of turbulent transport. In *Proc. 2nd IUGG–IMIAM Symp. on Atmospheric Diffusion in Environmental Pollution*. Academic.

MURTHY, C. R. & CSANADY G. T. 1971 Experimental studies of relative diffusion in Lake Huron. *J. Phys. Oceanogr.* **1**, 17–24.

NEWMAN, G. R. & HERRING, J. R. 1979 A test field model study of passive scalar in isotropic turbulence. *J. Fluid Mech.* **94**, 163–194.

NEWMAN, G. R., LAUNDER, B.E. & LUMLEY, J. L. 1981 Modelling the behaviour of homogeneous scalar turbulence. *J. Fluid Mech.* **111**, 217–232.

SAWFORD, B. L. 1982 Comparison of some different approximations in the statistical theory of relative dispersion. *Q. J. R. Met. Soc.* **108**, 191–208.

SMITH, F. B. & HAY, J. S. 1961 The expansion of clusters of particles in the atmosphere. *Q. J. R. Met. Soc.* **87**, 89–91.

TAYLOR, G. I. 1921 Diffusion by continuous movements. *Proc. Lond. Math. Soc.* (*Ser.* 2), **20**, 196–211.

WARHAFT, Z. & LUMLEY, J. L. 1978 An experimental study of the decay of temperature fluctuations in grid-generated turbulence. *J. Fluid Mech.* **88**, 659–684.

WILSON, D. J., ROBINS, A. G. & FACKRELL, J. E. 1982 Predicting the spatial distribution of concentration fluctuations from a ground level source. *Atmos. Env.* **16**, 497–504.

WILSON, D. J., FACKRELL, J. E. & ROBINS, A. G. 1982 Concentration fluctuations in an elevated plume: a diffusion–dissipation approximation. *Atmos. Environ.* **16**, 2581–2589.

Atmospheric Environment Vol. 18, No. 1, pp. 121–123, 1984
Printed in Great Britain.

0004–6981/84 $3.00 + 0.00

THE VARIANCE IN TIME-AVERAGED SAMPLES FROM AN INTERMITTENT PLUME

R. I. SYKES

Aeronautical Research Associates of Princeton, Inc., 50 Washington Road, P.O. Box 2229, Princeton, NJ 08540, U.S.A.

(*First received* 31 *May* 1983 *and in final form* 5 *July* 1983)

Abstract—Gifford's (1959) fluctuating plume model is extended to obtain an expression for the autocorrelation function for concentration fluctuations. This is then used to derive results for the reduction in sample variance as the averaging time is increased. A simple exponential shape assumption for the autocorrelation function is shown to give reasonable results, but the integral time scale for the concentration field is very much shorter than the Eulerian integral time scale of the velocity field for highly intermittent plumes. A simple expression for the time scale in terms of the ensemble mean and variance of the concentration is proposed.

INTRODUCTION

Any measured value of scalar concentration in a turbulent flow field is a time-averaged sample from a stochastic field. There is consequently a random component to the measurement which depends on the statistical variation of the instantaneous concentration field. As the averaging time is increased (in a stationary flow) the measured value approaches the ensemble average, and the random component diminishes. In practice, averaging times are often too short to make the random component negligible, therefore it is useful to have an estimate of the expected variation in the sample.

The variance in a time-averaged concentration is expressible in terms of the ensemble fluctuation variance, $\langle c'^2 \rangle$, and the fluctuation autocorrelation function, given by

$$\rho(\tau) = \frac{\langle c'(t)c'(t+\tau)\rangle}{\langle c'^2\rangle},$$

where angular brackets denote ensemble averages and c' is the instantaneous concentration fluctuation about the mean, $\langle c \rangle$. If we define a time average concentration for an averaging time, T, by

$$\bar{c}(t) = \int_{t-T/2}^{t+T/2} c(t')\,dt',$$

then

$$\langle \bar{c} \rangle = \langle c \rangle,$$

and

$$\langle \bar{c}'^2 \rangle = \frac{2\langle c'^2\rangle}{T}\int_0^T \left(1-\frac{\tau}{T}\right)\rho(\tau)\,d\tau, \qquad (1)$$

where $\bar{c}' = \bar{c} - \langle c \rangle$. For a derivation of these results, see Tennekes and Lumley (1972).

Equation (1) is a useful starting point because there are methods available for predicting the ensemble variance, $\langle c'^2 \rangle$, e.g. the particle-pair dispersion model of Durbin (1980), or second-order closure methods (Lewellen and Sykes, 1983). Given $\langle c'^2 \rangle$, we still need the autocorrelation function to calculate $\langle \bar{c}'^2 \rangle$. Venkatram (1979) has considered this problem, and postulated an exponential form for $\rho(\tau)$, using an integral timescale obtained from the fluctuating Eulerian velocity field; this was also the form used by Lewellen and Sykes (1983). The exponential is justified by the observation that the results from (1) are insensitive to the shape of $\rho(\tau)$ (provided that ρ tends to zero reasonably quickly as $\tau \to \infty$), but we shall show herein that the velocity timescale is inappropriate for a highly fluctuating plume which has $\langle c'^2 \rangle \gg \langle c \rangle^2$.

THEORETICAL MODEL

The basis of our theoretical model for estimating the autocorrelation function is Gifford's (1959) fluctuating plume model. This simple idealization has been shown to be capable of describing the early meander phase of a plume (Fackrell and Robins, 1982), and this is precisely the regime where $\langle c'^2 \rangle \gg \langle c \rangle^2$ and the concentration fluctuation timescale is quite different from the velocity timescale. The model does assume a significant mean wind, so that the pollutant is transported downstream, and our results will be valid in the neighborhood of the mean transport direction.

We can readily see that $\langle c'^2 \rangle > \langle c \rangle^2$, together with the restriction $c \geq 0$, implies an intermittent variable, so that there is a strong possibility that there are multiple scales involved. Gifford incorporates this idea in a two-scale model where he expresses the instantaneous concentration as

$$c(x,y,z) = \frac{Q}{2\pi U\sigma_i^2}\exp\left[-\frac{(y-Y)^2+(z-Z)^2}{2\sigma_i^2}\right], \qquad (2)$$

where x is the streamwise coordinate, y, z are lateral coordinates, Q is the release rate, U is the mean velocity, σ_i is the instantaneous width of the plume and (Y, Z) is the instantaneous location of the plume centroid. Y and Z are random variables which are normally (and independently) distributed with zero mean, and variance σ_y^2 and σ_z^2, respectively. We, therefore, have a simple model of a meandering plume, in which the width of the instantaneous plume, σ_i and the range of the meander are functions of downstream distance, x. For our purposes, we do not need to know the downstream development since we want to predict the autocorrelation for an Eulerian measurement; we therefore ignore the x-dependence and work only with the local description. We shall also assume transverse isotropy, so that $\sigma_y^2 = \sigma_z^2$, since this makes the algebra less cumbersome without any fundamental loss of generality.

Gifford shows that the fluctuating plume model gives

$$\langle c \rangle = \frac{Q}{2\pi U(\sigma_i^2 + \sigma_y^2)} \exp\left[-\frac{(y^2+z^2)}{2(\sigma_i^2+\sigma_y^2)} \right] \quad (3)$$

$$\langle c'^2 \rangle = \frac{Q^2}{(2\pi U)^2} \frac{\exp\left(-\frac{(y^2+z^2)}{(2\sigma_y^2+\sigma_i^2)} \right)}{\sigma_i^2(2\sigma_y^2+\sigma_i^2)} - \langle c \rangle^2. \quad (4)$$

To calculate $\rho(\tau)$, we need the correlations $\langle c_1 c_2 \rangle$ where $c_i \equiv c(t_i)$, i.e. time-displaced correlations. From (2), we may write

$$c_1 c_2 = \frac{Q^2}{4\pi^2 U^2 \sigma_i^4} \times \exp\left[-\frac{(y-Y_1)^2 + (z-Z_1)^2 + (y-Y_2)^2 + (z-Z_2)^2}{2\sigma_i^2} \right], \quad (5)$$

where $(Y_1, Z_1) \equiv (Y(t_1), Z(t_1))$ and similarly for t_2. Thus

$$\langle c_1 c_2 \rangle = \iiiint c_1 c_2 P(Y_1, Z_1, Y_2, Z_2)\, dY_1\, dZ_1\, dY_2\, dZ_2, \quad (6)$$

where $c_1 c_2$ is given by (5), and $P(Y_1, Z_1, Y_2, Z_2)$ is the joint probability distribution of Y and Z at times t_1 and t_2. Since Y and Z are assumed independent, $P(Y_1, Z_1, Y_2, Z_2) = P(Y_1, Y_2)\, P(Z_1, Z_2)$, and isotropy allows us to write

$$\langle c_1 c_2 \rangle = \left(\frac{Q}{2\pi U \sigma_i^2} \right)^2 F(y)\, F(z),$$

where

$$F(y) = \iint \exp\left[\frac{-(y-Y_1)^2 - (y-Y_2)^2}{2\sigma_i^2} \right] P(Y_1, Y_2)\, dY_1\, dY_2. \quad (7)$$

In order to solve (7), we must postulate a form for the joint pdf, $P(Y_1, Y_2)$. This was not included in Gifford's original model since it was not required for the calculation of ensemble variance, but we shall propose that Y_1 and Y_2 are joint normally distributed, with a correlation coefficient r, so that $\langle Y_1^2 \rangle = \langle Y_2^2 \rangle = \sigma_y^2$ and $\langle Y_1 Y_2 \rangle = r\sigma_y^2$.

We shall assume the autocorrelation function of the plume position, $r(t_2 - t_1)$, to be exponential, and since variations in Y arise from the meander component of the turbulence, the integral timescale should be the Eulerian integral timescale of the velocity fluctuations, T_E. Thus

$$r = \exp(-|t_2 - t_1|/T_E)$$

and $T_E = \lambda/U$, where λ is an integral length scale of the turbulent eddies.

Our supposed distribution for Y_1, Y_2 implies

$$P(Y_1, Y_2) = \frac{1}{2\pi\sigma_y^2(1-r^2)^{1/2}} \times \exp\left[-\frac{(Y_1^2 - 2rY_1Y_2 + Y_2^2)}{2\sigma_y^2(1-r^2)} \right]. \quad (8)$$

Substituting (8) into (7) and performing the integrations gives, after some algebraic manipulation,

$$F(y) = \frac{\sigma_i^4}{[(\sigma_i^2+\sigma_y^2)^2 - r^2\sigma_y^4]} \exp\left[-\frac{y^2}{\sigma_i^2 + (1+r)\sigma_y^2} \right].$$

Hence

$$\langle c(t)c(t+\tau) \rangle = \frac{Q^2}{4\pi^2 U^2 [(\sigma_i^2+\sigma_y^2)^2 - r^2\sigma_y^4]} \exp\left[-\frac{y^2+z^2}{\sigma_i^2 + (1+r)\sigma_y^2} \right], \quad (9)$$

where $r = \exp(-\tau/T_E)$.

Using the relationship

$$\langle c'(t)c'(t+\tau) \rangle = \langle c(t)c(t+\tau) \rangle - \langle c \rangle^2,$$

it is easy to verify that $\langle c'(t)c'(t+\tau) \rangle \to \langle c'^2 \rangle$ as $\tau \to 0$ and vanishes as $\tau \to \infty$, consistent with Gifford's results (3) and (4).

We now have a closed form for the concentration autocorrelation function which we can substitute in (1) to obtain time-averaged sample variances. The function is quite complicated in general, but is simpler on the plume axis, $y = z = 0$, where

$$\rho(\tau) = \frac{\sigma_i^2(\sigma_i^2 + 2\sigma_y^2)\, e^{-2\tau/T_E}}{[(\sigma_i^2+\sigma_y^2)^2 - e^{-2\tau/T_E}\sigma_y^4]}. \quad (10)$$

This expression can be used to give the concentration integral timescale,

$$T_c = \int_0^\infty \rho(\tau)\, d\tau = T_E \frac{\sigma_i^2(\sigma_i^2+2\sigma_y^2)}{2\sigma_y^4} \ln\left[\frac{(\sigma_i^2+\sigma_y^2)^2}{\sigma_i^4 + 2\sigma_i^2\sigma_y^2} \right]. \quad (11)$$

As $\sigma_i/\sigma_y \to 0, T_c \sim T_E\,\sigma_i^2/\sigma_y^2 \ln[\sigma_y^2/2\sigma_i^2] \ll T_E$, so that T_E is inappropriate for the highly intermittent plume with a large ratio of $\langle c'^2\rangle/\langle c\rangle^2$.

AN ESTIMATE OF THE VARIANCE

We wish to obtain a simple method of estimating the variance in a time-average sample given the ensemble mean and variance only so that we can use the results from this simple model in conjunction with other methods. We therefore replace (10) by the assumption

$$\rho(\tau) = e^{-\tau/T_c} \tag{12}$$

and estimate

$$T_c = T_E \frac{\langle c\rangle_0^2}{2\langle c'^2\rangle_0} \ln\left[1 + 2\frac{\langle c'^2\rangle_0}{\langle c\rangle_0^2}\right] \tag{13}$$

where the subscript zero denotes center-line values. (13) is consistent with (11) in the limit $\sigma_i/\sigma_y \to 0$, and we have inserted the factor of 2 in the logarithm to ensure that $T_c \to T_E$ as $\langle c'^2\rangle/\langle c\rangle^2 \to 0$. Strictly the fluctuating plume model gives $T_c \leqslant T_E/2$, but the model is not appropriate when $\sigma_i \gg \sigma_y$ and we do not have any firm information about the behavior of T_c. Equation (13) implies that we recover Venkatram's (1979) model with $T_c = T_E$ when $\langle c'^2\rangle \ll \langle c\rangle^2$. In any case, Venkatram has shown that (12) implies

$$\frac{\langle \bar{c}'^2\rangle}{\langle c'^2\rangle} = \frac{2(\beta - 1 + e^{-\beta})}{\beta^2}, \tag{14}$$

where $\beta = T/T_c$. This gives

$$\frac{\langle \bar{c}'^2\rangle}{\langle c'^2\rangle} \sim \frac{2T_c}{T} \text{ for } T \to \infty. \tag{15}$$

Thus, on the center line at least, we see that time-averaging a highly intermittent plume gives

$$\langle \bar{c}'^2\rangle_0 = \frac{T_E}{T} \ln\left[1 + 2\frac{\langle c'^2\rangle_0}{\langle c\rangle_0^2}\right] \langle c\rangle_0^2, \tag{16}$$

i.e. there is only a logarithmic dependence on the actual ensemble variance, the time-average result being much more nearly proportional to the square of the mean. This is due to the fact that the instantaneous plume is not resolved by the time-average, i.e. the plume passes over the sampler much faster than the sample time, so that there is hardly any information about the width of the instantaneous plume, and only a logarithmic dependence remains.

Figures 1 and 2 show comparisons between numerical calculations of the variance using equation (10), and the simple estimates from (13) and (14). The results on the center-line are reasonably good for the two values of $\langle c'^2\rangle_0/\langle c\rangle_0^2$ considered, namely 5 and 50. The figures also show the result for $T_c = T_E$, and demonstrate the very large difference in variance reduction for the large variance cases. At $y = 2\sigma_y$, the agreement is actually more precise, showing that the integral time scale, T_c, is not constant across the plume.

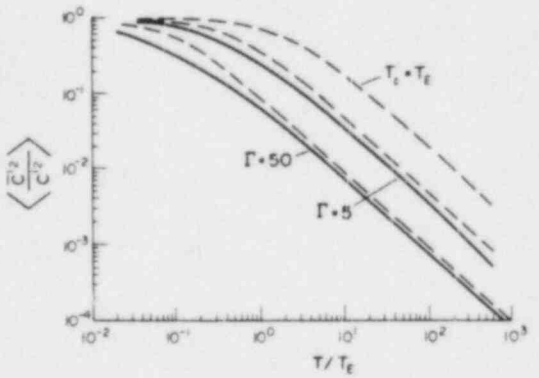

Fig. 1. Reduction of variance by time-averaging on the plume centerline, $y = z = 0$, for different values of the variance to near ratio, $\Gamma = \langle c'^2\rangle_0/\langle c\rangle_0^2$. Solid lines represent the full integral, short dashes correspond to the simple formulae (12) and (13). Also shown is the limiting result for $T_c = T_E$ in (13).

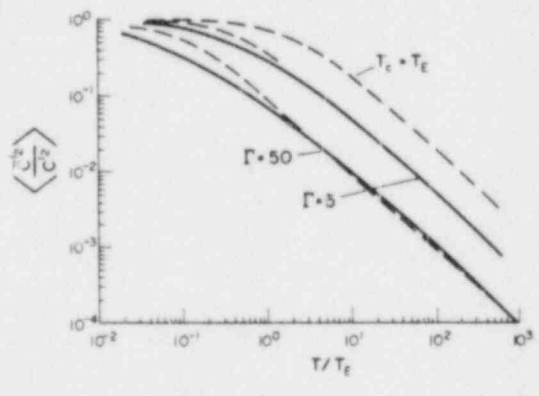

Fig. 2. As Fig. 1 but off-axis at $y = 2\sigma_y$, $z = 0$.

However, discrepancies between the simple estimate and the full integral are not unreasonably large anywhere in the plume, and the simple formulation is adequately justified.

Acknowledgements—This work was partially supported by EPRI with G. R. Hilst as project manager and by NRC with R. F. Abbey as project manager.

REFERENCES

Durbin P. A. (1980) A stochastic model of two-particle dispersion and concentration fluctuations in homogeneous turbulence. *J. Fluid Mech.* **100**, 279–302.

Fackrell J. E. and Robins A. G. (1982) The effects of source size on concentration fluctuations in plumes. *Boundary-Layer Met.* **22**, 335–350.

Gifford F. (1959) Statistical properties of a fluctuating plume dispersal model. *Adv. Geophys.* **6**, 117–137.

Lewellen W. S. and Sykes R. I. (1983) On the use of Concentration Variance Predictions as a Measure of Natural Uncertainty in Observed Concentration Samples. *Proc. 6th Symp. of Turb. and Diff.*, AMS, Boston, MA.

Tennekes H. and Lumley J. L. (1972) *A First Course in Turbulence*. MIT Press, Cambridge, MA.

Venkatram A. (1979) The expected deviation of observed concentrations from predicted ensemble means. *Atmospheric Environment* **13**, 1547–1549.

NRC FORM 335 (11 81)

U.S. NUCLEAR REGULATORY COMMISSION

BIBLIOGRAPHIC DATA SHEET

1. REPORT NUMBER (Assigned by DDC)
NUREG/CR-4157
ARAP Report No. 472

4. TITLE AND SUBTITLE (Add Volume No., if appropriate)
A Scientific Critique of Available Models for Real-Time Simulations of Dispersion

2. (Leave blank)

3. RECIPIENT'S ACCESSION NO.

7. AUTHOR(S)
W.S. Lewellen and R.I. Sykes

5. DATE REPORT COMPLETED
MONTH: January YEAR: 1985

9. PERFORMING ORGANIZATION NAME AND MAILING ADDRESS (Include Zip Code)
Aeronautical Research Associates of Princeton, Inc.
50 Washington Road
Post Office Box 2229
Princeton, New Jersey 08540

DATE REPORT ISSUED
MONTH: March YEAR: 1985

6. (Leave blank)

8. (Leave blank)

12. SPONSORING ORGANIZATION NAME AND MAILING ADDRESS (Include Zip Code)
Division of Radiation Programs and Earth Sciences
Office of Nuclear Regulatory Research
U.S. Nuclear Regulatory Commission
Washington, D.C. 20555

10. PROJECT/TASK/WORK UNIT NO.

11. FIN NO.
B0446

13. TYPE OF REPORT
Technical

PERIOD COVERED (Inclusive dates)

15. SUPPLEMENTARY NOTES

14. (Leave blank)

16. ABSTRACT (200 words or less)

This report provides an evaluation of several available dispersion models to determine their suitability for providing the capability for estimating the effects of accidental discharges of radioactive material at nuclear power plants. A critique of the assumptions involved and a review of existing verification studies are made for models ranging from the Gaussian plume with straight line winds to models which attempt a complete solution of the primitive equations of motion. It is demonstrated that although even the simple models are capable of providing reasonably accurate predictions under ideal conditions, there are reasons to expect relatively severe limits on plume predictability when certain emission conditions are combined with certain meteorological conditions. The usefulness of a real-time dispersion model is thus likely to be dependent on a complementary estimate of the variability expected about the mean dispersion for the conditions existing at that time. This report is one of a set of three dealing with real-time dispersion models. The other two deal with the uncertainties involved in the deposition module of dispersion models and the results of testing some of the dispersion models reviewed in this report by comparing them with the data collected at the Idaho National Engineering Laboratory in July, 1981 during an NRC sponsored field test.

17. KEY WORDS AND DOCUMENT ANALYSIS

17a. DESCRIPTORS

atmospheric dispersion
deposition velocity
dispersion models
dry deposition
model uncertainty
precipitation scavenging
turbulent transfer
wet deposition

17b. IDENTIFIERS/OPEN-ENDED TERMS

18. AVAILABILITY STATEMENT
Unlimited

19. SECURITY CLASS (This report)
Unclassified

21. NO. OF PAGES

20. SECURITY CLASS (This page)
Unclassified

22. PRICE
$